# SOURCE OR SINK?
## A MODELING STUDY OF INORGANIC CARBON CYCLING ON THE SCOTIAN SHELF

by

Krysten Rutherford

Submitted in partial fulfillment of the requirements
for the degree of Doctor of Philosophy

at

Dalhousie University
Halifax, Nova Scotia
November 2021

*Dedicated to my family: my mom, Susan, who inspired my love of science and has supported me no matter what; my older sister, Shari, who never entertains my self-doubt and always knows the right usage of a semi-colon; and my late father, Hugh, whom I carry with me always.*

# TABLE OF CONTENTS

# LIST OF TABLES

# LIST OF FIGURES

# ABSTRACT

The Scotian Shelf, located in the highly dynamic northwestern North Atlantic along the eastern Canadian seaboard, has been the focus of much debate as previous studies have yielded conflicting estimates of air-sea $CO_2$ flux on this mid-latitude shelf. To resolve these inconsistent estimates of air-sea $CO_2$ flux, a quantitative understanding of the underlying carbon transport mechanisms is needed. The Continental Shelf Pump (CSP), which is thought to apply to mid- to high-latitude shelves, posits that the effective transport of carbon from these shelves to the subsurface open ocean creates a sustained sink of $CO_2$. In contrast, the Scotian Shelf behaves as a sustained source of $CO_2$ to the atmosphere, and knowledge about the regional transport mechanisms that could be driving this net outgassing of $CO_2$ has been lacking. My thesis contributes to a better understanding of the observed $CO_2$ flux on the Scotian Shelf, and how it may change in the future. First, I introduce an analysis of dye and age tracers to quantify transport timescales and pathways in a numerical model of the northwestern North Atlantic. Secondly, I present a validation of the inorganic carbon component of the model, and evaluate spatial and temporal variability of the simulated air-sea $CO_2$ flux. Then I use the dye tracers in the carbon model to determine what transport mechanism is underlying the observed air-sea $CO_2$ flux. Lastly, I show future model projections to illustrate how a changing climate may affect carbon transport, air-sea flux, and pH on the northwestern North Atlantic shelf.

# LIST OF ABBREVIATIONS AND SYMBOLS USED

| Abbreviations | Description | Units |
|---|---|---|
| GoM | Gulf of Maine | |
| SS | Scotian Shelf | |
| GB | Grand Banks | |
| LS | Labrador Sea | |
| ENS | East Newfoundland Shelf | |
| Slp | Slope water | |
| Slp-S | Shallow Slope water (>200 m) | |
| Slp-D | Deep Slope water (<200 m) | |
| GoSL | Gulf of St. Lawrence | |
| SLE | St. Lawrence River Estuary | |
| NW | northwest | |
| LC | Labrador Current | |
| NSC | Nova Scotia Current | |
| SC | Shelfbreak Current | |
| NS | Nova Scotia | |
| Nfld | Newfoundland | |
| GFDL | Geophysical Fluid Dynamics Lab | |
| BNAM | Bedford Institute of Oceanography North Atlantic Model | |
| TTD | Transit time distribution | |
| CART | Constituent-oriented age and residence time theory | |
| MRT | Mean residence time | |
| ROMS | Regional Ocean Modelling System | |
| GLS | Generic Length Scale | |
| ECMWF | European Centre for Medium-Range Weather Forecasts | |

| Abbreviations | Description | Units |
|---|---|---|
| HSIMT | High-order Spatial Interpolation at the Middle Temporal level advection scheme | |
| TRANS | Type of dye tracer simulation, dyes are initialized once | |
| AGE | Type of dye tracer simulation, dyes are constantly reinitialized | |
| STN | Station | |
| CI | Confidence Interval | |
| $S_p$ | Ratio of river plume width to shelf width (from *Sharples et al.*, 2017) | |
| SOCAT | Surface Ocean $CO_2$ Atlas | |
| GLODAP | Global Ocean Data Analysis Project | |
| AZMP | Atlantic Zone Monitoring Program | |
| DFO | Department of Fisheries and Oceans Canada | |
| NEMO | Nucleus for European Modelling of the Ocean | |
| Chl | Chlorophyll | |
| Dal-SOOP | Dalhousie Ship of Opportunity Program | |
| CCS | California Current System | |
| LCS | Labrador Current System | |
| HAL | Halifax Line | |
| BB | Brown Banks Line | |
| LOU | Louisbourg Line | |
| HL2 | Station 2 on the Halifax Line | |
| RMSE | Root-mean square error | |

| Symbols | Description | Units |
|---|---|---|
| $T$ | Temperature | °C |
| $DIC$ | Dissolved Inorganic Carbon | mmol C $m^{-3}$ |
| $DIC_{eq}$ | Equilibirum Dissolved Inorganic Carbon | mmol C $m^{-3}$ |
| $NO_3$ | Nitrate | |
| $DIC - DIC_{eq}$ | Carbon disequilibirum | mmol C $m^{-3}$ |
| $TA$ | Total Alkalinity | meq $m^{-3}$ |
| $S$ | Salinity | |
| $CO_2$ | Carbon Dioxide | |
| $pCO_2$ | Partial pressure of carbon dioxide | $\mu$atm |
| K1,K2 | Dissociation constants | |
| $a(t,x)$ | Mean age | days |
| $c(t,x,\tau)$ | Distribution of ages | |
| $C(x,t)$ | Passive dye tracer concentration | kg $m^{-3}$ |
| $\alpha(x,t)$ | Age concentration tracer | kg $m^{-3}$ $day^{-1}$ |
| $\tau_R$ | Mean residence time | days |
| $\Delta pCO_2$ | Anomolies in $pCO_2$ relative to reference value | $\mu$atm |

# ACKNOWLEDGEMENTS

To suggest that I did this PhD on my own would be a gross underestimation of the amazing support I have received over the years. When I started my degree, thinking I'd only be in Halifax for a couple years to do a Master's, I knew no one in the city and knew even less about oceanography. As I am now wrapping up my PhD, I can undoubtedly say that I know too many people in Halifax to count and I know slightly more about oceanography than when I started. The friendships and contacts I have made while at Dalhousie have honestly been one of the best parts of my experience here, and without them, I'm sure I would have run away ages ago to go live in the woods.

To start, my supervisor, Dr. Katja Fennel, has obviously been one of the biggest influences on my time here. She has been endlessly supportive while simultaneously pushing me to be a better scientist. I like to think that I have become a much better researcher over the years, which is absolutely a result of Katja's guidance and support. I, of course, additionally need to thank my supervising committee: Drs. Helmuth Thomas, Christopher Algar, and Eric Oliver. All of these committee members have provided invaluable feedback, tough questions, and generous support throughout my degree, which I am very thankful for. I also need to thank my additional collaborators, Dasha Atamanchuk, Douglas Wallace, Jasmine John, and Dave Brickman, as well as my external examiner, Joseph Salisbury, who generously agreed to be a part of my final thesis defence. Our Graduate Secretary, Lori Lawton, has also been an invaluable resource over the years, and I'm so thankful for all of her help throughout my thesis.

Having been here for quite some time, I have also had the pleasure of working with many people in the MEMG lab group, some who have come and gone, or some who have come and stayed. They have all listened to many of my presentations, critiqued my figures, bolstered my confidence when I needed it, and supplied endless laughter. Although there truly are too many of them to name, honourable mentions go to: Arnaud Laurent for always having the answer; Chris Gordon for boosting my confidence before many presentations; Angela Kuhn and Luiqian Yu for being the wise colleauges in the office next door; Benjamin Richaud for being a great office mate and scientific debater; Katie Brennan for making the steep initial transition into my degree seem much more manageable; Fehmi

Dilmahamod for keeping me laughing (mainly by always trying to scare me); and Lina Garcia-Suarez for support with my last chapter.

Outside of my lab group, I have been incredibly lucky to be a part of many extracurriculars both in and out of the Oceanography Department. The support (and distraction) of the many people I have met along the way has been invaluable. Those groups include most notably DOSA, the Sunday Suppers family, and my EDNA pals. Lorenza Raimondi (the other half of Krystenza) has obviously been one of my biggest supports throughout my thesis and I'm so lucky to have gone through this experience with her. I'm so glad I always had her office to go to or, when COVID-19 hit, her phone to call when things were just a little too overwhelming. Colleen Wilson has been another major support during my degree. She is one of my favourite adventure buddies and ice cream pals, and I'm so privileged to have gotten to take many weekends to explore this province with her. I am additionally forever thankful to Nadine Lehmann and Christoph Renkl for coffee chats and raclette nights; Jenna Hare for her amazing *LaTeX* and Matlab help, and always being an excellent listener; plus, of course, Heather Weston, Jonathan Izett, Stefanie Anna Mellon, Delphine Durette Morin, Mays Markabi, Jacoba Mol, Myriam Lacharite, Laura Green, Jackie Fulton, Esther Gomes, Heather Townsend, and honestly too many people to list. All of these marvelous people made Halifax my home away from home.

There are many other friends who have come to visit and called me often. I may not always get to see them, but they are always there when I need them. My gratitude goes out specifically to Alanna Williams, one of my longest friends and an extension of my family; and Ginelle Johnson and Kelley Robins, who are two of the funniest people I know.

Lastly, I would absolutely not be here without the support of my family, specifically my mom, Susan, and sister, Shari. They had no idea the endeavour I was embarking on when I moved to Halifax (or that I'd stay so long), but have always been my number one cheerleaders and inspirations. They even edited and proofread many of my emails, abstracts, and, most recently, this thesis. I am so lucky to have them in my corner and to have been able to look up to them over the years. Growing up with such amazing female role models undeniably shaped my journey and who I am today.

# CHAPTER 1

# INTRODUCTION

As the use of fossil fuels has steadily increased over the last century, we have seen a rapid rise in atmospheric anthropogenic $CO_2$ (*Keeling et al.*, 1976), which inevitably impacts the balance of $CO_2$ between atmosphere and ocean. Studies have shown that net global ocean $CO_2$ uptake is 1.5-2.0 Pg-C $y^{-1}$, approximately 25% of the industrial atmospheric emissions (e.g. *Takahashi et al.*, 2009). Although mitigating global warming, this anthropogenic $CO_2$ uptake by the ocean leads to many changes in the ocean's biogeochemistry, such as ocean acidification, which has many associated damaging effects on ecosystems (*Lee et al.*, 2006). It is therefore important to understand the processes underlying oceanic $CO_2$ uptake, both now and in the future. Ocean margins are of particular interest due to their high rates of primary production (*Chen and Borges*, 2009), susceptibility to increasing atmospheric $CO_2$ on much shorter timescales than the open ocean (*Cai et al.*, 2010), and disproportionately contributing to global fluxes (*Laruelle et al.*, 2010).

Quantifying shelf-wide $CO_2$ fluxes and understanding the underlying processes is not straightforward. Flux estimates on continental shelves come with large uncertainties: air-sea fluxes are associated with complex shelf dynamics (*Laruelle et al.*, 2014), and have large spatial and temporal variability (*Previdi et al.*, 2009). Many studies have been aimed at characterizing $CO_2$ flux on continental shelves from local to regional and global scales (e.g. *Cai et al.*, 2006, 2010; *Laruelle et al.*, 2014, 2015; *Roobaert et al.*, 2019; *Bourgeois et al.*, 2016; *Fennel et al.*, 2019). From global syntheses, a latitudinal trend in continental shelf source-sink behavior has emerged, where mid- to high-latitudes act as net sinks of atmospheric $CO_2$ and those at low latitudes act as net sources of $CO_2$ (see Figure 1.1; e.g. *Chen and Borges*, 2009; *Cai et al.*, 2006; *Laruelle et al.*, 2014; *Roobaert et al.*, 2019).

A mechanism that is frequently used to explain net $CO_2$ uptake in mid- to high-latitude shelf systems is the Continental Shelf Pump (CSP). *Tsunogai et al.* (1999) proposed this mechanism, which relies on cross-shelf advection moving cold dense, carbon-rich shelf water into the deep open ocean, thus creating a sink of $CO_2$. The CSP relies on large seasonal changes in temperature, which are not found at lower latitudes. Instead, upwelling transport mechanisms are often observed on low-latitude shelves.

There are, of course, deviations from the described global-scale flux pattern. For example, the Scotian Shelf is a mid-latitude shelf located along eastern Canada, which would indicate that it should act as a sink of $CO_2$. It has, however, been reported to act as a large net source of $CO_2$ in local studies, which used direct measurements from a moored CARIOCA buoy located 30 km offshore on the Scotian Shelf (*Shadwick et al.*, 2010, 2011; *Shadwick and Thomas*, 2014). To explain the reported outgassing on the Scotian Shelf, it has been proposed that this mid-latitude shelf acts as an upwelling system (e.g. *Shadwick et al.*, 2010; *Burt et al.*, 2013), where deep carbon-rich waters are brought onto the shelf, promoting a release of $CO_2$ to the atmosphere. This hypothesized upwelling mechanism counters the CSP mechanism that is thought to act on mid-latitude shelves. The overarching motivation of my thesis is to better understand the source or sink behavior of the Scotian Shelf and what transport processes are underlying this behavior.

The Scotian Shelf is approximately 700 km long and varies in width between 120-240 km (see Figure 1.2). The shelf is heavily influenced by the Labrador Current System (*Loder et al.*, 1998; *Fratantoni and Pickart*, 2007). The Labrador Current carries cold, carbon-rich water along the shelf break here, turning at the tip of Grand Banks to travel southwestward and form the shelf-break current along the Scotian Shelf. There is additionally an inner branch of this southward transport, originating with shelf-ocean exchange between the Labrador Sea and the Labrador Shelf, and can be traced as far south as the Middle Atlantic Bight and Cape Hatteras (*Chapman and Beardsley*, 1989; *Mountain*, 1991). Farther offshore is the Gulf Stream, which travels northward and carries warm and salty subtropical water. The dynamic confluence of the Gulf Stream and Labrador Current affects the whole shelf north of Cape Hatteras and makes it a dynamically unique region to study.

My thesis work aims to improve our understanding of how biogeochemical and physical processes influence air-sea $CO_2$ flux, and transport and transformation of inorganic carbon on the Scotian Shelf, both now and in the future, by using a biogeochemical model in

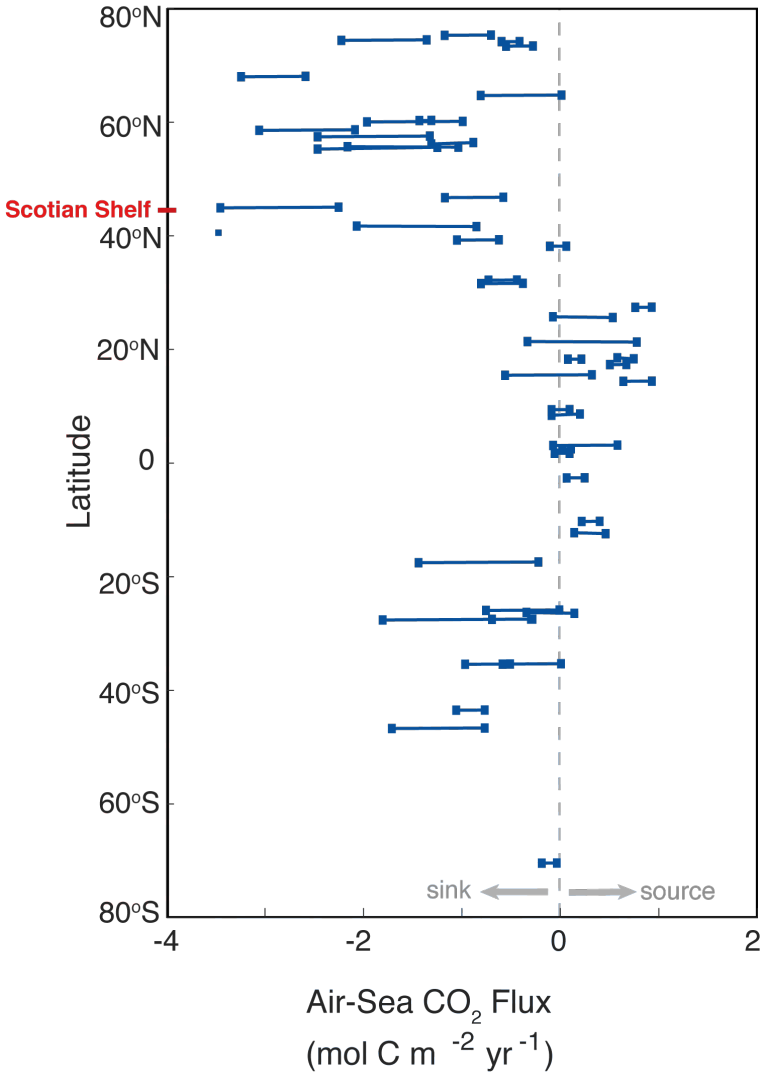


Figure 1.1: Adaptation of *Roobaert et al.* (2019), indicating latitudinal trends in air-sea $CO_2$ fluxes, with the latitude of the Scotian Shelf indicated on the y-axis.

conjunction with observations. Numerical models are useful tools for investigating the complex interaction of processes affecting carbon cycling. Models can help interpret sparse measurements through mechanistic representations of the relevant processes and can be used to make future projections. My thesis will investigate the processes impacting air-sea $CO_2$ flux on the Scotian Shelf with the use of a Regional Ocean Modeling System (ROMS; *Haidvogel et al.*, 2008) model of Atlantic Canadian shelf waters (Atlantic Canada Model, ACM; *Brennan et al.*, 2016; *Laurent et al.*, 2021). The physical ROMS model is coupled with a biogeochemical module (*Fennel et al.*, 2006, 2008), which includes the inorganic carbon variables. I will investigate both present and future ocean circulation

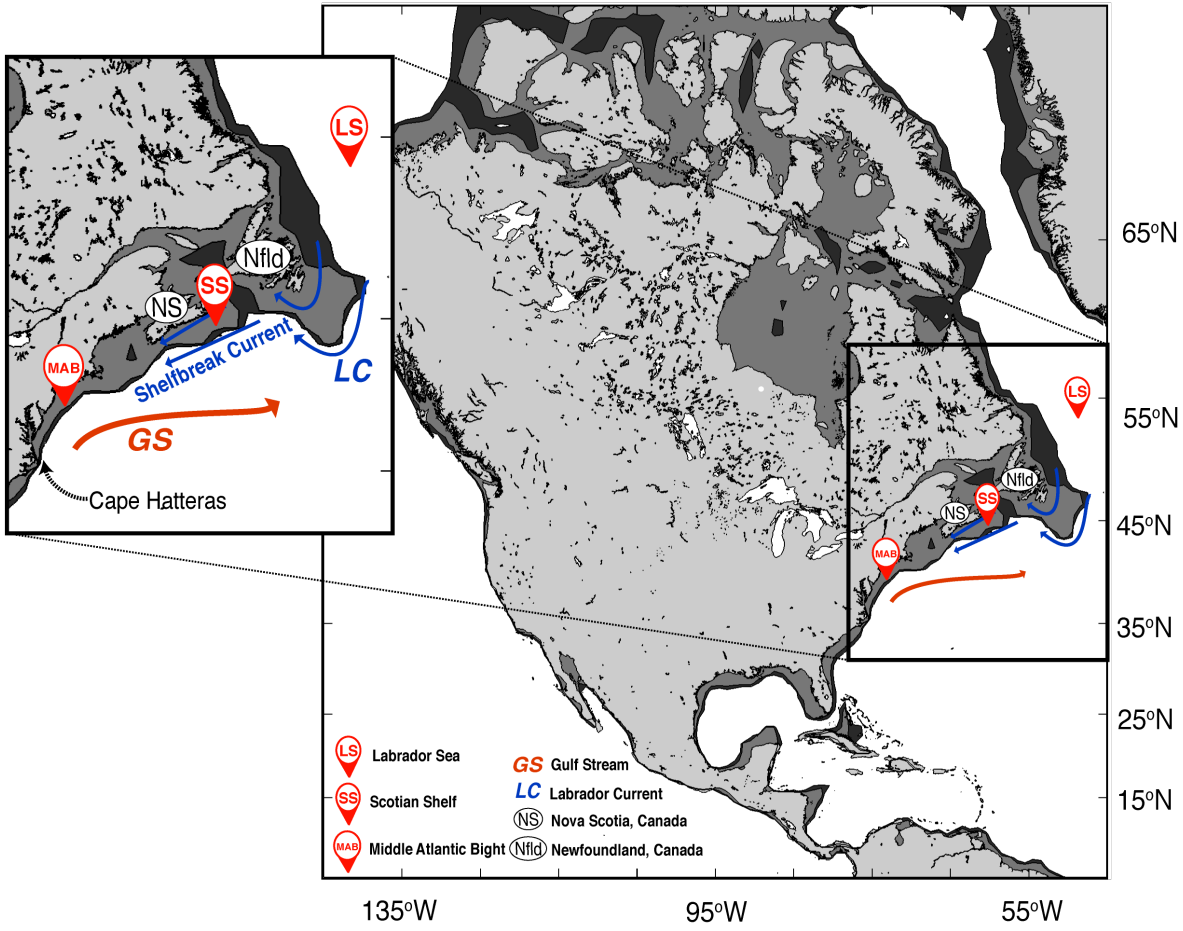


Figure 1.2: Map of North America. Black area indicates 500 m depth and dark grey indicates 200 m depth. Important locations and circulation features off the coast of eastern Canada are indicated by the arrows.

to determine how inorganic carbon is being transported onto and off the Scotian Shelf. More specifically, my research aims to address four main objectives, each of which forms a chapter in my thesis:

1. Quantify and evaluate transport timescales and pathways in a model of the northwestern North Atlantic.

2. Develop and validate an inorganic carbon model for the northwestern North Atlantic to evaluate temporal and spatial variability of air-sea $CO_2$ flux.

3. Improve understanding of the transport mechanisms underlying these carbon fluxes

by simulating and quantifying carbon transport pathways and timescales with the help of dye and age tracers in the numerical model.

4. Generate future model projections to assess how a changing climate will affect retention times and carbon transport on the northwestern North Atlantic shelf.

## 1.1 Diagnosing transit times on the northwestern North Atlantic continental shelf

Many studies have used transport timescales to complement the investigation of biogeochemical processes. For instance, (*Holzer and Primeau*, 2006) used transport diagnostics, such as residence time, to track the movement of the great ocean conveyer (*Broecker*, 1991), which has ultimate control over inter-basin transport and nutrient distributions. *Laruelle et al.* (2013) used freshwater residence time in their multi-scale segmentation approach towards understanding the connection between rivers, and coastal and continental shelf waters, and the implications of this connection on regional and global air-sea $CO_2$ flux. *Cao et al.* (2009) used ventilation timescales to assess the effect of ocean transport on $CO_2$ uptake and how different ventilation rates can appreciably affect projected future anthropogenic $CO_2$ in global ocean models. I implemented dye and age tracers in our model of the North Atlantic to evaluate transport times and pathways. Qualitatively, the dye simulations allow me to track where and how fast water is moving throughout the model domain, especially across the shelf break. Quantitatively, the dyes allow me to calculate the relative contribution of source waters in setting the biogeochemical properties in various shelf locations and to determine the effects of transport timescales on biogeochemical properties. I specifically examined the validity of the previously proposed CSP and upwelling mechanisms on the Scotian Shelf and implemented numerical dye tracers in my model to track the movement of different water masses to investigate these carbon transport mechanisms. Specific questions I address are:

- What are the retention times and dominant transport pathways in the Northwest Atlantic?
- What are the relative contributions of source waters to setting biogeochemical properties on the shelf regions here?

## 1.2 A modeling study of temporal and spatial $pCO_2$ variability on the biologically active and temperature-dominated Scotian Shelf

Estimates of the net air-sea flux of $CO_2$ for the Scotian Shelf are conflicting. Global studies, such as that performed by *Laruelle et al.* (2014), identify the Scotian Shelf as a sink ($-0.33 \pm 0.25$ mol C m$^{-2}$ yr$^{-1}$) of $CO_2$ from the atmosphere. In contrast, the regional study by *Shadwick et al.* (2011), using observations from a moored CARIOCA buoy located 30 km off the coast of Halifax, estimated that the Scotian Shelf acts as a net source ($+1.42 \pm 0.28$ mol C m$^{-2}$ yr$^{-1}$) of $CO_2$ to the atmosphere. *Signorini et al.* (2013), in a regional study of the eastern coast of North America, also classified the Scotian Shelf as a net sink ($-1.10 \pm 0.25$ mol C m$^{-2}$ yr$^{-1}$) of $CO_2$. Considering the conflicting estimates for the Scotian Shelf, my work aims to combine high-resolution observational datasets with our regional model of the northwest North Atlantic to better understand the temporal and spatial variability of $pCO_2$ on a seasonal scale and estimate the air-sea $CO_2$ flux here. Specific questions I address are:

- Is the Scotian Shelf, as a whole, acting as a net source or net sink of atmospheric $CO_2$?
- Can one station of extended time series data accurately describe shelf-wide dynamics of $CO_2$ fluxes?

## 1.3 Elucidating coastal ocean carbon transport processes: A novel approach applied to the northwest North Atlantic shelf

The consensus view of many global syntheses of coastal air-sea $CO_2$ flux is that mid- to high-latitude shelves act as net sinks (i.e. take up $CO_2$ from the atmosphere) whereas low-latitude shelves act as net sources of $CO_2$ (see for example: *Cai et al.*, 2006; *Chen and Borges*, 2009; *Laruelle et al.*, 2014; *Roobaert et al.*, 2019). However, regional observations and our regional model indicate that the Scotian Shelf deviates from this global trend in $CO_2$ fluxes, acting as a large net source of $CO_2$. I use my model analyses to elucidate the underlying processes that can sustain the outgassing of $CO_2$ on the mid-latitude Scotian

Shelf. I use the passive dye tracers to elucidate where the majority of the water on the Scotian Shelf is coming from, and analyze what changes are occurring to the carbonate chemistry of water as it travels to the Scotian Shelf. More specifically:

- What transport mechanisms are acting on the Scotian Shelf to sustain it as a source of atmospheric $CO_2$? For example:
  - Is DIC-rich deep ocean water being upwelled onto the shelf creating a source of $CO_2$?
  - Is cold, nutrient-rich Labrador Current water being transported onto the shelf, being warmed and creating a source of $CO_2$?

## 1.4 Shifting circulation under a changing climate: Biogeochemical impacts in the northwest North Atlantic

*Claret et al.* (2018) used the global Geophysical Fluid Dynamics Lab (GFDL) model and projected rapid deoxygenation on the shelves along eastern Canada over the next century as a result of shifting regional circulation features. It is therefore reasonable to assume that we could see some dramatic changes to the carbonate chemistry here as a result of circulation changes as well. These effects are, of course, compounded by the rising atmospheric $CO_2$ and increasing temperatures, and could cause many negative effects in the shelf ecosystem, for example due to ocean acidification. It is known that global climate models are too coarse to adequately resolve shelf circulation and biogeochemical processes in this region (*Loder et al.*, 2015; *Lavoie et al.*, 2019) and thus are not capable of distinguishing small-scale features related to carbon transport. I therefore use the output from the global GFDL model to force our regional model of the northwest North Atlantic to more accurately represent small-scale carbon transport on the Scotian Shelf under a future climate scenario and study how this potential future state will affect the carbonate chemistry here. Specific questions I address are:

- How will the carbonate chemistry on the shelves along eastern Canada be impacted under a future scenario where the shelf-break current vanishes?

- What future changes to the shelf-wide carbonate chemistry can be attributed to circulation changes versus atmospheric inputs?

# CHAPTER 2

# DIAGNOSING TRANSIT TIMES ON THE NORTHWESTERN NORTH ATLANTIC CONTINENTAL SHELF [1]

## 2.1 Abstract

The circulation in the northwestern North Atlantic Ocean is highly complex, characterized by the confluence of two major western boundary current systems and several shelf currents. Here we present the first comprehensive analysis of transport paths and timescales for the northwestern North Atlantic shelf, which is useful for estimating ventilation rates, describing circulation and mixing, characterizing the composition of water masses with respect to different source regions, and elucidating rates and patterns of biogeochemical processing, species dispersal, and genetic connectivity. Our analysis uses dye and age tracers within a high-resolution circulation model of the region, divided into 9 subregions, to diagnose retention times, transport pathways, and transit times. Retention times are shortest on the Scotian Shelf ($\sim$3 months), where the inshore and shelf-break branches of the coastal current system result in high along-shelf transport to the southwest, and on the Grand Banks ($\sim$3 months). Larger retention times are simulated in the Gulf of St. Lawrence ($\sim$12 months) and the Gulf of Maine ($\sim$6 months). Source-water analysis shows that Scotian Shelf water is primarily comprised of waters from the Grand Banks and Gulf of St. Lawrence, with varying composition across the shelf. Contributions from

[1] Rutherford, K., and K. Fennel, Diagnosing transit times on the northwestern North Atlantic continental shelf, Ocean Science, 14, 1207–1221, 2018.
Author contribution: KR and KF conceived the study. KR carried out the model simulations and analysis. KR and KF discussed the results and wrote the manuscript.

the Gulf of St. Lawrence are larger at nearshore locations, whereas locations near the shelf break have larger contributions from the Grand Banks and slope waters. Waters from the deep slope have little connectivity with the shelf, because the shelf-break current inhibits transport across the shelf break. Grand Banks and Gulf of St. Lawrence waters are therefore dominant controls on biogeochemical properties, and on setting and sustaining planktonic communities on the Scotian Shelf.

## 2.2 Introduction

Biogeochemical cycling and property distributions in aquatic systems, including in lakes, estuaries, and ocean basins, depend on water transport paths and timescales. Analysis of transport paths and timescales has been used to estimate ventilation rates (*Jenkins*, 1987; *England*, 1995; *Hohmann et al.*, 1998; *Cao et al.*, 2009), to describe circulation and mixing (*Fine*, 1995; *Haine et al.*, 1998; *Schlosser et al.*, 2001; *Wunsch*, 2002), and to investigate river plume dynamics (*Zhang et al.*, 2010, 2012). These analyses can either be the focus of or complement investigations into biogeochemical processes. For example, *Holzer and Primeau* (2006) used residence time, a diagnostic of transport timescales, to investigate the role of the global overturning circulation in controlling inter-basin transport and nutrient distributions. *Cao et al.* (2009) used ventilation timescales to assess the effect of ocean transport on $CO_2$ uptake and how different ventilation rates can affect projected anthropogenic carbon in global ocean models. *Laruelle et al.* (2013) estimated freshwater residence times in the coastal ocean to better understand the connection between rivers and coastal waters, and their effect on regional and global air-sea $CO_2$ flux. In a recent study, *Xue et al.* (2011) used flushing times to discuss carbon export from the continental shelf of the East China Sea. *Ho et al.* (2017) used residence time estimates to infer carbon export fluxes from a mangrove-dominated estuary. These examples show that transport timescales are widely used measures for the analysis of biogeochemical distributions and fluxes.

Transport paths and timescales can be obtained with the help of tracers, either through direct measurement of appropriate chemical tracers that are injected into aquatic systems deliberately (e.g. *Banyte et al.*, 2013; *Ho et al.*, 2017) or unintentionally (*Beining and Roether*, 1996; *Karstensen and Tomczak*, 1998), or with the help of dye and age tracers in numerical models (e.g. *England*, 1995; *Delhez et al.*, 1999; *Banas and Hickey*, 2005; *Zhang et al.*, 2010). Due to practical considerations such as cost, the application of chemical

tracers for direct measurement remains limited, and numerical tracers are often used. Models can scale up from sparse measurements through mechanistic representations of the relevant processes and achieve high spatial and temporal resolution. Various methods for determining timescales and quantifying ocean age and ventilation rates in numerical models have been used (*Jenkins*, 1987; *Sarmiento et al.*, 1990; *Thiele and Sarmiento*, 1990; *England*, 1995).

Through the implementation of dye and age tracers in a high-resolution regional circulation model, this present study aims to determine circulation pathways, transport timescales, and residence times for the northwestern (NW) North Atlantic shelf, which is characterized by complex circulation and is undergoing rapid changes. Although previous studies have quantified shelf basin particle retention (*Rogers*, 2015), shelf residence times as part of global studies (*Bourgeois et al.*, 2016; *Sharples et al.*, 2017), and transport times from the St. Lawrence River to the Scotian Shelf (*Sutcliffe et al.*, 1976; *Smith*, 1989; *Shan et al.*, 2016), this is the first comprehensive analysis of residence times and transport pathways and timescales in the NW North Atlantic.

The region has experienced rapid oxygen loss over past decades both on the Scotian Shelf (*Gilbert et al.*, 2010) and in bottom waters in the Lower St. Lawrence Estuary in the Gulf of St. Lawrence (*Gilbert et al.*, 2005), with negative effects on the coastal ecosystem (*Bianucci et al.*, 2016; *Brennan et al.*, 2016a). Furthermore, the region's status as a source or sink of atmospheric $CO_2$ is unresolved, with conflicting reports of the Scotian Shelf as a region of net outgassing (*Shadwick et al.*, 2010) and net uptake (*Signorini et al.*, 2013). Coastal upwelling, defined as upwelling of water from below the seasonal thermocline within 10 km of the coast, has been reported along the southern shore of Nova Scotia during the late summer months due to upwelling-favourable winds along the coast (*Petrie et al.*, 1987; *Shan et al.*, 2016). *Shadwick et al.* (2010) and *Burt et al.* (2013) have proposed that upwelling also occurs at the shelf break bringing subsurface slope waters onto the Scotian Shelf to explain the reported outgassing of $CO_2$, but this is counter to the hypothesized behavior of mid- and high-latitude shelves as net sinks (*Tsunogai et al.*, 1999; *Cai et al.*, 2006). Ocean circulation and mixing are important controls on oxygen ventilation and net air-sea $CO_2$ flux. By elucidating transport pathways and quantifying the associated timescales for different subregions in the NW North Atlantic, we aim to improve mechanistic understanding of the physical influences on regional biogeochemical

cycling, in particular deoxygenation and net air-sea $CO_2$ flux.

We follow established methodology for quantifying the related concepts of water age and residence time. Age, $a$, is a local measure, in other words it is unique to each water parcel, and thus recognizes spatial heterogeneity (*Delhez et al.*, 1999; *Monsen et al.*, 2002). The age of a water parcel is defined as the time since that parcel left a specified point location, surface, or volume where its age is set to zero (*Delhez et al.*, 1999) and is a Lagrangian concept since it is a characteristic of the fluid parcel (*Deleersnijder et al.*, 2001). There are two main approaches to calculating age in numerical models: Green's function-based transit time distribution (TTD) theory (*Hall and Plumb*, 1994; *Holzer and Hall*, 2000; *Haine and Hall*, 2002; *Hall and Haine*, 2002) and constituent-oriented age and residence time theory (CART; *Delhez et al.*, 1999; *Deleersnijder et al.*, 2001; *Delhez et al.*, 2004; *Delhez*, 2006; *Delhez and Deleersnijder*, 2006). TTD is best used for steady flow applications and computes the full spectrum or distribution of transit times in a water parcel using Green's functions (*Haine and Hall*, 2002), while CART is better suited to time-varying flow, and is especially useful for highly resolved coastal applications. The present study uses CART, which calculates the mean age as a mass-weighted average of the distribution of ages, $c(t, x, \tau)$, present in each water parcel (*Delhez et al.*, 1999). A fuller explanation of CART theory is given in Section 2.4.1.

Residence time, a complement to age, is also a local measure unique to each water parcel. Local residence time estimates can be averaged to quantify mean residence time (also referred to as flushing time or retention time; *Agmon*, 1984; *Monsen et al.*, 2002), which applies to the larger control volume. Mean residence time, defined as the time it takes for a water parcel to leave a control volume or source volume, is frequently used to quantify the renewal of water in a defined body of water and can be used to assess the influence of hydrodynamic processes on aquatic systems. Since residence time is a function of both space and time (by definition, every water parcel has its own unique path and history, each with a different residence time), it is necessary to describe residence time in a finite volume as a distribution (*Delhez et al.*, 2004). From this distribution, the mean residence time, $\tau_R$, can be calculated as the first moment of the residence time distribution (*Agmon*, 1984; *Berezhkovskii et al.*, 1998). Although knowledge of $\tau_R$ does not identify the underlying physical processes or a system's unique spatial distribution of water retention, it is useful for comparing different regions (*Monsen et al.*, 2002).

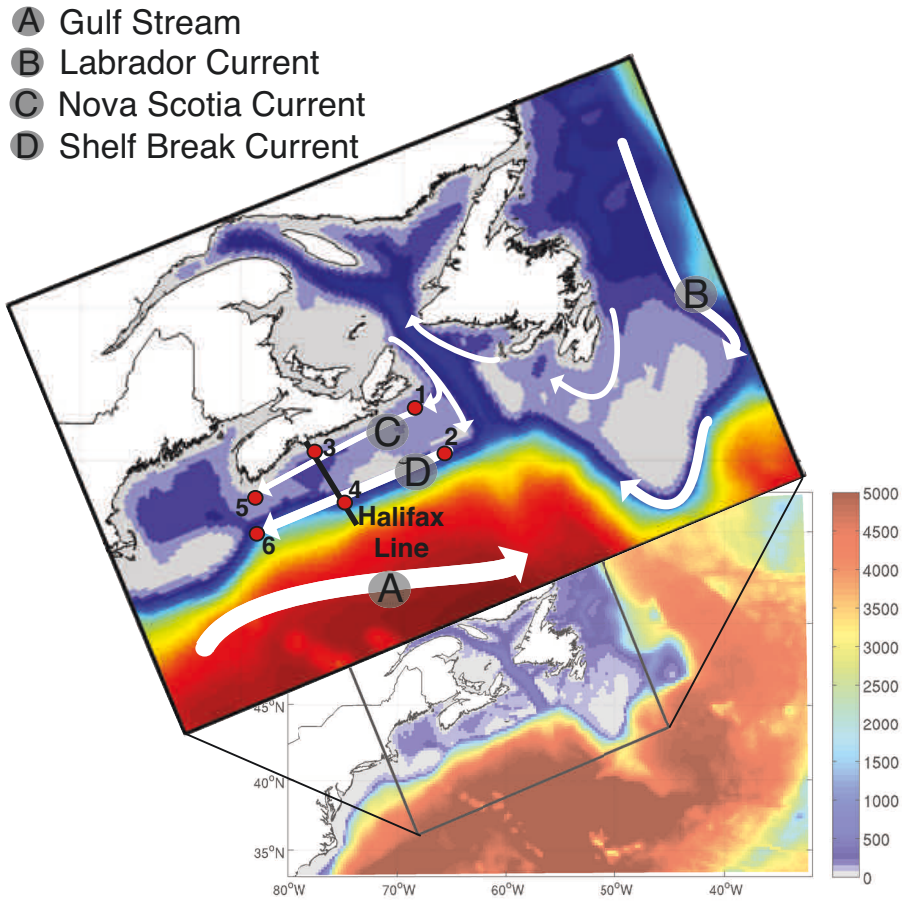


Figure 2.1: Bathymetric map of the NW Atlantic, with the model domain and general circulation structure shown in the upper panel. The Halifax Line, a transect across the Scotian Shelf, is shown by the bold black line. Station locations are numbered and indicated by red points along the Scotian Shelf.

In this study, we use a high-resolution circulation model for the NW North Atlantic (*Brennan et al.*, 2016) that is implemented using the Regional Ocean Modeling System (ROMS; *Haidvogel et al.*, 2008). Within the model domain, we distinguish 9 different subregions and track their source-water movements with passive dye tracers and associated age tracers following CART. The simulated dye tracer distributions illustrate how water circulates throughout the domain, and enable quantification of mean residence time in four shelf regions: the Grand Banks, the Gulf of St. Lawrence, the Scotian Shelf, and the Gulf of Maine. Mass fractions of each of the dyes in the Gulf of St. Lawrence, Scotian Shelf, and Gulf of Maine illustrate how the different source regions are contributing at different locations and on average. Lastly, the age of these dyes indicates how long it takes water to travel throughout the domain.

## 2.3 Study region

The NW North Atlantic (Figure 2.1), off the eastern coast of Canada, is uniquely located at the junction of the subpolar and subtropical gyres (*Loder et al.*, 1997; *Hannah et al.*, 2001). The circulation is dominated by the southward transport of Arctic waters via the Labrador Current System (*Loder et al.*, 1998; *Fratantoni and Pickart*, 2007). The outflow from the Denmark and Davis Straits in the north, which make up the Labrador Current, accumulates along the northwestern North Atlantic continental shelf separating cold, fresh shelf waters from warm, salty slope waters (*Beardsley and Boicourt*, 1981; *Loder et al.*, 1998; *Fratantoni and Pickart*, 2007).

The Scotian Shelf (Figure 2.2), a 700 km-long portion of the continental shelf centrally located in the NW North Atlantic, is characterized by currents moving to the southwest with inshore and shelf-break branches. The inshore Nova Scotia Current (NSC) originates in the Gulf of St. Lawrence, turns onto the Scotian Shelf at Cabot Strait, moves southwestward along the coast, and enters the Gulf of Maine at Cape Sable. The shelf-break current is an extension of the Labrador Current (*Hannah et al.*, 2001; *Han*, 2003). Since the NSC plays a dominant role in the alongshore transport on the Scotian Shelf, much of the water within 60 km of shore and top 100 m is composed of Gulf of St. Lawrence–originating water (*Dever et al.*, 2016). Freshwater discharge from the St. Lawrence River additionally impacts the seasonal cycle of the NSC transport (*Dever et al.*, 2016), and both the NSC and shelf-break current are strongest in the winter and weakest in the summer (*Shan et al.*, 2016). Overall, this demonstrates the important connectivity between the Gulf of St. Lawrence and the Scotian Shelf. Transit times from the St. Lawrence River (at Quebec City) to Halifax and Cape Sable have been previously estimated as 6 to 7 months (*Sutcliffe et al.*, 1976; *Shan et al.*, 2016) and 8 to 9 months (*Smith*, 1989; *Shan et al.*, 2016), respectively.

Small-scale circulation patterns on the shelf are influenced by topographic features, such as banks and basins, creating anticyclonic and cyclonic features (*Han*, 2003). In deep shelf basins and along the shelf break, the contribution from slope waters becomes more important (*Dever et al.*, 2016), with onshore flow of slope water through several cross-shelf channels (*Shan et al.*, 2016).

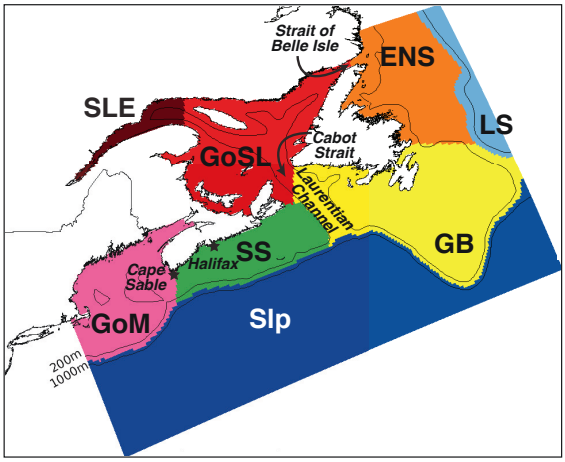


Figure 2.2: Division of the model domain for initialization of dye tracers. Regions are as follows: offshore segment (Slp), which is further divided into 2 depth levels (200 m and above, and below 200 m); Labrador Sea (LS), East Newfoundland Shelf (ENS), Grand Banks (GB), St. Lawrence Estuary (SLE), Gulf of St. Lawrence (GoSL), Scotian Shelf (SS), and Gulf of Maine (GoM).

## 2.4 Methods

### 2.4.1 CART theory: quantifying age

Most methods for quantifying age are based on the idea that in each water parcel there is a distribution of ages, $c(t, x, \tau)$, as shown schematically in Figure 2.3. All equations to calculate age are based on this age distribution in a water parcel at position $x$ and at time $t$, where $\tau$ is the age or time since the water parcel left its source region. The age distribution is subject to the following dynamical equation:

$$\frac{\partial c(\tau)}{\partial t} = -\nabla(\mathbf{u}c - \mathbf{K}\nabla c) - \frac{\partial c(\tau)}{\partial \tau} \tag{2.1}$$

where $\mathbf{u}$ is the velocity at time $t$ and location $x$, and $\mathbf{K}\nabla c$ is the subgrid-scale flux parameterization, with the eddy diffusivity tensor $\mathbf{K}$ (*Delhez et al.*, 1999). The first two terms on the right side represent water being advected and diffused, respectively, which will add and subtract from the age distribution. The last term represents the aging of the distribution (Figure 2.3).

For coastal applications, such as in the present study, calculating the entire spectrum of ages in Figure 2.3 is computationally not feasible and instead we calculate the mass-weighted average of the spectrum of ages, i.e. the mean age (CART method). To implement

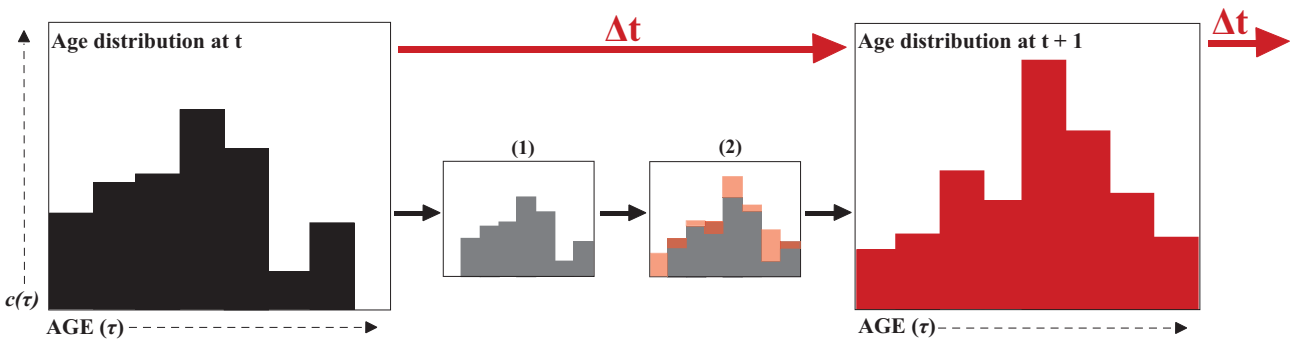


Figure 2.3: Each water parcel is characterized by a distribution of ages, as described in equation (1) and indicated in the left panel. With each time step, this distribution ages as indicated by the shift to small panel (1); additionally, water is advecting/diffusing in/out of the water parcel resulting in different age components being added and subtracted as indicated by the transition from (1) to (2). Together, these two processes produce the distribution at the next time step shown in the right panel.

this method in numerical models, two tracers need to be simulated: (1) a passive dye tracer, $C(x,t)$, that is purely advected and diffused throughout the domain, and (2) an age concentration tracer, $\alpha(x,t)$, that is coupled with the passive dye tracer and only starts to increase once the coupled tracer has left its source region. This second tracer essentially tracks the time since the associated dye tracer has last left its initialization region and is only defined where the dye tracer is present (i.e. where $C > 0$). Mean age is then calculated as a ratio of these two tracers.

Equations governing the dye and age concentration tracers are derived as follows. It can be assumed that all tracer leaves the domain as $\tau$ approaches infinity; in other words, as $\tau$ becomes infinitely large, the age spectrum distribution approaches zero (i.e. $\lim_{\tau\to\infty} c_i(t,x,\tau) = 0$). With this boundary condition, Equation 2.1 can be integrated with respect to $\tau$ and using

$$C(t,x) = \int_0^\infty c(t,x,\tau)d\tau. \tag{2.2}$$

The resulting equation

$$\frac{\partial C}{\partial t} = -\nabla(\mathbf{u}C - \mathbf{K}\nabla C) \tag{2.3}$$

is used to track the dye tracer concentration, $C$ (*Delhez et al.*, 1999).

The age concentration tracer, $\alpha(t, x)$, is defined as the first moment of the age distribution, $c(t, x, \tau)$, and is obtained by multiplying Equation 2.1 by $\tau$, integrating with respect to $\tau$ and making use of the fact that

$$\alpha(t, x) = \int_0^\infty \tau c(t, x, \tau) d\tau \tag{2.4}$$

which yields

$$\frac{\partial \alpha}{\partial t} = C - \nabla(\mathbf{u}\alpha - \mathbf{K}\nabla\alpha). \tag{2.5}$$

Equation 2.5 is coupled with Equation 2.3 such that $\alpha$ will grow proportional in time with each time step when $C > 0$ .

The mean age, $a(t, x)$, is defined by the first moment of the age distribution normalized by the dye tracer concentration

$$a(t, x) = \frac{1}{C(t, x)} \int_0^\infty \tau c(t, x, \tau) d\tau. \tag{2.6}$$

In other words, the age is calculated by dividing the age concentration tracer, $\alpha(t, x)$, by the dye tracer, $C(t, x)$, as in equation 2.6,

$$a(t, x) = \frac{\alpha(t, x)}{C(t, x)}. \tag{2.7}$$

These equations can be applied to any number of independent tracers with separate $C_i(t, x)$, $\alpha_i(t, x)$, and $a_i(t, x)$, as in this study. It is straightforward to implement Equations 2.3 and 2.5 in ROMS.

### 2.4.2 Quantifying mean residence time

Residence time, similar to age, is a local measure described by a distribution. Here, we calculate the mean residence time (MRT), which has also been referred to as "mean passage time" (*Agmon*, 1984), "average lifetime" (*Berezhkovskii et al.*, 1998), and "flushing time" (*Monsen et al.*, 2002), and describes the average time water or a constituent (e.g. a dissolved tracer) spends in a defined control volume.

Residence time is best defined in a probabilistic framework (*Agmon*, 1984; *Berezhkovskii et al.*, 1998). The probability that a particle, $P$, which at time $t_o = 0$ was located at $x_o$ in domain $X$, is found at point $x \in X$ at time $t$, is given by the probability $p(x, t|X)$. Then

survival probability, or the probability of $P$ remaining in the domain $X$, is

$$S(t|X) \equiv \int_X p(x,t|X)dx. \tag{2.8}$$

The lifetime distribution, $F(t|X)$, which is similar to the age distribution and essentially describes how long the particle $P$ spends within the domain $X$, is then described as

$$F(t|X) = -\frac{\partial S(t|X)}{\partial t}. \tag{2.9}$$

Similar to the calculation of the mean age, the mean lifetime or mean residence time of $P, \tau_P$, is calculated as the first moment of the lifetime distribution

$$\tau_P = -\int_0^\infty \frac{\partial S(t|X)}{\partial t} t dt = \int_0^\infty S(t|X)dt. \tag{2.10}$$

The same principles used to find the residence time of a single particle can be applied to calculate the MRT of all particles contained in domain $X$ at $t_o$, e.g. a passive dye tracer homogeneously initialized within $X$. In practice, the lifetime distribution for this scenario is described as the distribution of dye mass, $C_m$, leaving the domain

$$F(t|X) = -\frac{\partial C_m}{\partial t}. \tag{2.11}$$

MRT is calculated as the first moment of $F(t|X)$ (i.e. the weighted sum of the dye tracer mass leaving the control domain at each time step), integrating to the end of the simulation, $t_n$,

$$\tau_R = -\int_0^{t_n} \frac{\partial C_m}{\partial t} t dt. \tag{2.12}$$

MRT is different from residence time and age, which are local quantities. Its calculation requires only the implementation of a passive dye tracer.

### 2.4.3 Model domain and setup

Our model is based on ROMS version 3.5, a terrain-following, free-surface, primitive equation ocean model (*Haidvogel et al.*, 2008), implemented with 30 vertical levels and approximately 10 km horizontal resolution (240×120 horizontal grid cells). The model domain includes the Gulf of Maine, Scotian Shelf, East Newfoundland Shelf, Grand Banks, and Gulf of St. Lawrence (see Figure 2.2), and is described in detail in *Brennan*

*et al.* (2016), who have shown it to realistically represent the regional circulation patterns. Our implementation uses the GLS vertical mixing scheme (*Umlauf and Burchard*, 2003; *Warner et al.*, 2005), atmospheric surface forcing from the European Centre for Medium-Range Weather Forecasts (ECMWF) ERA-Interim global atmospheric reanalysis (*Dee et al.*, 2011), and the *h*igh-order *s*patial *i*nterpolation at the *m*iddle *t*emporal level (HSIMT) advection scheme for tracers (*Wu and Zhu*, 2010). HSIMT is flux-based, 3rd-order accurate, mass-conservative, oscillation-free, and positive-definite with low dissipation and no overshooting. Boundary conditions for temperature, salinity, and transport are defined using *Urrego-Blanco and Sheng*'s (2012) regional physical ocean model of the NW North Atlantic (their model domain is shown as background in Figure 2.1), with open boundary transports augmented by barotropic tides from *Egbert and Erofeeva*. The model's temperature and salinity is nudged towards *Urrego-Blanco and Sheng*'s (2012) solution in a 10-grid-cell-wide buffer zone along the open boundaries. Nudging strength decays linearly away from the boundary to a value of zero at the 11th grid cell. Our model is able to resolve mesoscale features in the region and captures the reported coastal upwelling (see Appendix A for further details; *Petrie et al.*, 1987; *Shan et al.*, 2016). Our model simulation with dye tracers is initialized on January 1, 1999, from *Urrego-Blanco and Sheng*'s (2012) solution and run for 6 to 9 years.

### 2.4.4 Numerical dye and age tracer setup

Numerical dyes are used to mark the 8 chosen subregions (Figure 2.2). The offshore segment (Slp) is divided into two layers (200 m and above defined as Slp-S, and below 200 m defined as Slp-D), each with its associated dye. In each subregion, the initial dye concentration is set to 1 kg $m^{-3}$ and the initial age tracer is 0 kg s $m^{-3}$. Two types of numerical tracer experiments are performed. The first type, referred to as TRANS, qualitatively shows the circulation patterns and transit pathways, and is used for the quantification of residence times in selected subregions of the model domain. Here dyes are initialized only once at the beginning of the simulation, allowed to advect and diffuse throughout the domain, and their concentration decays within the source region over the 6-year simulation. The second type of experiment, referred to as AGE, is used to calculate dye mass fractions and ages, and is run for 9 years to ensure that a dynamic steady state is reached for the dye and age tracers. Here dyes are constantly forced to the initial value in their source regions, effectively re-initializing the dyes at every time step and forcing

their ages to zero at the source. Age only starts to increase when the dye leaves the source region, allowing the analysis of age at any point within the domain and the calculation of mean age in subregions that are fully contained within the model domain, i.e. the GoSL, SS, and GoM. As stated already in Section 2.4.1, age is undefined in areas where the released tracer has not yet reached (i.e. where C is equal to zero). When interpreting dye mass fractions, it is important to note that dye endmembers are strictly defined by their initial subregion. For example, GB-dyed water that enters the SS region will remain GB-originating water, no matter whether it first travelled into the GoSL or entered the SS directly.

## 2.5 Results

### 2.5.1 Dye tracer distributions

The distributions of the vertically averaged dye tracers at 6 months after initialization from the TRANS experiment (Figure 2.4) show intricate transport patterns on the shelf and indicate that cross-shelf exchange is inhibited in some regions. Notably, neither Slp-D nor Slp-S dye has moved onto the shelf within the first 6 months of the simulation, except for intrusions of Slp-D dye into the deep Laurentian and Northwest Channels. Significant cross-shelf exchange has occurred only at the northernmost region of the Labrador Shelf where a sizeable fraction of LS dye has moved onto the shelf. Another fraction of the LS dye has moved along the shelf break around the Grand Banks and along the edge of the Scotian Shelf, following the 200 m isobath, with a small branch moving into the Gulf of St. Lawrence at the mouth of the Laurentian Channel.

GB dye has moved into the Gulf of St. Lawrence and onto the Scotian Shelf, with larger concentrations on the outer shelf, but has not crossed the shelf break. GB dye has remained the longest in the Laurentian Channel and a portion of GB dye has remained highly localized on the southern tip of the Grand Banks, while the rest of the region is occupied by ENS dye. The distribution of GoSL dye within the Gulf of St. Lawrence also indicates some regions with relatively large retention times, e.g. shallow parts around Prince Edward Island and north of Anticosti Island. A portion of the GoSL dye has moved onto the Scotian Shelf. SS dye has moved quickly to the south, but very little has crossed the shelf break. On the Scotian Shelf, the coastal and shelf-break currents have caused the dye to move particularly fast near the coast and just inside of the shelf break, while dye

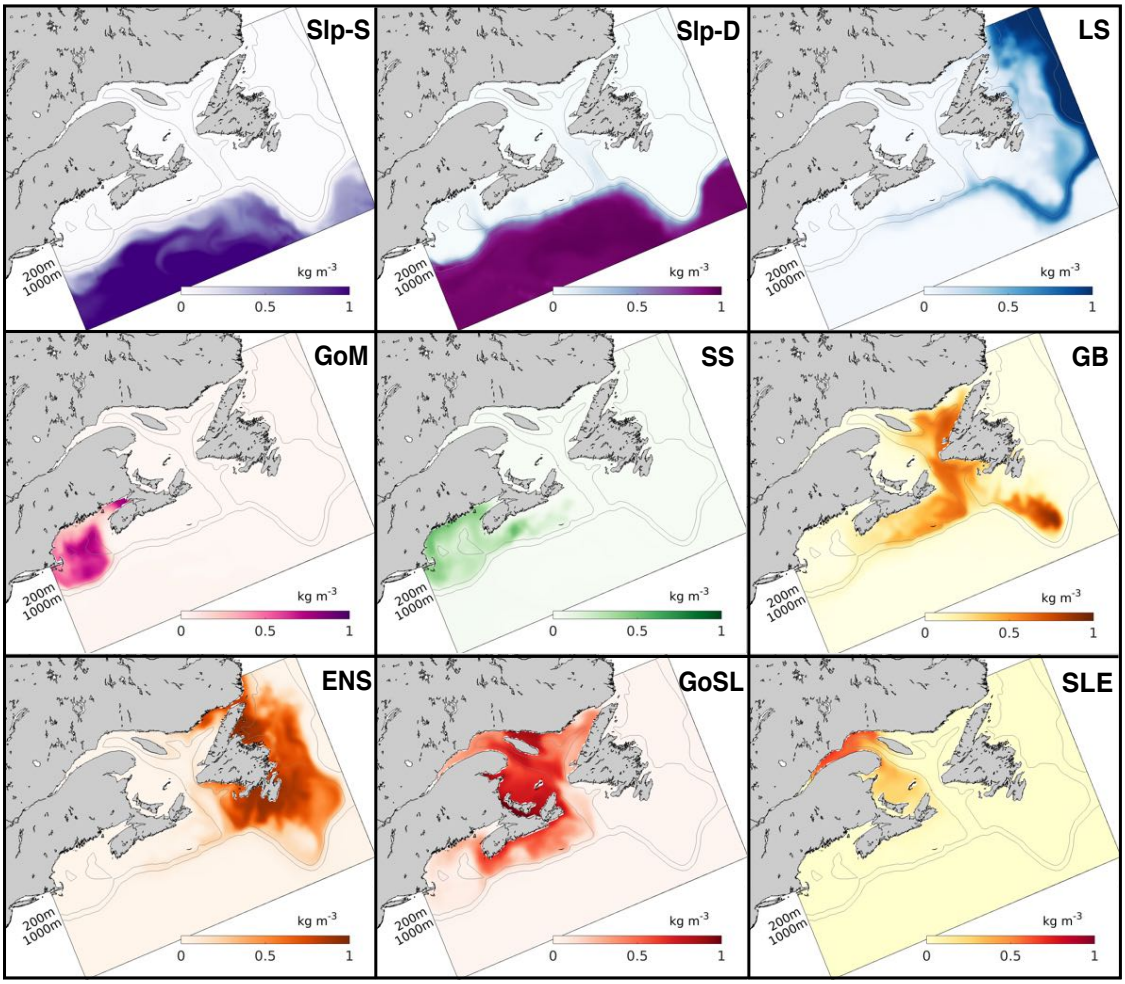


Figure 2.4: Maps of vertical mean dye concentration on June 16, 1999 (6 months into the TRANS simulation).

was retained slightly longer mid-shelf. GoM dye has slowly circulated in the Gulf before leaving the domain.

Transects of dye concentrations and currents along the Halifax Line (Figure 2.1) at the same time and from the same experiment (TRANS) are shown in Figure 2.5. These transects illustrate that the shelf-break current, visible by the LS dye, acts like a wall along the shelf break inhibiting cross-shelf exchange. Little Slp-D dye travels onto the shelf, and similarly little SS dye travels off the shelf.

### 2.5.2 Mean residence times

Time series of the dye mass leaving their source regions per unit time from the TRANS experiment were used to calculate mean residence times. Two examples, for the Scotian

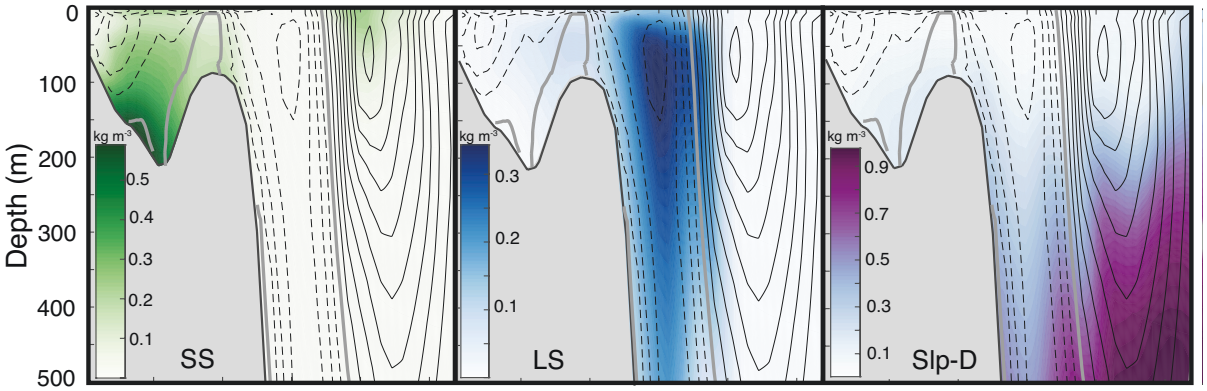


Figure 2.5: Dye concentration (colors) and 5-day average velocities (isolines) along the Halifax Line (HAL) transect on June 16, 1999 (6 months into TRANS simulation). Northward flow (into the page) is indicated by solid lines, zero flow by the thick grey line, and southward flow (out of the page) by dashed lines. Interval between isolines is 0.03 m $s^{-1}$.

Shelf and Gulf of St. Lawrence, are shown in Figure 2.6. In general, a large pulse of mass leaves each subregion initially, then the amount of mass leaving per unit time decays. SS dye leaves its source region much more rapidly than GoSL dye. The latter displays seasonality that is correlated with the discharge from the St. Lawrence River, when taking into account a lag of 8 months. River discharge peaks in late spring/early summer, with a second, smaller pulse in November. The rate of GoSL mass leaving the Gulf increases in late fall/early winter. The delay of 8 months from peak discharge to peak in mass export from the Gulf is consistent with previous estimates of transport time from the St. Lawrence River to the Scotian Shelf (*Sutcliffe et al.*, 1976; *Smith*, 1989; *Shan et al.*, 2016), which assumes that the dye is entrained in the river plume. This timing indicates that the seasonal increase in dye mass leaving the Gulf is enhanced by increased river discharge into the Gulf.

MRTs, calculated as the first moment of these histograms (see Equation 2.12), are 88.1 days for the GB calculated without the Laurentian Channel (126 days with Laurentian Channel), 367 days for the GoSL, 81.4 days for the SS, and 251 days for the GoM. The Scotian Shelf and Grand Banks have the shortest mean residence times, approximately one third of that of the Gulf of Maine and one quarter of that of the Gulf of St. Lawrence. As described in Section 2.5.1, the SS dye moves quickly to the south, hence mean residence time is short. Similarly, GB dye moves quickly to the south into the Gulf of St. Lawerence

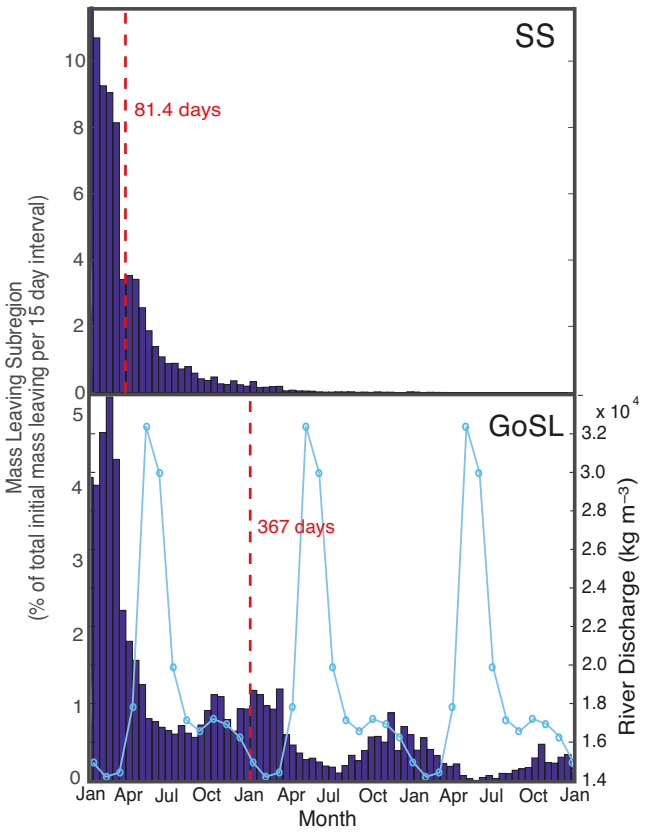


Figure 2.6: Histograms (lifetime distribution) of mass of the SS and GoSL dyes leaving their source regions over time. Mass is reported as a fraction of the initial mass present in each region. Mean residence times are reported in red, calculated as the weighted average of the mass leaving each subregion per unit time (Equation 2.12). St. Lawrence River discharge is indicated by the light blue curve in the bottom panel (see right y-axis).

and onto the Scotian Shelf, with some dye remaining on a localized patch on the southern tip of Grand Banks. There is a high concentration of GB dye in the Laurentian Channel (Figure 2.4) indicating a longer retention of GB dye here. The Gulf of Maine and Gulf of St. Lawrence are semi-enclosed basins and more retentive.

### 2.5.3 Mass fractions

The AGE simulation was used to calculate the mass fractions from different source regions for selected regions and locations (Figure 2.8, Table 2.1). Mass fractions were spun-up for 3 years until they reached a dynamic steady state (Figure 2.7). Mass fractions reported in Figure 2.8 and Table 2.1 were calculated as the average fractions after the 3-year spin-up.

Figure 2.8a shows the mass fraction of each dye contributing to the total dye mass in the Gulf of St. Lawrence, Scotian Shelf, and Gulf of Maine regions, not considering the

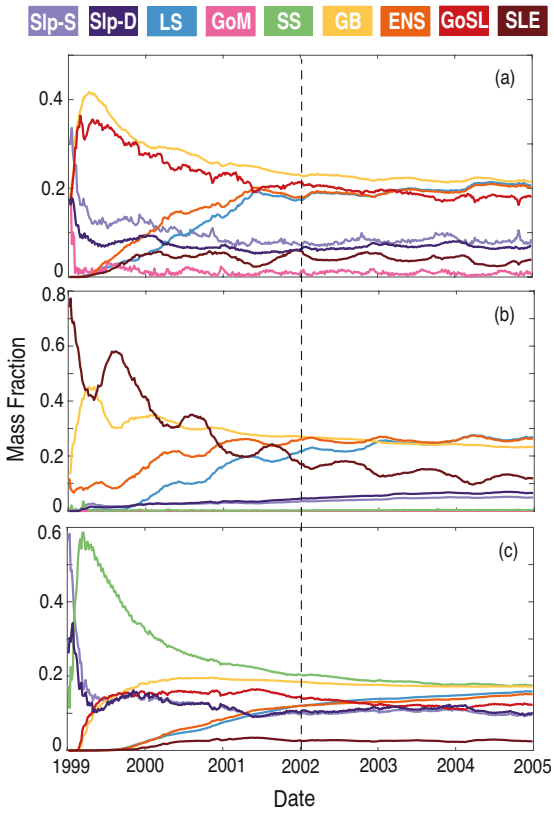


Figure 2.7: Mass fractions of each dye in (a) SS (b) GoSL (c) GoM. Mass fractions are spun-up for 3 years, as noted by the vertical dashed line. The average mass fractions are calculated after this spin-up period.

dye initialized in the analyzed region. The main contributions to Scotian Shelf waters are from the GoSL, GB, LS, and ENS regions. The main contributions to the Gulf of St. Lawrence are from the ENS, GB, and LS regions. The Gulf of Maine has nearly equal contributions from most dyes, except for the SLE dye which makes up only a quarter of the contribution (Table 2.1; SLE contributing 3% compared to 11-13%), and the SS and GB dyes contributing approximately 50% more than the other dyes (Table 2.1; SS and GB contributing 18-20% compared to 11-13%). The dye contributions at specific stations on the Scotian Shelf (Figure 2.8b) illustrate heterogeneity in source-water distributions. For example, the contributions of GoSL dye are high close to shore and minimal near the shelf break. The Nova Scotia Current carries GoSL water along the coast resulting in the high dye contributions at the nearshore stations.

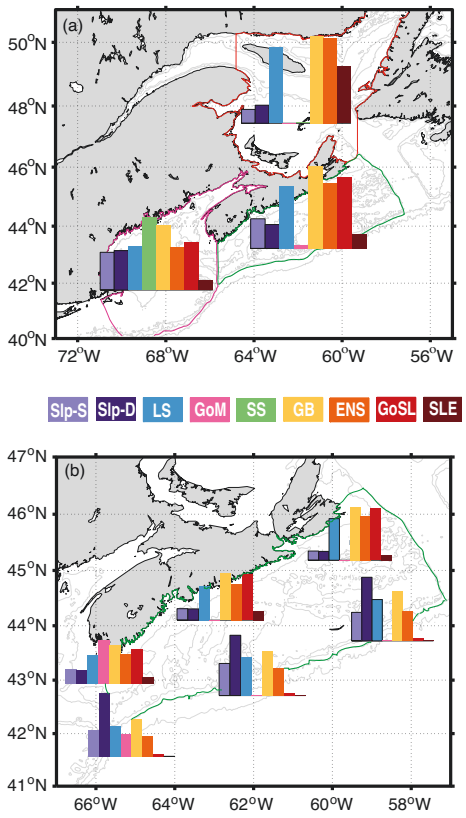


Figure 2.8: (a) Mass fractions of each dye in the three main regions of interest: GoSL (outlined in red), SS (outlined in green), and GoM (outlined in pink). (b) Mass fractions of each dye at six different stations on SS compared to the overall mass fractions of SS (see Table 2 for exact station locations).

### 2.5.4 Ages

Water ages from the different source regions were calculated, as described in Section 2.4.1, from the AGE experiment. They are shown as spatial distributions for three selected source regions in Figure 2.9 and reported as mean ages for the Scotian Shelf and Gulf of St. Lawrence in Table 2.1. Mean ages are spatially averaged over each subregion and time averaged over a dynamic steady state unique to each dye. See supplemental figures in Appendix A for time series of these mean ages illustrating the spin-up period required to reach a dynamic steady state. Mean ages reflect two important transport timescales: (1) the duration of transport from source region to the present location, and (2) the mean residence time within the present region. The latter is important when considering mean differences between regions; for example, longer residence times in the Gulf of St. Lawrence contribute to larger mean ages here as compared to the Scotian Shelf. The

former contributes to relative differences in ages within a region; for example, on the Scotian Shelf, longer transport times across the shelf contribute to larger LS ages nearshore compared to near the shelf break.

The surface age distributions (Figure 2.9) illustrate the length of transport from a source region to any given location in the model domain and reflect specific transport pathways in the region. GB has low ages on the Scotian Shelf (less than 300 days), indicating the quick transport over the Laurentian Channel to the Scotian Shelf, rather than first entering the Gulf of St. Lawrence. GB dye that first enters the Gulf of St. Lawrence before being transported along the Scotian Shelf via the NSC is found farthest inshore, illustrated by larger ages here. LS water has ages less than 200 days on the East Newfoundland Shelf and Grand Banks, demonstrating the quick transport onto the shelf here. Although LS ages along the shelf break are relatively small ($\sim$200 days), LS water ages are at least three times larger farther inshore on the Scotian Shelf (500-600 days). The large transport times onto the Scotian Shelf are not a result of slow transport south, indicated by small shelf break LS ages, but rather a result of LS dye first traveling into the Gulf of St. Lawrence before reaching the inner Scotian Shelf. Slp dye similarly moves easily onto Grand Banks, through the Laurentian Channel, and into Gulf of Maine, but it cannot quickly and directly flow onto the Scotian Shelf. The importance of these transport pathways is illustrated by comparing the dye mass contributions (Figure 2.8) to the mean ages. In each subregion, the waters with the lowest dye contributions tend to have the highest mean ages and vice versa. In the Gulf of St. Lawrence, the LS, GB and ENS dyes have the highest contributions and some of the lowest mean ages: 915, 639, and 766 days, respectively. On the Scotian Shelf, GB, and GoSL dyes have the highest contributions and the lowest ages of 206 and 112 days, respectively.

## 2.6 Discussion

### 2.6.1 Regional circulation features

The simulation of numerical tracers in our model illustrates its accurate representation of circulation features described in previous studies of the region. Circulation in the North Atlantic is dominated by the subpolar gyre, specifically the equatorward transport of the Labrador Current (*Loder et al.*, 1998; *Fratantoni and Pickart*, 2007). The Labrador Current originates as part of the East Greenland Current, flowing out of the Denmark Strait

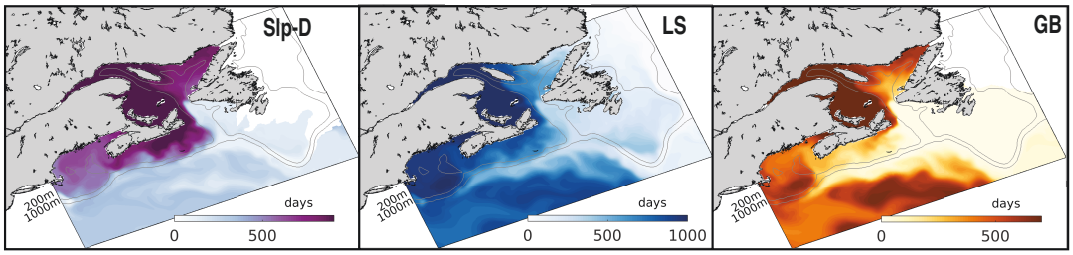


Figure 2.9: Surface age (days) as determined from the AGE experiment. Snapshot from last year of 6 year simulation (June 10, 2004). White areas are regions where dye concentrations $< 0.001$ kg m$^{-3}$.

Table 2.1: Dye mass fractions and mean age (days) of each of the dyes in the shelf regions.

| | | **Slp-S** | **Slp-D** | **LS** | **GoM** | **SS** | **GB** | **ENS** | **GoSL** | **SLE** |
|---|---|---|---|---|---|---|---|---|---|---|
| MASS FRACTION | GoSL | 0.041 | 0.054 | 0.224 | 0.000 | 0.003 | 0.258 | 0.252 | – | 0.168 |
| | SS | 0.084 | 0.067 | 0.177 | 0.009 | – | 0.234 | 0.185 | 0.202 | 0.042 |
| | STN 1 | 0.043 | 0.041 | 0.195 | 0.000 | – | 0.250 | 0.206 | 0.241 | 0.024 |
| | STN 2 | 0.132 | 0.296 | 0.192 | 0.000 | – | 0.229 | 0.139 | 0.012 | 0.000 |
| | STN 3 | 0.058 | 0.058 | 0.175 | 0.000 | – | 0.240 | 0.187 | 0.236 | 0.046 |
| | STN 4 | 0.156 | 0.293 | 0.186 | 0.002 | – | 0.216 | 0.135 | 0.012 | 0.000 |
| | STN 5 | 0.070 | 0.062 | 0.136 | 0.208 | – | 0.187 | 0.142 | 0.164 | 0.031 |
| | STN 6 | 0.129 | 0.320 | 0.150 | 0.110 | – | 0.180 | 0.100 | 0.010 | 0.001 |
| | GoM | 0.106 | 0.110 | 0.122 | – | 0.202 | 0.180 | 0.120 | 0.134 | 0.026 |
| MEAN AGE | GoSL (days) | 1010 | 1030 | 915 | 1750 | 1170 | 639 | 766 | – | 346 |
| | *Standard Deviation* | 67.6 | 67.4 | 62.9 | 57.4 | 82.5 | 47.3 | 56.5 | – | 15.2 |
| | SS (days) | 496 | 648 | 728 | 1140 | – | 206 | 587 | 112 | 324 |
| | *Standard Deviation* | 50.3 | 54.4 | 46.2 | 106 | – | 37.3 | 48.1 | 16.3 | 19.6 |

southward (*Fratantoni and Pickart*, 2007). The movement of LS dye equatorward in our model simulation, notably following the shelf break of the Scotian Shelf, represents the dominant movement of Arctic-origin waters southwestward.

The Labrador Current, reinforced by a branch of Cabot Strait outflow, makes up the shelf-break current (*Beardsley and Boicourt*, 1981; *Loder et al.*, 1998), which agrees with our findings that LS water, combined with GB and GoSL outflow through the Cabot Strait, is a dominant component of the shelf-break current. Previous studies found that Labrador Sea water only penetrates the Gulf of St. Lawrence through the Strait of Belle Isle and through the northeastern part of the Cabot Strait (*Galbraith et al.*, 2013). Our study finds

similar results, with limited penetration of the LS dye into the Gulf of St. Lawrence, except through the Laurentian Channel and Strait of Belle Isle. Similarly, it is thought that limited Labrador Sea water penetrates the Scotian Shelf through canyons and gullies along the shelf break (*Han*, 2003), consistent with the vertical mean dye concentration maps (Figure 2.4). Studies also found that upper slope flow occurs between the 200 m and 500 m isobaths, consistent with downstream remnants of the shelf-edge Labrador Current (*Han et al.*, 1997; *Loder et al.*, 1998, 2003; *Fratantoni and Pickart*, 2007). LS water in our model similarly follows the 200 m isobath along the slope. *Loder et al.* (2003) and *Hannah et al.* (1996, 2001) report that density fields suggest that there is limited movement of subpolar water southward past the western edge of the Scotian Shelf, which agrees with our results. LS water is young along the shelf break (less than 200 days) but becomes much older once in the Gulf of Maine (over 1000 days). The long transit time of LS dye into the Gulf of Maine suggests that this is not a dominant pathway in the system.

On the Scotian Shelf, past studies have revealed that the dominant circulation pattern is the southwestward flow with seasonal variability in both the Nova Scotia Current (directly along the coast) and the shelf-break current (farther offshore) (e.g. *Drinkwater et al.*, 1979; *Han et al.*, 1997). We note the same dominant circulation structure in our model. GoSL dyes flow through the Cabot Strait onto the Scotian Shelf and, combined with GB and LS dyes as an extension of the Labrador Current, form the noted nearshore and shelf break southwestward flow. The Slp dyes flow northeastward further offshore.

### 2.6.2 Mean residence times

The mean residence times in the region are: 88.1 days on the Grand Banks, 367 days in the Gulf of St. Lawrence, 81.4 days on the Scotian Shelf, and 251 days in the Gulf of Maine. High transport directly along the shelf, with inner-shelf and shelf-break branches (*Han et al.*, 1997), carries SS dye quickly to the southwest into the Gulf of Maine rather than crossing the shelf break. Quantitatively, this quick transport is reflected by relatively short mean residence times on the Scotian Shelf (81.4 days).

Few studies have looked at quantifying retention times on the Scotian Shelf and surrounding regions. *Rogers* (2015) did, however, look at the retention of particles in shelf basins. *Rogers*' numerical modeling study of the region used particle tracking to calculate the retention of particles in two basins on the shelf: the Lahave and Emerald Basins. Max retention times were calculated as 166 days in the Lahave Basin and 111 days in Emerald

Basin in summer at 200 m release depth. These results, although calculated over different scales and regions of the Scotian Shelf, are similar in magnitude to the mean residence times calculated in our model.

In a larger scale study, *Bourgeois et al.* (2016) divided the global continental shelves into 43 segments and calculated the residence time in each segment of a global model with an average model resolution of 38 km in our region (ranging from 31 to 45 km). Their Florida Upwelling segment contains the Scotian Shelf, Gulf of Maine, and most of the eastern United States shelves. Their Sea of Labrador segment includes the Labrador Sea, East Newfoundland Shelf, Grand Banks, and Gulf of St. Lawrence. *Bourgeois et al.* (2016) reported residence times of $12 \pm 0.6$ and $36 \pm 11$ days for the Florida Upwelling and Sea of Labrador segments, respectively. These residence times are much shorter than the estimates from our model simulations, likely as a result of the coarser resolution ($\sim$38 km vs. $\sim$10 km in ours) missing important circulation features like the shelf-break current. Differences in approaches to calculating residence time may also contribute. *Bourgeois et al.*'s (2016) residence times are also shorter for other regions when compared to previous studies including the North Sea (*Jickells*, 1998; *Delhez et al.*, 2004), Baltic Sea (*Jickells*, 1998), South Atlantic Bight (*Jickells*, 1998), and the Yellow and East China Seas (*Men and Liu*, 2014).

*Sharples et al.* (2017) calculated residence times for $5\times5^o$ coastal ocean grid cells around the globe, based on a sequence of theoretical arguments and empirical relationships about ocean-shelf exchange processes. While their analysis does not use subregions as defined in our study, we can make rough comparisons between our model mean residence times and theirs. For the North Atlantic, *Sharples et al.* (2017) calculated a mean residence time of 14 days for Grand Banks (95% confidence interval (CI): 9-26 days), 105 days for the Gulf of St. Lawrence (95% CI: 62-199 days), 126 days for the Scotian Shelf (95% CI: 74-235 days), and 217 days in the Gulf of Maine (95% CI: 115-509 days). Their estimates for the Scotian Shelf and Gulf of Maine are similar to those calculated here, but are much smaller for the Gulf of St. Lawrence and Grand Banks (approximately a third and a sixth, respectively) than ours. *Sharples et al.*'s (2017) calculation focuses on river plume export across the shelf break without the use of numerical models. They divide global continental shelves based on the ratio of the plume width to the shelf width, $S_p$, which determines the assumptions needed to calculate residence time. Since the Scotian

Shelf has an $S_p < 1$, it is assumed that the salinity plume is confined to the shelf and that exchange with the open ocean is controlled by exchange across the shelf break. It is then assumed that residence time is controlled by Ekman cross-shelf break transport and a lumped transport representing the mean non-wind driven export that can affect residence times on such shelves. Their calculation is therefore very different than the one performed in the present study, resulting in discrepencies in reported residence times.

### 2.6.3 Transport times

Since the St. Lawrence River and the Gulf of St. Lawrence have a strong influence on the hydrography of the Scotian Shelf, previous studies have estimated the time for St. Lawrence River discharge to reach Halifax and Cape Sable. *Shan et al.* (2016) calculated the lag between the discharge peak from the St. Lawrence River and the low-salinity signal at Halifax and Cape Sable in their model simulations. They found that water exiting the St. Lawrence River took 7 months to travel from Quebec City to Halifax and 8 months to travel to Cape Sable. *Sutcliffe et al.* (1976) compared the temperature and salinity of the St. Lawrence River to different stations along the Scotian Shelf to determine the time for river discharge to reach these locations. They found, similar to *Shan et al.* (2016), that St. Lawrence River discharge reaches Halifax in approximately 6 months. *Smith* (1989) similarly compared the seasonal cycle of current velocity, surface salinity and temperature at different locations and found that St. Lawrence River discharge reached Cape Sable in 8 to 9 months.

In our study, we can compare the age of SLE dye on the Scotian Shelf to these transit estimates, as the age of SLE dye estimates the time for water leaving the estuary to reach specific points on the shelf. We calculated that SLE dye has an average age of 324 days (10.5 months) on the Scotian Shelf, which is longer than in these past studies. Looking at specific locations (Halifax and Cape Sable), the age of SLE dye near Halifax is approximately 9 months (seasonally varies from 6.5 - 12.5 months) and 11.5 months (seasonally varies from 8 - 15 months) near Cape Sable. These estimates are larger than those previously reported but with a similar delay in St. Lawrence River water delivery between Halifax and Cape Sable. For a more direct comparison, we calculated the lag between the St. Lawrence River discharge peak and low-salinity signals at Halifax and Cape Sable in our model simulation, as in *Shan et al.* (2016). The lag at each of these locations, respectively, was on average 4.8 and 5.5 months, with some interannual

variability in lag times. Our calculated lags are smaller than the age estimates but close in magnitude to those from *Sutcliffe et al.* (1976), *Smith* (1989), and *Shan et al.* (2016). The differences between our age calculation and calculating the lag between peak river discharge and low-salinity signal stems from the fact that the age is a time-integrated measure rather than a propagation of the maximum signal. At certain times of the year, the age of St. Lawrence Estuary water at Halifax, for instance, can reach as low as 6.5 months, which is comparable to previous studies. In other words, it takes longer for river water to reach each of the stations when not during peak river discharge and the age calculation reflects averaging over these times.

### 2.6.4 Transport mechanisms

Previous studies have reported that nutrient-rich slope water flows onshore via major cross-shelf channels, such as through the Laurentian Channel, Scotian Gulf and Northeast Channel (*Smith et al.*, 2001). Our study illustrates that the shelf-break current, marked by the LS dye, creates a barrier along the Scotian Shelf that prevents deep slope water from reaching the shelf and similarly prevents surface SS water from being exported to the adjacent open ocean. Small amounts of water marked by LS dye enter the Scotian Shelf through cross-shelf channels, and onshore transport of water marked by Slp dye occurs through the Laurentian Channel and Northeast Channel. However, there is almost no direct onshore transport of Slp-dyed water onto the Scotian Shelf. Slp-dyed water has low ages (Figure 2.9) and significant mass fractions (Figure 2.8, Table 2.1) only near the shelf break; past the mid-shelf ages are much larger and mass fractions lower. We do not find evidence in support for significant upwelling of nutrient-rich slope water onto the Scotian Shelf as suggested by *Shadwick et al.* (2010) and *Burt et al.* (2013).

In our simulation, waters marked by GB and GoSL dyes have the highest mass fractions on the Scotian Shelf overall, as indicated by large mass fractions (Figure 2.8, Table 2.1) and associated low ages (Figure 2.9), and are therefore important source waters for setting the properties on the Scotian Shelf. Although the mean residence time in the Gulf of St. Lawrence is large (367 days), once this water exits the Gulf, it moves quickly along the Scotian Shelf. Similarly, water marked by GB dye moves quickly across the Laurentian Channel onto and along the Scotian Shelf. These pathways have been noted in previous studies. *Han* (2003) has shown that Gulf of St. Lawrence water moves through the Cabot Strait along the eastern edge of the Scotian Shelf, while flow from the Newfoundland Shelf

directly contributes to Scotian Shelf circulation through crossovers across the Laurentian Channel and along the shelf edge.

### 2.6.5 Impacts on regional zooplankton distributions

The importance of the NSC, previously estimated to account for 75% of the net annual transport along the shelf (*Drinkwater et al.*, 1979), for setting biological properties on the Scotian Shelf has been investigated in previous studies. For example, *Tremblay and Roff* (1983), *Sameoto and Herman* (1990), *Herman et al.* (1991), and *Sameoto and Herman* (1992) have evaluated the effects of the NSC on the local copepod community. There are three main species of copepods on the Shelf: *Calanus finmarchicus*, *Calanus glacialis*, and *Calanus hyperboreus*. The former dominates the southwestern half of the shelf, whereas the latter two species are dominant on the northeastern half. *C. glacialis* and *C. hyperboreus* are northern species with breeding populations in the cold water of the Gulf of St. Lawrence and Labrador Current, carried to the Scotian Shelf via the NSC and shelf-break current (*Fleminger and Hulsemann*, 1977; *Tremblay and Roff*, 1983; *Conover*, 1988). The outflow from the Gulf of St. Lawrence affects the entire northeast portion of the Scotian Shelf (*Trites and Walton*, 1975; *Bugden et al.*, 1982), acting as a dominant control on the copepod population here (*Sameoto and Herman*, 1992). *Calanus* species also overwinter in basins deeper than 200 m along the Scotian Shelf (*Sameoto and Herman*, 1990; *Herman et al.*, 1991) and there is a small contribution from slope waters to shelf *C. finamrchicus*, and *C. hyperboreus* populations (*Lewis and Sameoto*, 1988). By calculating the time for water to travel from the Gulf of St. Lawrence to the Scotian Shelf, one can estimate the maturity stage of copepods along the shelf, assuming breeding in the Gulf. It is expected that with a 3-month transit time from the Gulf to Halifax copepods will have matured to stage C4 and migrate downwards to the deep basins in the NE shelf (*Sameoto and Herman*, 1992). It is unlikely that *C. glacialis* and *C. hyperboreus* could exist on the shelf for long without the infusion from the Gulf; *C. finmarchicus* overwinter and are therefore less reliant on the Gulf of St. Lawrence (*Sameoto and Herman*, 1992). The transport pathways in this region, mainly the transport of GoSL and GB waters onto the Scotian Shelf to form the NSC and shelf-break current, are therefore very important controls on setting species populations here.

## 2.7 Conclusion

In our model simulations, dye tracer distributions and transit timescales are in good agreement with previous modeling and observational studies. Water marked by LS dye flows along the 200 m isobath, forming the shelf-break current which limits the lateral transport of water on- and off-shelf. Waters marked by LS and Slp flow relatively unimpeded onto the Newfoundland Shelf and Grand Banks, and through the Laurentian and the Northeastern Channels, but do not flow onto the Scotian Shelf. Water marked by LS and Slp dye that is present on the Scotian Shelf has first travelled into the Gulf of St. Lawrence. There is retention on the tip of the Grand Banks associated with the Labrador Current bifurcating around shallow bathymetry. This retention contributes to a larger mean residence time, compared to the Scotian Shelf. Waters marked by GB and GoSL dyes have the highest contributions on the Scotian Shelf (24% and 20% contributions, respectively) and some of the lowest ages (202 and 113 days, respectively). Some of the largest ages on the Scotian Shelf are from waters that must first travel into the Gulf of St. Lawrence before flowing onto the Scotian Shelf. These results reflect the fact that the main pathway onto the Scotian Shelf is first through the Laurentian Channel into the Gulf of St. Lawrence, and then out onto the shelf via the Cabot Strait. In the case of water marked by GB dye, transport occurs directly over the Laurentian Channel.

Our results highlight how useful regional models are in capturing fine-scale details of circulation and quantifying accurate transport times and pathways. Previous estimates of residence time for the NW North Atlantic shelves from a global model are too short, likely because the resolution is too coarse to capture the details of this dynamic system. The mean residence times and transport analyses calculated in this study provide useful information for understanding biological processes, such as the shelf-wide copepod community structure, and biogeochemical processes, such as carbon fluxes.

# CHAPTER 3

# A MODELING STUDY OF TEMPORAL AND SPATIAL $pCO_2$ VARIABILITY ON THE BIOLOGICALLY ACTIVE AND TEMPERATURE DOMINATED SCOTIAN SHELF [1]

## 3.1 Abstract

Continental shelves are thought to be affected disproportionately by climate change and are a large contributor to global air-sea carbon dioxide ($CO_2$) fluxes. It is often reported that low-latitude shelves tend to act as net sources of $CO_2$ whereas mid- and high-latitude shelves act as net sinks. Here, we combine a high-resolution regional model with surface water time series and repeat transect observations from the Scotian Shelf, a mid-latitude region in the northwest North Atlantic, to determine what processes are driving the temporal and spatial variability of partial pressure of $CO_2$ ($pCO_2$) on a seasonal scale. In contrast to the global trend, the Scotian Shelf acts as a net source. Surface $pCO_2$ undergoes a strong seasonal cycle with an amplitude of $\sim$200-250 $\mu$atm. These changes are associated with both a strong biological drawdown of Dissolved Inorganic Carbon

[1] Rutherford, K., K. Fennel, D. Atamanchuk, D. Wallace, and H. Thomas, A modeling study of temporal and spatial $pCO_2$ variability on the biologically active and temperature- dominated Scotian Shelf, Biogeosciences, 18(23), 6271-6286, 2021.
Author contribution: KR and KF conceived the research questions of this study. KR carried out the model simulations and analyses. DA, DW and HT implemented observational platforms and contributed the subsequent datasets. KR and KF discussed the results and wrote the manuscript, with inputs from DA, DW and HT.

(DIC) in spring (corresponding to a decrease in $pCO_2$ of 100-200 $\mu$atm), and pronounced effects of temperature, which ranges from $0^oC$ in the winter to near $20^oC$ in the summer, resulting in an increase in $pCO_2$ of $\sim$200-250 $\mu$atm. Throughout the summer, events with low surface water $pCO_2$ occur associated with coastal upwelling. This effect of upwelling on $pCO_2$ is also in contrast to the general assumption that upwelling increases surface $pCO_2$ by delivering DIC-enriched water to the surface. Aside from these localized events, $pCO_2$ is relatively uniform across the shelf. Our model agrees with regional observations, reproduces seasonal patterns of $pCO_2$, and simulates annual outgassing of $CO_2$ from the ocean of $+1.7 \pm 0.2$ mol C $m^{-2}$ $yr^{-1}$ for the Scotian Shelf, net uptake of $CO_2$ by the ocean of $-0.5 \pm 0.2$ mol C $m^{-2}$ $yr^{-1}$ for the Gulf of Maine, and uptake by the ocean of $-1.3 \pm 0.3$ mol C $m^{-2}$ $yr^{-1}$ for the Grand Banks.

## 3.2 Introduction

The global ocean acts as a major sink of $CO_2$ from the atmosphere (e.g., *Le Quéré et al.*, 2018; *Gruber et al.*, 2019; *Landschützer et al.*, 2014; *Rödenbeck et al.*, 2015), but it has been suggested that flux density (or flux per unit area) on continental shelves is larger than in the open ocean (*Chen et al.*, 2013; *Laruelle et al.*, 2014). Therefore, compared to their size, continental shelves are thought to disproportionately contribute to global air-sea $CO_2$ fluxes (*Laruelle et al.*, 2010). Additionally, they are susceptible to climate change on much shorter timescales than the open ocean (*Cai et al.*, 2010) and are experiencing increasing impacts of human activity (*Cai*, 2011; *Doney*, 2010; *Gruber*, 2015). Given their high susceptibility to negative impacts from climate change, and their potentially significant contribution to global air-sea $CO_2$ fluxes, it is important to understand the drivers underlying inorganic carbon dynamics on continental shelves.

It is generally thought that continental shelves at mid- to high-latitudes act as net sinks of atmospheric $CO_2$ while those at low latitudes act as net sources (e.g. *Chen and Borges*, 2009; *Cai et al.*, 2006; *Laruelle et al.*, 2014; *Roobaert et al.*, 2019). There are, however, notable deviations from this global-scale pattern. The Scotian Shelf, a mid-latitude shelf off the coast of eastern Canada, is one example with large discrepancies between independent estimates of air-sea $CO_2$ flux (*Fennel et al.*, 2019). Direct measurements made using a moored CARIOCA buoy on the Scotian Shelf indicate that the shelf acts as a net source of $CO_2$ to the atmosphere (*Shadwick et al.*, 2010, 2011; *Shadwick and Thomas*, 2014). These

findings are in contrast to other studies using observations from the SOCAT database, indicating that the Scotian Shelf follows the global trend and acts as a net sink of $CO_2$ (*Laruelle et al.*, 2014, 2015; *Signorini et al.*, 2013). These contrasting results for the Scotian Shelf emphasize the large uncertainty inherent in shelf-wide $CO_2$ flux estimates.

Continental shelves are highly complex and dynamic regions where many biological and physical processes modulate $CO_2$ flux (*Laruelle et al.*, 2014, 2017; *Roobaert et al.*, 2019). The partial pressure of $CO_2$ ($pCO_2$) in the ocean is one of the key factors which determines the air-sea $CO_2$ flux. Recent global studies found that thermal controls dominate the seasonality of $pCO_2$ but that these alone cannot describe observed $pCO_2$ variations, particularly in temperate and high latitudes (*Roobaert et al.*, 2019). High rates of primary production on continental shelves (*Chen and Borges*, 2009) are another important driver of seasonal changes in $pCO_2$.

Continental margins are also subject to intense horizontal transport processes, which act as additional drivers of $CO_2$ fluxes. For example, the Continental Shelf Pump, a term first coined by *Tsunogai et al.* (1999) in relation to the East China Sea, describes the movement of shelf water high in dissolved inorganic carbon (DIC) across the shelf break to the subsurface open ocean leading to an influx of atmospheric $CO_2$. This mechanism is thought to mainly occur at mid- to high-latitude shelves since it relies on winter cooling to create dense shelf water that is transported to the open ocean's subsurface layers. Upwelling is another well-studied transport mechanism driving shelf-wide $CO_2$ dynamics. The California Current system is a typical example of an upwelling system (*Chavez et al.*, 2017; *Hickey*, 1998; *Fennel et al.*, 2019; *Feely et al.*, 2008). Here, winds drive coastal upwelling, which brings DIC-rich water to the surface along the continental shelf and creates favourable conditions for $CO_2$ outgassing to the atmosphere.

Altogether, these complex shelf dynamics lead to large spatial and temporal variability of $pCO_2$ (*Previdi et al.*, 2009). Such large variability combined with limited data availability for many continental shelves make it difficult to accurately constrain $CO_2$ fluxes. Limited data availability in space and time, often with seasonal biases, is a prime source of uncertainty in flux estimates that can only be overcome with more uniformly distributed sampling. To fully capture how ocean margins are reacting to perturbations caused by the steady input of anthropogenic $CO_2$ to the atmosphere, it is important to understand the processes underlying both spatial and temporal evolution of shelf-wide $pCO_2$.

Numerical models can be useful when investigating such complex interactions and constraining $CO_2$ flux since they can interpret sparse measurements through the mechanistic representations of relevant processes. In the present study, we employ a high-resolution biogeochemical model of the northwest North Atlantic to examine the magnitude, variability, and sign of the air-sea $CO_2$ flux on the Scotian Shelf. Previous studies have evaluated our model's ability to represent the physical (*Brennan et al.*, 2016; *Rutherford and Fennel*, 2018) and biological (*Laurent et al.*, 2021) dynamics of the region. Here, we focus solely on the model representation of inorganic carbon dynamics, especially the spatial and temporal variability of $pCO_2$ on a seasonal scale on the Scotian Shelf in light of new, high-resolution, shelf-wide observations.

Our overall goal is to show how both biological and transport processes work together seasonally on the Scotian Shelf to set shelf-wide surface $pCO_2$. We additionally discuss event-based variability of the air-sea $CO_2$ flux, and, especially, how short-term, upwelling-favourable wind events throughout the summer create spatial variability of $CO_2$ on the Scotian Shelf. To accomplish these goals, our paper: (1) discusses the seasonal cycle of $pCO_2$ across the shelf; (2) investigates the spatial variability of $pCO_2$, particularly during the summer months, and (3) reports shelf-wide air-sea $CO_2$ flux estimates in comparison to previously reported estimates. We discuss the importance of our findings in terms of global patterns of air-sea $CO_2$ flux and carbon cycling.

## 3.3 Study region

The Scotian Shelf (Figure 3.1) is uniquely located at the junction of the subpolar and subtropical gyres (*Loder et al.*, 1997; *Hannah et al.*, 2001). Regional circulation is dominated by southward transport of the Labrador Current (*Loder et al.*, 1998; *Fratantoni and Pickart*, 2007). As a result, cool Arctic-derived water accumulates along the northwestern North Atlantic continental shelf separating fresh shelf waters from warmer and salty slope waters (*Beardsley and Boicourt*, 1981; *Loder et al.*, 1998; *Fratantoni and Pickart*, 2007).

The Scotian Shelf in particular is controlled by inshore and shelf-break branches of the southwestward moving current. The shelf-break branch inhibits the movement of water across the shelf break of the Scotian Shelf (*Rutherford and Fennel*, 2018). As a result, water moves predominantly along-shelf so that residence times in the region are relatively long, with water being retained on the Scotian Shelf for an average of 3 months before

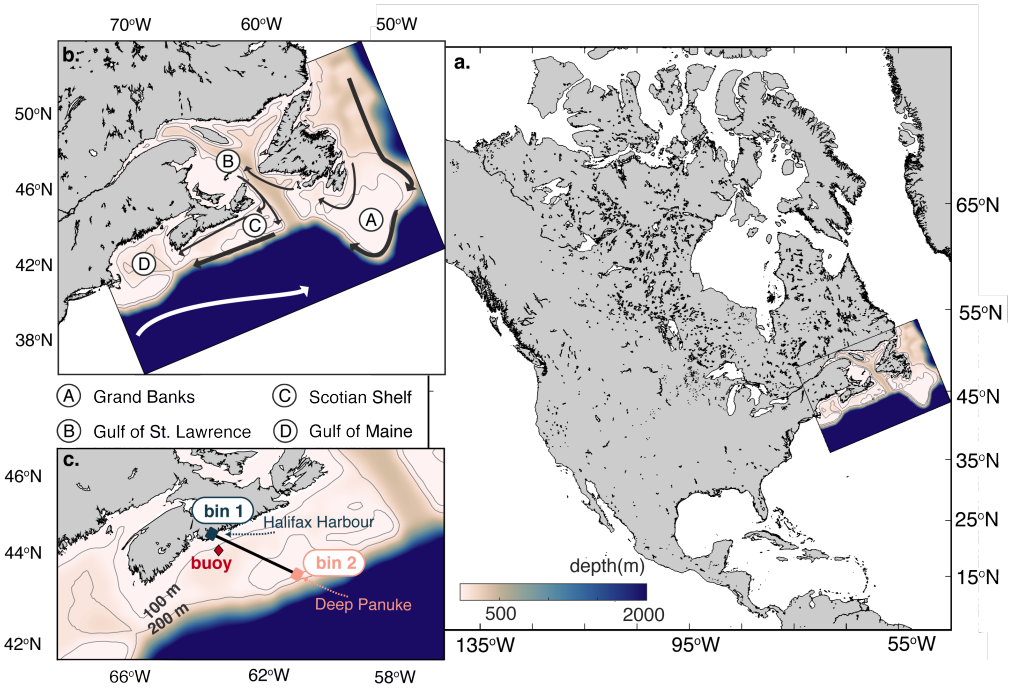


Figure 3.1: Bathymetric maps of the model domain. (a) Map of North America, including the location of the model domain. (b) A zoomed-in map of the model domain with mean current locations. (c) Zoomed-in map of the Scotian Shelf, and indicates the location of the CARIOCA buoy (red diamond) and the Atlantic Condor Transect (black line). Bin 1 (Halifax Harbour) and bin 2 (Deep Panuke) are used for analyses of spatial variability. All maps show the 100 m and 200 m isobaths.

moving further southwest on the shelf (*Rutherford and Fennel*, 2018). In terms of vertical structure, the Scotian Shelf shifts between a two-layer system in the winter, when a cold, fresh layer sits over a warm, salty deep layer, and a three-layer system in the spring and summer, when a warm surface layer forms in the top 20 m above the cold intermediate layer between 20–100 m, and the warm and salty deep layer (*Dever et al.*, 2016).

The Scotian Shelf is additionally characterized by a large, shelf-wide spring bloom initiated in late-March (*Ross et al.*, 2017; *Fournier et al.*, 1977; *Mills and Fournier*, 1979), when the mixed layer is still relatively deep and temperature is at its coldest (*Craig et al.*, 2015). The initiation of the spring bloom in late March has rapid and large impacts on the observed $pCO_2$ seasonality (*Shadwick et al.*, 2010, 2011).

## 3.4 Methods

### 3.4.1 Model setup and initialization

#### 3.4.1.1 Physical model setup

We employ a biogeochemical model, based on *Fennel et al.* (2006), *Fennel and Wilkin* (2009), and *Laurent et al.* (2021) that is part of the Regional Ocean Modelling System (ROMS, v.3.5; *Haidvogel et al.*, 2008). The physical model implementation, described in more detail in *Brennan et al.* (2016), has 30 vertical levels and approximately 10 km horizontal resolution (240x120 horizontal grid cells), uses the GLS vertical mixing scheme (*Umlauf and Burchard*, 2003; *Warner et al.*, 2005), atmospheric surface forcing from the European Centre for Medium-Range Weather Forecasts (ECMWF) global atmospheric reanalysis (*Dee et al.*, 2011), and the "high-order spatial interpolation at the middle temporal level" (HSIMT) advection scheme for tracers (*Wu and Zhu*, 2010). Physical initial and boundary conditions are defined using the regional physical ocean model of the northwest North Atlantic of *Urrego-Blanco and Sheng* (2012). Temperature and salinity are nudged towards the climatology of *Geshelin et al.* (1999) in a 10-grid-cell-wide buffer zone along open boundaries. Nudging strength decays linearly away from the boundaries to a value of zero in the 11th grid cell from the boundary. Tides are imposed from *Egbert and Erofeeva*. Climatological river discharge is imposed for 12 major rivers and uses observed long-term monthly means from Water Survey Canada. Full details on the physical model setup and its validation can be found in *Brennan et al.* (2016) and *Rutherford and Fennel* (2018). These studies have shown that our model simulates the vertical structure and seasonal cycling of temperature and salinity on the shelf well. The model captures mesoscale features and the coastal upwelling events, and simulates the volume transport throughout the region in agreement with observation-based estimates.

#### 3.4.1.2 Biogeochemical module

The biogeochemical model is based on the nitrogen-cycle model with inorganic carbon component of *Fennel et al.* (2006) and *Fennel and Wilkin* (2009) but was recently expanded to include 2 phytoplankton and 2 zooplankton functional groups (*Laurent et al.*, 2021). For a detailed description and validation of the biological model, we refer to *Laurent et al.* (2021), who compared the model output with glider transects of temperature, salinity, and chlorophyll and in situ measurements of chlorophyll and nitrate. The model was

evaluated on a seasonal scale for the entire model domain, mainly in the surface (top 100 m). *Laurent et al.* (2021) showed that the model outperforms global models for the region for all variables and that the timing of the spring bloom is well represented, but the model slightly underestimates the magnitude of the bloom and tends to overestimate nitrate throughout the year.

For calculating air-sea $CO_2$ flux, according to the carbonate chemistry model of *Zeebe and Wolf-Gladrow* (2001), we use dissociation constants (K1 and K2) from *Millero* (1995) using *Mehrbach et al.* (1973) data on the seawater scale which are deemed appropriate for the typical salinity ranges from 27 to 36.6 in the model domain (lower salinities are highly localized in the Gulf of St. Lawrence Estuary). Atmospheric $pCO_2$ is set to the seasonal cycle and secular trend derived from Sable Island monitoring data contributed by Environment Canada's Greenhouse Gas Measurement Program (*Environment and Climate Change Canada*, 2017). The long term linear trend in the atmospheric $pCO_2$ is $\sim$+2 $\mu$atm year$^{-1}$ (see Supplement for the full trend equation and figure). $CO_2$ solubility is calculated with the *Weiss* (1974) formulation. The gas transfer coefficient of *Ho et al.* (2006) is used and depends on wind speed at 10 m above the sea surface and the Schmidt number. Further details of the biogeochemical model, including the carbonate chemistry equations, can be found in *Laurent et al.* (2017, Supporting Information). Carbon initialization, boundary conditions, and climatological nudging are calculated from relationships with temperature and salinity determined from bottle data for the region. DIC is nudged in an 80-grid-cell-wide buffer zone along the eastern boundary, with nudging linearly decaying away from a nudging timescale of 60 days at the boundary to a value of 0 in the 81st grid cell. At all other boundaries, a 10-grid buffer zone is used, as with temperature and salinity. Use of a wider boundary nudging zone along the eastern boundary was found to be beneficial in imposing low-frequency variability from the Labrador Sea at the northeastern boundary. The nudging zones are not used in the analysis.

Nitrate concentrations in rivers are prescribed from Global NEWS model output *Seitzinger et al.* (2005). DIC and total alkalinity (TA) in rivers were calculated by fitting a linear relationship with salinity from Gulf of St. Lawrence bottle data and extrapolating to river water salinity. The model is initialized on January 1, 1999, from *Urrego-Blanco and Sheng*'s (2012) solution for temperature and salinity. Nitrate ($NO_3^-$) concentrations are initialized

from the regional climatologies as in *Laurent et al.* (2021). DIC and TA initial and boundary conditions were created from observationally based relationships with temperature (T) and salinity (S) using bottle data from regional cruises from 1997-2011 encompassing as far south as the Gulf of Maine and as far north as the Labrador Sea (observations from DFO's AZMP program, see: dfo-mpo.gc.ca/science/data-donnees/azmp-pmza/index-eng.html#publications). Initialization relationships used only observations from December, January, and February (TA = 43S + 800, $r^2$ = 0.96; DIC = 1153 – 21.6T + 29.1S – 0.41$T^2$ + 0.63ST, $r^2$ = 0.90). Boundary conditions used observations that encompassed the entire year (TA = 41S + 875, $r^2$ = 0.92; DIC =912.6 – 2.5T + 35.7S – 0.45$T^2$ + 0.12ST, $r^2$ = 0.80). The model is run for 16 years (1999-2014) with daily output. The present study analyses the model output from 2006-2014, with focus on year 2006. See the Supplement for a comparison of surface $p$CO$_2$ throughout the simulation and a brief validation of TA and DIC.

#### 3.4.1.3 Taylor decomposition of upwelling events

To better understand the effects of coastal upwelling on surface $p$CO$_2$, we perform a Taylor Decomposition on the model output during one of the upwelling events focused on in this study, following a similar methodology to *Rheuban et al.* (2019), and *Hauri et al.* (2020). Here, we investigate the influence of T, S, DIC, and TA on $p$CO$_2$ following the equation

$$pCO_2 = f(T, S, DIC, TA) \tag{3.1}$$

where $f$ indicates the CO2SYS set of equations. We calculated anomalies, $\Delta$ $p$CO$_2$, from a reference value, $p$CO$_{2,0}$:

$$\Delta pCO_2 = pCO_2 - pCO_{2,0} \tag{3.2}$$

The reference values for each variable were calculated as the average of that variable along the Condor transect (see Figure 3.1) in the upper 40 m (i.e., the part of the water column affected by the upwelling event). We decomposed $\Delta$ $p$CO$_2$ relatively simply into

perturbations related to T, S, DIC, and TA calculated as follows:

$$\Delta pCO_{2,T} = f(T, S_0, DIC_0, TA_0) - pCO_{2,0} \tag{3.3}$$

$$\Delta pCO_{2,S} = f(T_0, S, DIC_0, TA_0) - pCO_{2,0} \tag{3.4}$$

$$\Delta pCO_{2,DIC} = f(T_0, S_0, DIC, TA_0) - pCO_{2,0} \tag{3.5}$$

$$\Delta pCO_{2,TA} = f(T_0, S_0, DIC_0, TA) - pCO_{2,0} \tag{3.6}$$

We refer the reader to *Rheuban et al.* (2019) for a more detailed description of the Taylor Decomposition methodology.

### 3.4.2 Observational datasets

The moored CARIOCA buoy was located at Station 2 on the Halifax Line. Station 2 (HL2; 44.3$^o$N, 63.3$^o$W) is located about 30 km offshore from Halifax, Nova Scotia, and occupied monthly by Bedford Institute of Oceanography. The buoy measured surface water (at approximately 1 m depth) temperature, conductivity, $p$CO$_2$, salinity, and Chl-a fluorescence every hour and was deployed from 2007 to 2014 with several gaps in data due to calibration and maintenance (see Table S1 in Supplement). $p$CO$_2$ was estimated using an automated spectrophotometric technique (*Lemay et al.*, 2018). The raw $p$CO$_2$ data contained high-amplitude spikes, with increases from 400 $\mu$atm to over 1000 $\mu$atm within a few hours, which were measuring artifacts and did not represent $p$CO$_2$ of surrounding water. These spikes were removed by binning all years of the $p$CO$_2$ observations into a 365-day of year (DOY) seasonal cycle. Any points that were outside 1.5 standard deviations of the 1-month moving average $p$CO$_2$ were discarded. This method removed only the extreme values and maintained much of the observed variability (see Figure 3.2).

The sensor-based underway system, Dal-SOOP (*Arruda et al.*, 2020), was installed on the multipurpose platform supply vessel Atlantic Condor (operated by Atlantic Towing Ltd.) and has been measuring a suite of biogeochemical parameters, including $p$CO$_2$, in the surface water since May 2017. The ship transits weekly to biweekly between the Halifax Harbour (Bin 1) and the Deep Panuke gas platform off Sable Island (Bin 2) on the Scotian Shelf (Figure 3.1). The Atlantic Condor $p$CO$_2$ data underwent standard QA/QC procedures, which included pre-, post-deployment and regular zero-calibration of the $p$CO$_2$ sensor (Pro-Oceanus Inc, Canada) and associated data corrections. The QC'd data has been deposited into the Surface Ocean CO$_2$ Atlas (SOCAT v.2020), where it was attributed

an accuracy of $\pm$ 10 $\mu$atm. Performance of the novel Dal-SOOP system was assessed during a 2-month transatlantic cruise in comparison with a conventional $pCO_2$ equilibrator and showed good agreement with the latter (i.e. 5.7 $\pm$ 4.0 $\mu$atm; *Arruda et al.*, 2020).

During the QC/QA procedure, some data collected in close proximity to Halifax, and corresponding to the outbound transects, were removed. Some of these data were biased high and attributed to prolonged ship layover in port allowing for a build-up of high $pCO_2$ within the Dal-SOOP system due to respiration. The active pumping that delivers fresh seawater to the measurement system is triggered by a GPS signal when the ship leaves the harbour; as a result, there can be a delayed response from the $pCO_2$ sensor to the much lower $pCO_2$ signals observed immediately outside the harbour. To account for the bias, values that were 2 standard deviations from the mean $pCO_2$ value for the latitudinal bin closest to the Halifax Harbour were removed for some transects. Only three transects were removed.

The CARIOCA and Atlantic Condor transect observations were mapped onto year 2006 for comparison directly with this year in the model using the linear trend in atmospheric $pCO_2$ (+ 2 $\mu$atm year$^{-1}$). Where numbers are reported comparing the model mean to observations, the observations were mapped to year 2010 (the median year of our model simulation). For comparison of the modelled flux to the flux estimates from the CARIOCA buoy, years 2006-2014 in the model were used and no mapping of the observations was performed.

## 3.5 Results

### 3.5.1 $CO_2$ time series and transect

Both the model and observations at the CARIOCA buoy location (see Figure 3.1) are shown as a seasonal cycle in Figure 3.2 (chlorophyll, $pCO_2$, temperature, and temperature-normalized $pCO_2$). The buoy observations show a distinct and recurring seasonal cycle in $pCO_2$. Specifically, $pCO_2$ slightly decreases (from $\sim$450 to 425 $\mu$atm) from day 0 to 75. In late March, at approximately day 75, there is a large (100-200 $\mu$atm) and rapid (over $\sim$25 days) drop of $pCO_2$ associated with DIC drawdown due to the spring bloom (the dashed line indicates the peak in chlorophyll and its alignment with the lowest $pCO_2$ value). This drawdown of DIC occurs while the surface temperature is relatively constant and at its annual minimum.

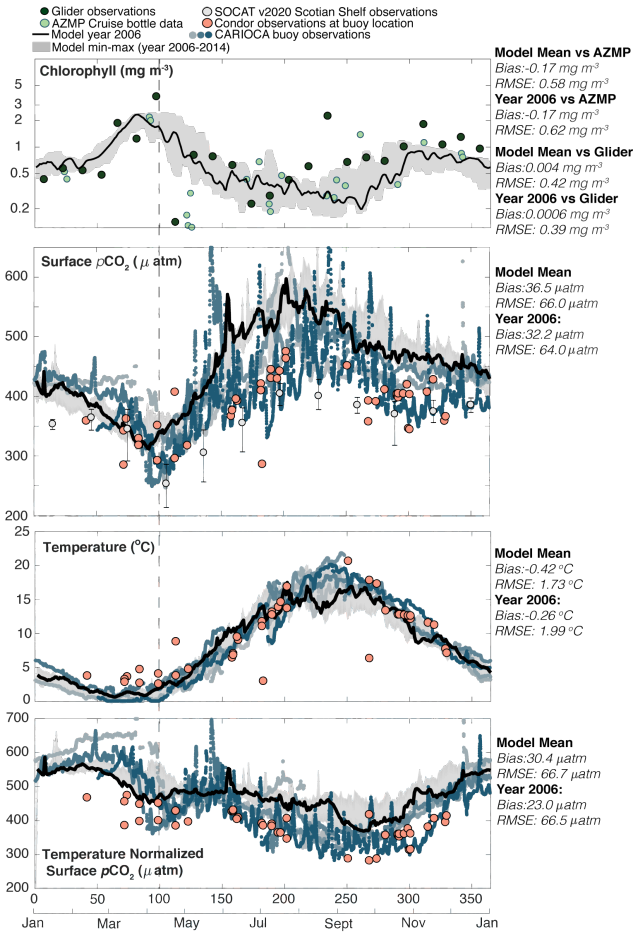


Figure 3.2: Seasonal (from top to bottom, with RMSE and bias in reference to year 2006) (a) chlorophyll (Glider: RMSE: 0.39 mg $m^{-3}$, bias: 0.0006 mg $m^{-3}$; AZMP: RMSE: 0.62 mg $m^{-3}$, bias: -0.17 mg $m^{-3}$); (b) $pCO_2$ (RMSE: 64.0 $\mu$atm , bias: 32.2 $\mu$atm ); (c) temperature (RMSE: 1.99 $^o$C, bias: -0.26 $^o$C); (d) temperature-normalized $pCO_2$ following Takahashi et al. (2002) (RMSE: 66.5 $\mu$atm, bias: 23.0 $\mu$atm) at STN 2 on the Scotian Shelf. The model year 2006 is shown with the thick black line and min-max in the model from years 2006-2014 with the grey shaded area in all panels. In (a) the dark green points are AZMP bottle data and light green points are glider data. In (b-d) observations from the moored CARIOCA buoy are shown as small blue points, with lighter shades of blue indicating earlier observations and darker shades indicating more recent observations, and observations from the Atlantic Condor transects at approximately the same location as the buoy are shown in large pink points. Both the Condor and CARIOCA buoy observations are mapped to year 2006 using the atmospheric trend in $pCO_2$. Light grey points are monthly mean SOCAT observations for the entire Scotian Shelf and the error bars are the 10th and 90th percentiles.

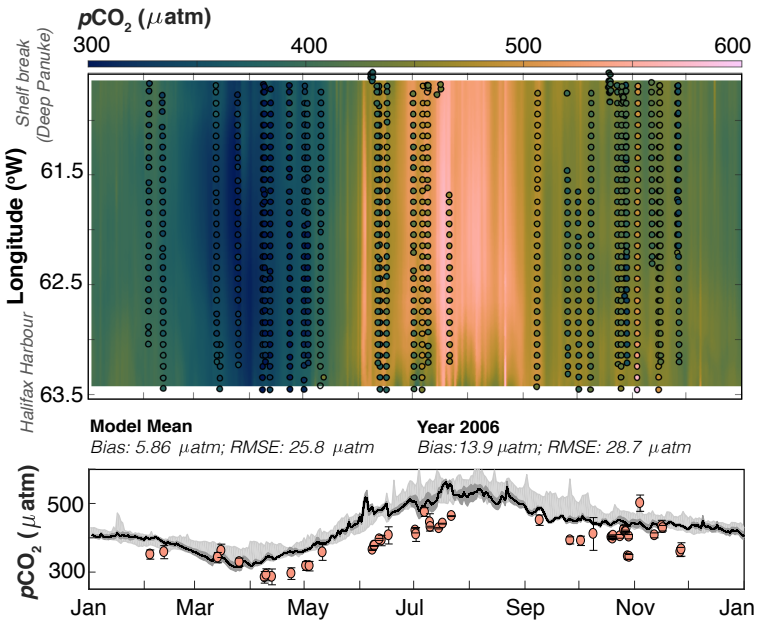


Figure 3.3: Model-data comparison along the Atlantic Condor transect. The top panel shows $pCO_2$ (in colour) evolving over time (x-axis) along the transect (longitude on the y-axis; Halifax Harbour to shelf break). The background is the model average $pCO_2$ along the transect and the points are the Atlantic Condor data binned into $0.1^o$ longitudinal bins. The bottom panel shows the average $pCO_2$ along the transect (y-axis) as it evolves over the seasonal cycle (x-axis). The line is year 2006 from the model averaged across the transect, the dark grey shaded area is the standard deviation, and the light grey shaded area is the min-max $pCO_2$ along the transect from 2006-2014. The points are the average and the error bars are standard deviation of observational $pCO_2$ across each transect. The Condor observations are mapped to year 2006 in both panels using the atmospheric trend in $pCO_2$. RMSE: 28.7 $\mu$atm; Bias: 13.9 $\mu$atm.

Following the drop in $pCO_2$ associated with the spring bloom, around day 100, surface water starts to warm, and this warming dominates the $pCO_2$ seasonal cycle with a maximum value of approximately 450–500 $\mu$atm reached around day 200-250 (mid to late summer). Around day 250, temperatures and $pCO_2$ start to decrease. Also shown is the temperature-normalized $pCO_2$ using the *Takahashi et al.* (2002) method for removing the thermal component of $pCO_2$ variations. The biological drawdown of DIC is visible in the temperature-normalized $pCO_2$ during the spring bloom starting around day 75 and a further decline throughout summer from day 150 to 250. This indicates that the overall increase in the non-normalized $pCO_2$ in summer is driven by increasing temperatures, and that biological processes tend to draw down DIC during this period.

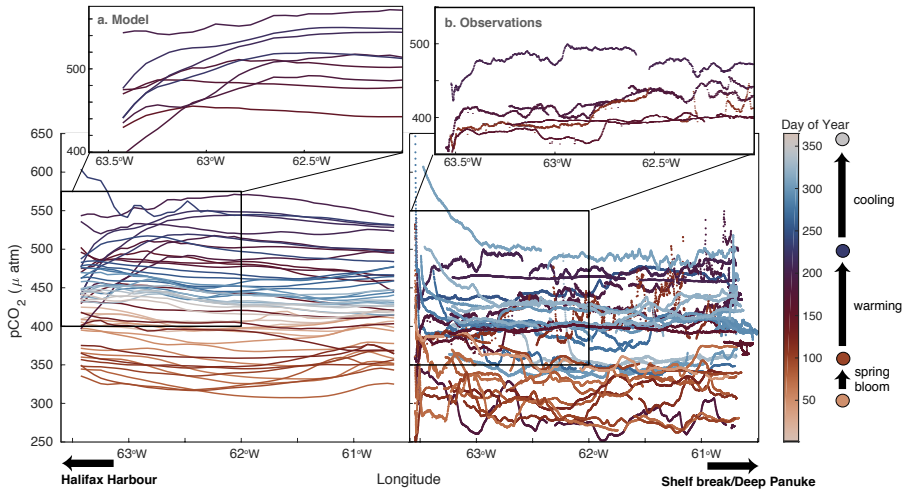


Figure 3.4: Temporal evolution of $pCO_2$ across the Atlantic Condor transect. X-axis is longitude, with the Halifax Harbour indicated on the left-hand side and the shelf break indicated on the right-hand side of each panel; Y-axis is $pCO_2$; and the colour indicates the day of the year. The left panel is year 2006 of the model along the transect every 7 days. The right panel are all of the observations along the transect. The upper insets zoom in on the indicated boxes showing only the events with lower $p$CO2 nearshore in the summer months (dark red/purple cololoured lines).

Most of the Atlantic Condor observations at this location fall within the envelope of the buoy observations' $pCO_2$ seasonal cycle. The monthly mean SOCAT v2020 $pCO_2$ for the entire Scotian Shelf also falls within the spread of buoy observations for most months. Exceptions include February and August, when the SOCAT observations are lower than the buoy observations, and September and October, when the SOCAT observations are at the low end of the buoy observations.

In terms of quantitative metrics, the model (year 2006) at the buoy location has an overall bias of 32.2 $\mu$atm and RMSE of 64.0 $\mu$atm compared to the buoy data. The model underestimates $pCO_2$ throughout January and February (day 0-80) partly because its spring bloom starts earlier than in the observations. The bloom-related minimum in $pCO_2$ in the model is approximately 50-75 $\mu$atm higher than the buoy observations and approximately 25–50 $\mu$atm higher than the Atlantic Condor observations. Temperature then dominates the $pCO_2$ seasonality in the model over a similar period as in the observations. During the summer (day 150-300), the model overestimates $pCO_2$ but follows a similar cycle as the observations throughout the remainder of the year. The temperature-normalized $pCO_2$ has similar biases (underestimation from day 0-80; overestimation from day 150-300), an

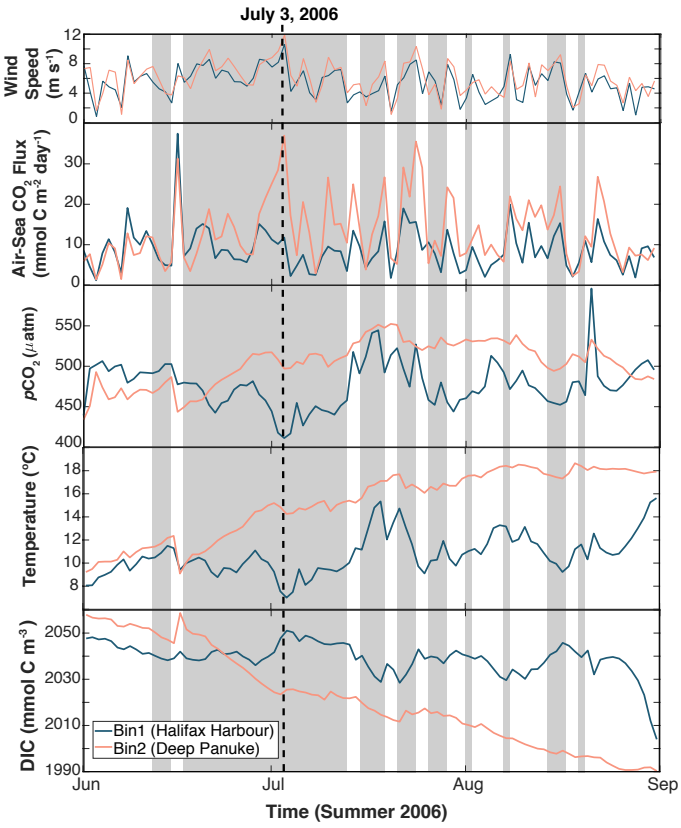


Figure 3.5: Time series of variables in two bins along the Condor Transect (see Figure 3.1) during summer 2006. From top to bottom: (a) wind speed, (b) air-sea $CO_2$ flux, (c) $pCO_2$, (d) temperature and (e) dissolved inorganic carbon (DIC). Shaded area indicates when there was upwelling-favourable winds nearshore (Bin 1). The blue lines indicate the values from the nearshore bin closest to the Halifax Harbour and the pink lines indicate values from the offshore bin near the Deep Panuke oil platform.

RMSE of 66.5 $\mu$atm, and an overall bias of 23.0 $\mu$atm for year 2006.

A comparison of simulated $pCO_2$ with the Atlantic Condor Transect observations along the average ship track (Figure 3.1) is shown in Figure 3.3. Compared to the Atlantic Condor observations, the model (year 2006) has a bias of 13.9 $\mu$atm and an RMSE of 28.7 $\mu$atm. The model tends towards slightly higher $pCO_2$ across the shelf compared to the ship data, but the bias along the ship track is about half the magnitude as that at the buoy. The seasonal cycle along the ship track (Figure 3.3) is similar to that at the buoy (Figure 3.2). The top panel of Figure 3.3 shows qualitatively good agreement between the model and observations across the whole transect, which is reflected in the averaged $pCO_2$ in the bottom panel. The model does a very good job at representing $pCO_2$

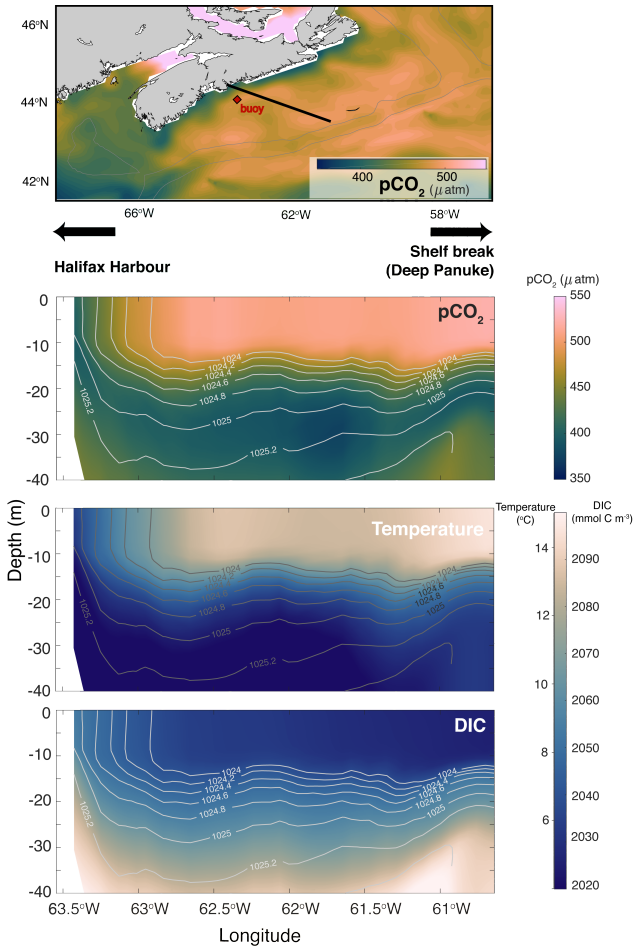


Figure 3.6: Surface map of $pCO_2$ (top panel), and transects along the average Atlantic Condor ship track of (top to bottom) $pCO_2$, temperature, and dissolved inorganic carbon (DIC) from the model taken during an upwelling event (Jul 3, 2006; see Figure 3.5). Contours in the transects are density. The top panel indicates the Condor transect with the black line and the location of the CARIOCA buoy with the red diamond.

throughout the winter (November through March) but does not reproduce the full spring bloom drop in $pCO_2$ across the whole shelf throughout April as observed. The model also overestimates $pCO_2$ throughout most of June and July. The seasonal cycle across the transect is relatively uniform throughout most of the year; however, there are some exceptions, for example, throughout July $pCO_2$ is relatively low near the shelf break in both the model and observations.

### 3.5.2 Effects of upwelling events

To better understand the effect of physical events on shelf-wide $pCO_2$, this section focuses on the cross-shelf variations in year 2006. Figure 3.4 shows the evolution of $pCO_2$

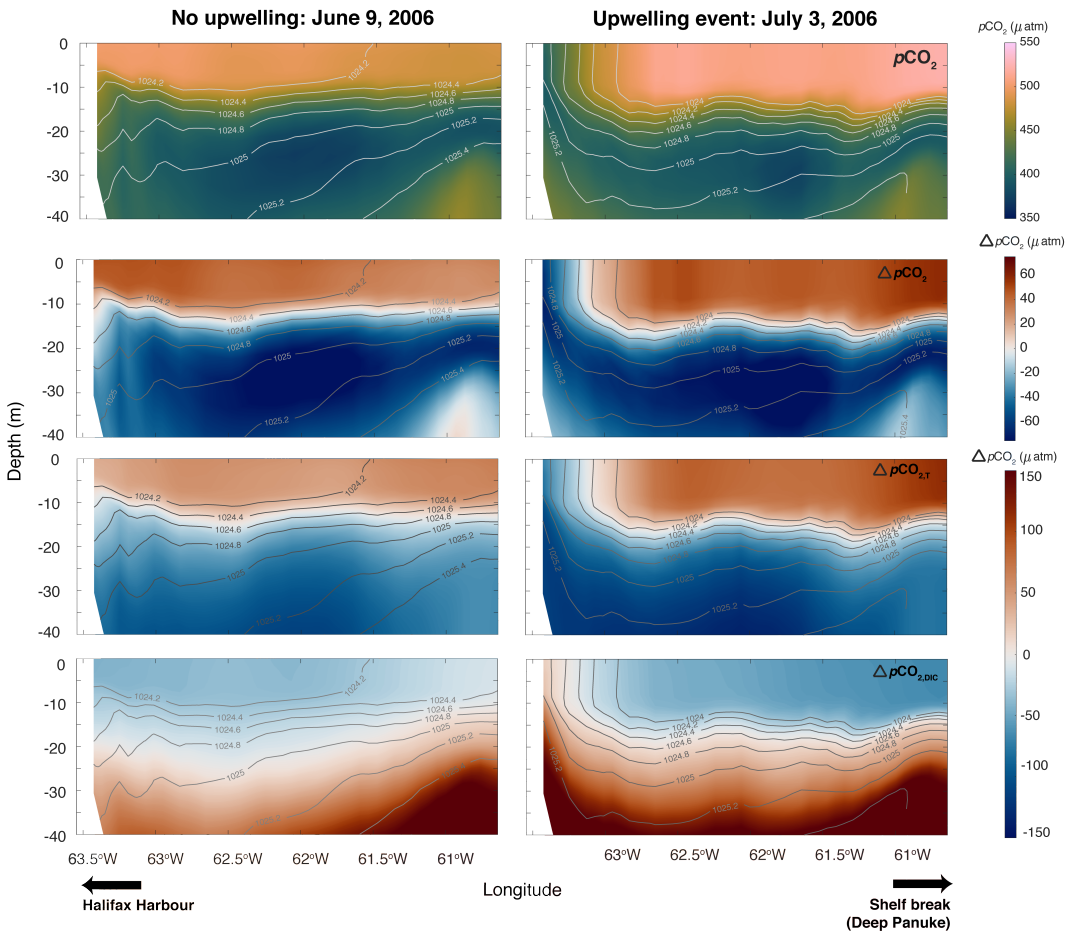


Figure 3.7: Taylor Decomposition of the upwelling event (right side; July 3, 2006) in Figure 3.6 compared to a non-upwelling event (left side; June 9, 2006). From top to bottom: (a) $p\mathrm{CO}_2$, (b) overall anomaly in $p\mathrm{CO}_2$ ($\Delta pCO_2$) from the mean $p\mathrm{CO}_2$ in the upper 40 m, (c) anomaly in $p\mathrm{CO}_2$ due to temperature changes ($\Delta pCO_{2,T}$), (d) anomaly in $p\mathrm{CO}_2$ due to DIC changes ($\Delta p\mathrm{CO}_{2,DIC}$).

along the Atlantic Condor transect throughout the year in both model (Figure 3.4a) and observations (Figure 3.4b). As in Figure 3.2 and Figure 3.3, the seasonal cycle of $p\mathrm{CO}_2$ extends across the entire shelf. Starting in January (light beige), $p\mathrm{CO}_2$ is around 400 $\mu$atm. In March ($\sim$day 50; golden orange colour), $p\mathrm{CO}_2$ starts to decrease, reaching a minimum of approximately 325 $\mu$atm in the model and around 275-300 $\mu$atm in the observations (day 100; dark brown colour). $p\mathrm{CO}_2$ subsequently increases again due to warming in the late spring/early summer and reaches a maximum of about 550 $\mu$atm in the model and 525 $\mu$atm in the observations (day 200; purple values). Following this peak in $p\mathrm{CO}_2$, both the model and observations start to decline, associated with cooling (days 225 to 325;

purple to light blue). Small-scale spatial variability in the observations is not captured by the model, but may, at least in part, be due to measurement artifacts of the underway system.

The insets in Figure 3.4 highlight events in summer (purple) in the northwestern half of the transect closest to Halifax, when $pCO_2$ decreases by 50–100 $\mu$atm within $\sim$40 km off the coast in the model and approximately 25 km off the coast in the observations. With more obvious examples in the model than in the observations, we use the model to investigate into a possible explanation for this decreased $pCO_2$. Figure 3.5 highlights the differences in $pCO_2$, air-sea $CO_2$ flux, temperature, and DIC between two longitudinal bins along the Atlantic Condor transect throughout summer 2006 in the model. The bin locations are shown in Figure 3.1 and contrast data closest to the coastline (Halifax Harbour bin, 63.5$^o$W to 63$^o$W; blue) with data closest to the shelf break (Deep Panuke bin, 61$^o$W to 60.5$^o$W; pink). In the model throughout June to August 2006, there are low $pCO_2$ events nearshore corresponding to low temperature which occurs during upwelling-favourable winds. During some of these events, temperature nearshore is about 7$^o$C lower than near the shelf break. These upwelling events and the subsequent low $pCO_2$ signal result in a short-term lowering of air-sea $CO_2$ fluxes nearshore (blue) compared to farther offshore (pink) throughout the summer (at approximately half the flux value nearshore versus offshore throughout July).

The top panel in Figure 3.6 shows a snapshot of surface $pCO_2$ from the model during one of the upwelling events (July 3, 2006; vertical dashed line in Figure 3.5). $pCO_2$ is relatively uniform across most of the shelf. However, in a narrow band along the coastline, $pCO_2$ values are nearly 100 $\mu$atm lower than the rest of the shelf. The bottom panels in Figure 3.6 show transects of $pCO_2$, temperature and DIC with density contours along the Atlantic Condor transect for the same time slice (July 3, 2006). In these panels, the density gradients move upwards towards the coastline, consistent with upwelling events. This upwelling brings cooler temperatures and higher DIC concentrations to the surface along the coastline of Nova Scotia. The low $pCO_2$ bin ranges from 63.5$^o$W to 63$^o$W longitude in the model (approximately 63.5$^o$W to 63.3$^o$W longitude in the observations; Figure 3.4), and aligns with the surface area affected by the upwelling events (Figure 3.6) in the model. See the Supplement for more variables along the Condor transect during the July 3, 2006, upwelling event.

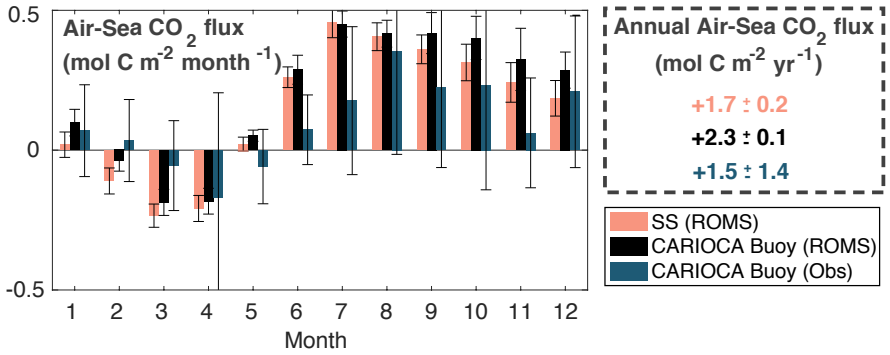


Figure 3.8: Monthly and annual air-sea $CO_2$ flux calculated from the model on the entire Scotian Shelf (pink), extracted at the CARIOCA buoy location (black), and from the buoy observations (blue). Flux is averaged over simulation years 2006-2014 for the model, and years 2007-2014 for the CARIOCA observations. Error bars are $\pm$ 1 standard deviations between years.

Figure 3.7 illustrates the results of the Taylor decomposition during the July 3, 2006, upwelling event with lower $pCO_2$ nearshore compared to a snapshot without upwelling (June 9, 2006) where surface $pCO_2$ is relatively uniform. The $pCO_2$ anomalies ($\Delta pCO_2$) show the deviations in each time slice from the mean $pCO_2$ in the upper 40 m. In both time slices, the surface $pCO_2$ is $\sim$50 $\mu$atm higher than the mean $pCO_2$ value in the upper 40 m. However, in the upwelling case, the upwelled water is 40-50 $\mu$atm lower than the mean $pCO_2$. In both time slices, across most of the transect, temperature is acting to increase $pCO_2$ ($\Delta pCO_{2,T}$; by $\sim$50-60 $\mu$atm on June 9, 2006 and by $\sim$75-100 $\mu$atm on July 3, 2006) in the top 10-15 m from the mean value whereas DIC is acting to decrease $pCO_2$ ($\Delta pCO_{2,DIC}$; by $\sim$10-20 $\mu$atm on June 9, 2006 and by $\sim$40-50 on July 3, 2006). However, in the upwelling region on July 3, temperature has the opposite effect and is acting to decrease $pCO_2$ by $\sim$50-60 $\mu$atm and DIC is acting to increase $pCO_2$ by only $\sim$5-10 $\mu$atm from the mean $pCO_2$ in the top 40 m. The effects of alkalinity ($\Delta pCO_{2,TA}$) and salinity ($\Delta pCO_{2,S}$) are much smaller across the shelf and in both time slices (see Supplement Figure S11). Comparisons of $\Delta pCO_{2,T}$ and $\Delta pCO_{2,DIC}$ illustrate that in the upwelled region, anomalies in $pCO_2$ from temperature are larger than those from DIC. However, if water from below 30 m was upwelled, DIC would likely start to outweigh the effect of temperature on $pCO_2$.

### 3.5.3 Regional flux estimates

The model-simulated air-sea $CO_2$ fluxes, integrated by month and year, and averaged over the simulation from 2006-2014, for the Scotian Shelf and at the buoy location are shown in Figure 3.8 in comparison to the flux calculated from the CARIOCA buoy observations. The uncertainty in the model estimates is calculated as the standard deviation between years. Annually, the averaged flux between the model and observations is comparable, and the flux estimates at the buoy location are significantly larger than the shelf-wide flux estimates. The model-estimated, annually integrated flux for the Scotian Shelf shows outgassing of $CO_2$ at +1.7 $\pm$ 0.2 mol C $m^{-2}$ $yr^{-1}$. At the buoy location, just outside the upwelling region, the model estimates net outgassing of +2.3 $\pm$ 0.1 mol C $m^{-2}$ $yr^{-1}$. From the buoy observations, the annually integrated $CO_2$ flux is estimated as net outgassing at +1.5 $\pm$ 1.4 mol C $m^{-2}$ $yr^{-1}$. Although our model-derived estimate is within the upper error-bound of the observation-based estimate, it is higher, which may be due to the model's overestimation of $pCO_2$, particularly throughout the summer months. There are also some differences in the seasonal cycle. In the model, the Scotian Shelf flux is lower in magnitude than the flux at the buoy location during most of the year, and particularly from June to January. Bin 1 along the Atlantic Condor transect (Halifax Harbour/upwelling bin, Figure 3.1) has an annually integrated flux of +2.2 $\pm$ 0.2 mol C $m^{-2}$ $yr^{-1}$, which is comparable to the annual flux of bin 2 (Deep Panuke/shelf break bin, Figure 3.1) at +2.0 $\pm$ 0.2 mol C $m^{-2}$ $yr^{-1}$ and the simulated flux at the buoy location. These results indicate that cross-shelf variability in air-sea $CO_2$ fluxes is small.

Figure 3.9 compares the model-derived, annual flux estimates from the present study for the Scotian Shelf (+1.7 $\pm$ 0.2 mol C $m^{-2}$ $yr^{-1}$), Grand Banks (–1.3 $\pm$ 0.3 mol C $m^{-2}$ $yr^{-1}$), and Gulf of Maine (–0.5 $\pm$ 0.2 mol C $m^{-2}$ $yr^{-1}$) to previously reported estimates. The model estimate for the Scotian Shelf agrees well with the estimates from *Shadwick et al.* (2011) but disagrees with those from *Signorini et al.* (2013), *Laruelle et al.* (2014), and *Laruelle et al.* (2015). *Laruelle et al.* (2014) define the shelf region as a larger area that encompasses both the Scotian Shelf and Gulf of Maine. *Laruelle et al.* (2015) calculate one flux estimate for both the Scotian Shelf and Gulf of Maine. *Signorini et al.* (2013) calculates separate estimates for Gulf of Maine and Scotian Shelf. The model estimate for the Gulf of Maine agrees best with the estimates from *Laruelle et al.* (2014), and *Laruelle et al.* (2015), and disagrees with the estimates from *Signorini et al.* (2013), and *Vandemark*

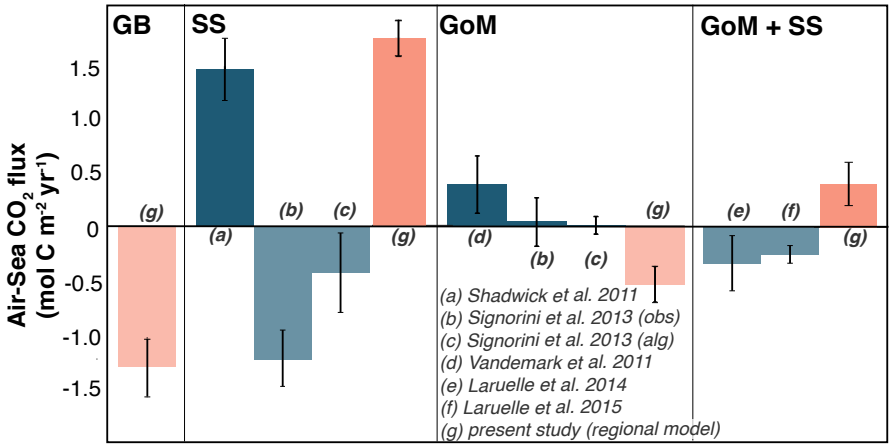


Figure 3.9: Annually integrated air-sea $CO_2$ flux for the Grand Banks (GB), Scotian Shelf (SS) and Gulf of Maine (GoM) in the model (pink) compared to literature values (blue). Positive values are net outgassing, indicated by solid bars, and negative values are net ingassing, indicated by faded bars.

*et al.* (2011).

## 3.6 Discussion

We have compared the inorganic carbon dynamics in our medium complexity biogeochemical model of the northwest North Atlantic against two different observational datasets of $pCO_2$, one of them highly resolved in time from a CARIOCA buoy and the other with high spatial resolution along a cross-shelf transect that is occupied approximately biweekly. The largest limitation of the model is that it is unable to capture the speed and magnitude of the DIC drawdown associated with the spring bloom throughout March and April (Figure 3.2 and Figure 3.3). The simulated $pCO_2$ starts to decline earlier and over a longer period than in both the buoy and transect observations, and the transect shows that this timing is consistent across the whole shelf. Additionally, the model does not reach the observed $pCO_2$ minimum during the bloom across the whole shelf. This discrepancy appears to be a result of the bloom initiation occurring slightly too early and the bloom spanning a longer period of time in the model, and also chlorophyll levels in the model not reaching the peak values that are observed (Figure 3.2a). This limitation aside, the overall seasonal cycle and switch between biological- and temperature-dominated signals in $pCO_2$ are well captured and the model simulates both the seasonal spatial and temporal variability of $pCO_2$ across

the Scotian Shelf reasonably well.

Notable occurrences of spatial variability of $pCO_2$ on the Scotian Shelf occur throughout the summer months in both the model and observations. With only 1-2 clear examples of lower $pCO_2$ within $\sim$25 km of shore in the observations, we used our model to hypothesize about a possible mechanism driving this variability. In the model, we found that coastal upwelling events are driving the summertime spatial variability of $pCO_2$ on the Scotian Shelf and could explain the variability in the observations as well. The physical dynamics of coastal upwelling is well-documented on the Scotian Shelf (*Petrie et al.*, 1987; *Shan et al.*, 2016). This upwelling only affects the nearshore region (within $\sim$20-40 km of shore in the model, depending on the event) where water from the cold intermediate layer is transported to the surface. In the model, this creates a coastal band of cold water at the surface that is high in DIC and low in $pCO_2$ (Figure 3.6). The difference between inshore and offshore temperatures ($7^oC$ and $15^oC$, respectively) during these events has a larger influence on the $pCO_2$ spatial variability than the DIC variations (2050 mmol C $m^{-3}$ inshore and 2020 mmol C $m^{-3}$ offshore; Figure 3.6) because the thermodynamic influence of temperature outweighs the effect of a slight increase in DIC, thus lowering $pCO_2$ (see the Taylor decomposition in Figure 3.7). In the example explored in the present study, the upwelled water comes from $\sim$20-25 m depth that has a $pCO_2$ approximately 100 $\mu$atm lower than the rest of the shelf. Temperature in the upwelled water is acting to lower $pCO_2$ by $\sim$150 $\mu$atm whereas DIC is acting to increase $pCO_2$ by $\sim$50 $\mu$atm compared to the rest of the shelf. If deeper water was being upwelled to the surface, DIC would likely start to be the dominant factor in setting $pCO_2$ during these events (Figure 3.7). For the given range of DIC values (2060 to 2020 mmol C $m^{-3}$) and a mean temperature of $11^oC$, the thermodynamic effect outweighs the effect of DIC differences for temperature changes larger than $4^oC$. Typically, it is thought that upwelling of subsurface waters rich in DIC leads to increased surface $pCO_2$ as is the case for the California Current System (CCS), encompassing the continental shelves off of Washington, Oregon, and California, where nearshore outgassing of $CO_2$ during upwelling events is well documented (*Fennel et al.*, 2019; *Chavez et al.*, 2017; *Evans et al.*, 2015; *Fiechter et al.*, 2014; *Turi et al.*, 2014). There are, however, large differences between the Scotian Shelf and the typical upwelling scenario of the CCS. For instance, the size and geometry of these shelves are quite different, which affects the type of water being upwelled to the surface. The California Shelf is an

active margin approximately 10 km wide (*Fennel et al.*, 2019) compared to the passive-margin Scotian Shelf with approximately 120-240 km width (*Shadwick et al.*, 2010). As a result, the upwelling in the CCS brings DIC rich water ($\sim$2200-2250 $\mu$mol kg$^{-1}$) from deep in the water column (below 150-200 m) of the open ocean across the shelf break to the surface of the shelf (*Feely et al.*, 2008). On the Scotian Shelf, it is only subsurface shelf water from between $\sim$20-25 m depth that is being upwelled, which is at a similar temperature to the upwelled water in the CCS (7-8$^o$C) but at a much lower DIC concentration (2050 mmol C m$^{-3}$).

Our regional model shows that upwelling events could be a large contributor to setting the $CO_2$ signal in the summer on the inner portion of the Scotian Shelf, acting to lower $pCO_2$ here and slightly reducing outgassing compared to the outer shelf. Throughout the remainder of the year, the $pCO_2$ distribution across the Scotian Shelf is relatively uniform (Figure 3.3). Comparison of the inner and outer shelf $pCO_2$ (Figure 3.4) shows the similar seasonality that is seen across the shelf, both in the model results and Atlantic Condor observations. Additionally, the simulated annual air-sea $CO_2$ flux in bin 1 (upwelling bin, Figure 3.1) is +2.2 $\pm$ 0.2 mol C m$^{-2}$ yr$^{-1}$ and similar to bin 2 (shelf break bin, Figure 3.1) where the annual flux is +2.0 $\pm$ 0.2 mol C m$^{-2}$ yr$^{-1}$. For comparison, the annual flux for the entire shelf flux is +1.7 $\pm$ 0.2 mol C m$^{-2}$ yr$^{-1}$ and the flux at the CARIOCA buoy is +2.3 $\pm$ 0.1 mol C m$^{-2}$ yr$^{-1}$. Our results indicate that the short-term upwelling events in the summer do not significantly affect the shelf-wide fluxes on an annual scale. The location of the CARIOCA buoy slightly overestimates shelfwide fluxes but is fairly representative of the shelf-wide $pCO_2$ dynamics overall.

According to the model, the Scotian Shelf acts as a net source of $CO_2$ to the atmosphere (+1.7 $\pm$ 0.2 mol C m$^{-2}$ yr$^{-1}$), the Gulf of Maine is a net sink of $CO_2$ (–0.5 $\pm$ 0.2 mol C m$^{-2}$ yr$^{-1}$), and the Grand Banks acts as a net sink of $CO_2$ (–1.3 $\pm$ 0.3 mol C m$^{-2}$ yr$^{-1}$). These results are in agreement with *Shadwick et al.* (2011) for the Scotian Shelf, and *Laruelle et al.* (2014) and *Laruelle et al.* (2015) for the Gulf of Maine. Our results disagree, however, with results from other global (*Laruelle et al.*, 2014) and regional studies (*Laruelle et al.*, 2015; *Signorini et al.*, 2013; *Vandemark et al.*, 2011). The discrepancy in reported air-sea $CO_2$ flux between these studies is partly a result of how each study defines the area of the Scotian Shelf and Gulf of Maine. For example, *Laruelle et al.* (2015) calculates one estimate for both the Scotian Shelf and Gulf of Maine. The

shelves of eastern North America are diverse, particularly in width and circulation features, and defining them as a single region is not representative. Additionally, the Scotian Shelf waters are strongly influenced by cold, carbon-rich Labrador Sea water, which is not the dominant endmember south of the Gulf of Maine (*Loder et al.*, 1998; *Rutherford and Fennel*, 2018; *Fennel et al.*, 2019). Calculating a single flux estimate for the entirety of this dynamically diverse region is problematic and will yield a different estimate than when considering smaller and more specific regions. However, this only partially explains the difference in flux estimates.

Another reason is that the global SOCAT database was missing important regional data until recently. *Signorini et al.* (2013) used data from version 1.5 and *Laruelle et al.* (2014) and *Laruelle et al.* (2015) used data from version 2.0 of the SOCAT database. Neither of the observational datasets used in the present study were included in SOCAT versions 1.5 and 2.0. Figure 3.10 illustrates the difference between different SOCAT versions for seasonal $pCO_2$ on the Scotian Shelf. SOCAT v2020 has consistently higher average $pCO_2$ values than v1.5 and v2, with at least double the number of years and a much larger number of observations going into each monthly average (on the order of 1000 to 10000 measurements in v2020 versus 100 to 1000 in v1.5 and v2). We believe that flux estimates using the updated SOCAT v2020 will agree better with our estimates and those of *Shadwick et al.* (2011) since SOCAT v2020 includes more observations with higher spatial and temporal resolution to better capture the distinct seasonal cycle here. Our study, however, only focuses on the recent seasonality of $pCO_2$, making it difficult to distinguish if earlier SOCAT versions miss the regional dynamics solely due to low resolution of observations, or if the estimates from the different SOCAT versions are reflective of a shift in the behaviour of the shelf system. More work should therefore be done to better understand how variability on longer timescales could be affecting regional $pCO_2$ and if that variability could also be a reason for the disagreement between the different SOCAT version.

In the present study, we have synthesized and compared our model simulations with high-resolution observations to highlight the dependence of Scotian Shelf $pCO_2$ seasonality on: (1) biological drawdown of DIC during the spring bloom, (2) temperature effects throughout the summer months, and (3) wind-driven coastal upwelling events. In Figure

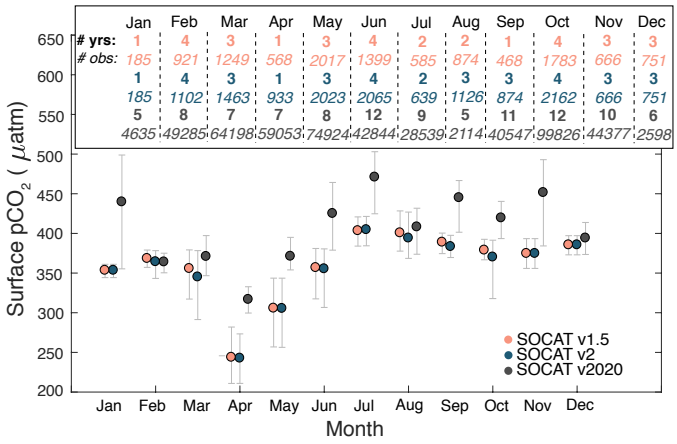


Figure 3.10: Comparison of the seasonal cycle of $pCO_2$ for the different versions of SOCAT for the Scotian Shelf, mapped to year 2006. The points indicate the mean for each month and the bars indicate the 5th and 95th percentile. Inset shows the number of years and number of observations used in each month for each version.

3.2d, the temperature-normalized $pCO_2$ shows the non-thermal $pCO_2$ signal, which distinguishes the influence of biological and transport processes on $pCO_2$ (*Takahashi et al.*, 2002). There is a clear decrease of $pCO_2$ associated with the spring bloom. The simulated decrease in $pCO_2$ is smaller than in the observations, likely due to the bloom occurring too early and over a more extended period in the model than the observations. In summer, temperature-normalized $pCO_2$ continues to decrease rather than follow the increasing temperature signal of non-normalized $pCO_2$. Previous studies have noted that, in summer, the thermodynamic signal in $pCO_2$ outweighs the influence of biological activity (*Shadwick et al.*, 2011; *Shadwick and Thomas*, 2014), which could explain the differences in seasonality between $pCO_2$ and temperature-normalized $pCO_2$ in the present study. We believe this thermodynamic influence is an important factor driving the net outgassing observed on the Scotian Shelf, particularly when combined with the delivery of DIC-rich water from the Labrador Sea.

Understanding what processes presently control $CO_2$ dynamics is important for projecting how the region will be affected by changes in climate. Previous studies have suggested that the frequency and intensity of coastal upwelling could increase (e.g., *Xiu et al.*, 2018). In the case of the Scotian Shelf, increased upwelling would lead to less outgassing or even net ingassing during summer along the coast of Nova Scotia. Climate change could therefore disproportionately affect the nearshore region here and lead to an intensification

of spatial gradients. Such an upwelling signal would be in addition to the effect of increasing atmospheric $CO_2$, which may be driving the entire Scotian Shelf towards a more neutral system with less outgassing. The effect of the thermal control on Scotian Shelf $pCO_2$ is also an important aspect to consider. As temperatures continue to rise, summer $pCO_2$ values will also likely increase, potentially offsetting some of the effect of increased atmospheric $CO_2$ but also affecting production and respiration rates. Of course, none of these factors act independently and will instead combine to alter both the seasonal and spatial patterns of $pCO_2$ in the region, making the overall outcome of climate-related perturbations on the Scotian Shelf difficult to predict. However, the implementation of a regional model that resolves current conditions well, as in the present study, is an important step towards projecting future climate-related changes in the region.

In this study, we have validated surface $pCO_2$ fields on a seasonal scale from a medium-complexity regional biogeochemical model for the northwest North Atlantic shelf region against $pCO_2$ observations from a CARIOCA buoy and repeated cross-shelf transects from a ship of opportunity that crosses the Scotian Shelf. Except for the strength and speed of the $pCO_2$ drawdown associated with the spring bloom, the model simulations represent the observed spatial and temporal variability of $pCO_2$ on the Scotian Shelf well. Contrary to most coastal upwelling systems, upwelling events in summer are acting to lower $pCO_2$ within $\sim$25 km of the coastline, as cold, carbon-enriched intermediate-layer water is brought to the surface. The lowering of surface $pCO_2$ during these events occurs because the temperature effect leading to a lowering of $pCO_2$ overwhelms the increase in $pCO_2$ associated with DIC enrichment. We found $pCO_2$ to be relatively uniform across the shelf, with the exception of a narrow band impacted by summer upwelling events. Overall, the Scotian Shelf acts as a net source of $CO_2$ (+1.7 $\pm$ 0.2 mol C $m^{-2}$ $yr^{-1}$), the Gulf of Maine is a net sink of $CO_2$ (–0.5 $\pm$ 0.2 mol C $m^{-2}$ $yr^{-1}$), and Grand Banks acts as a net sink of $CO_2$ (–1.3 $\pm$ 0.3 mol C $m^{-2}$ $yr^{-1}$) in our simulation. Combination of the model simulation and the highly resolved observational datasets emphasizes that the seasonal cycle of $pCO_2$ is driven by strong biological drawdown of DIC in early spring and a dominant thermal control throughout the summer months. Except for the short spring bloom period, surface $pCO_2$ is oversaturated with respect to atmospheric values, which results in net outgassing. Ongoing changes in climate and carbon cycling will likely alter both the seasonal and spatial patterns of $pCO_2$ on the Scotian Shelf.

# CHAPTER 4

# ELUCIDATING COASTAL OCEAN CARBON TRANSPORT PROCESSES: A NOVEL APPROACH APPLIED TO THE NORTHWEST NORTH ATLANTIC SHELF [1]

## 4.1 Abstract

A latitudinal pattern in coastal air-sea $CO_2$ flux has emerged where mid- and high-latitude shelves act as net sinks and low-latitude shelves as net sources to the atmosphere. Regional studies, however, report the mid-latitude Scotian Shelf at the eastern Canadian seaboard acts as a large source of $CO_2$, contradicting several global syntheses. Here, we combine observations and a regional biogeochemical model to explain, for the first time, why the Scotian Shelf outgasses $CO_2$. We employ a novel approach that uses passive dye tracers, allowing us to estimate how carbonate properties change along dominant transport pathways. We show that cold, carbon-rich subpolar North Atlantic water is a dominant endmember that warms and becomes oversaturated with $CO_2$ as it transits southwestward along the shelf, leading to net outgassing on the Scotian Shelf. Our approach explicitly considers the 3-dimensional nature of coastal ocean transport processes and should be applied to other shelf regions.

[1] Rutherford, K., and K. Fennel, Elucidating coastal ocean carbon transport processes: A novel approach applied to the northwest North Atlantic shelf, *Manuscript submitted to Geophysical Research Letters*.
Author Contributions: KR and KF conceived the study. KR carried out the model simulations and analysis. KR and KF discussed the results and wrote the manuscript.

## 4.2 Introduction

The ocean has taken up a major fraction of anthropogenic $CO_2$ emissions, but the magnitude, spatial distribution, temporal variability, and secular trend of this uptake remain poorly understood and quantified. Continental shelves in particular are known to be highly variable, both spatially and temporally (*Previdi et al.*, 2009; *Gruber*, 2015). They are likely to disproportionately feel the effects of climate change (*Laruelle et al.*, 2010) and respond on shorter timescales to increases in atmospheric $CO_2$ (*Cai et al.*, 2010).

The consensus view that seems to be emerging from several global syntheses of coastal air-sea $CO_2$ fluxes is that mid- to high-latitude shelves act as net sinks (i.e. take up $CO_2$ from the atmosphere) whereas low-latitude shelves act as net sources (i.e. release $CO_2$ to the atmosphere). For example, *Cai et al.* (2006) classified continental shelf observations from approximately 50 studies and estimated that mid- to high-latitude shelves take up 0.33 Pg C $yr^{-1}$ while low-latitude shelves outgas 0.11 Pg C $yr^{-1}$. *Chen and Borges* (2009) synthesized global $pCO_2$ observations from roughly 50 studies and found temperate and high-latitude shelves to be undersaturated in $CO_2$ and low-latitude shelves to be oversaturated. *Laruelle et al.* (2014) aggregated observations from the SOCAT v2.0 database (*Bakker et al.*, 2014) into 45 regions, and again found that low-latitude shelves show net outgassing, and mid- and high-latitude shelves net ingassing of $CO_2$. The most recent global synthesis of *Roobaert et al.* (2019) provided an updated estimate using SOCAT v4.0 (*Bakker et al.*, 2016) and found the same latitudinal trends as in the previous studies.

Contrary to this apparent consensus, *Vandemark et al.* (2011) reported that the mid-latitude Gulf of Maine (at approximately $42^oN$) acts as a weak net source of $CO_2$ of $+0.38\pm0.26$ mol $CO_2$ $m^{-2}$ $yr^{-1}$ and *Shadwick and Thomas* (2014) estimated that the Scotian Shelf, located to the north of the Gulf of Maine (at approximately 43-$44^oN$), acts as a large net source of $CO_2$ of $+1.42\pm0.28$ mol C $m^{-2}$ $yr^{-1}$. These estimates are in contradiction to the estimates of *Cai et al.* (2006), *Chen and Borges* (2009), *Laruelle et al.* (2014), *Roobaert et al.* (2019), and various others as illustrated in the compilation of North American coastal flux estimates in *Fennel et al.* (2019).

Similar contradictions are apparent in modelling studies. The global model of *Bourgeois et al.* (2016) simulated significant uptake ($-30$ mg C $m^{-2}$ $yr^{-1}$) for the Scotian Shelf

and Gulf of Maine combined (see Fig. 2 in *Fennel et al.*, 2019). In contrast, a high-resolution regional model simulated that the Scotian Shelf acts as a large source of $CO_2$ ($+1.7\pm0.2$ mol C $m^{-2}$ $yr^{-1}$), very similar to the observation-based estimates of *Shadwick and Thomas* (2014), and the Scotian Shelf and Gulf of Maine combined as a weak net source at $+0.5\pm0.2$ mol C $m^{-2}$ $yr^{-1}$ (*Rutherford et al.*, 2021).

A plausible mechanism that could explain the relatively large outgassing of $CO_2$ at this latitude, causing the Scotian Shelf to deviate substantially from the global pattern, has not been provided to date. *Shadwick et al.* (2010) and *Shadwick and Thomas* (2014) suggested that outgassing of $CO_2$ on the Scotian Shelf occurs because of upwelling of carbon-rich water, but did not specify whether they meant upwelling of slope water across the shelf break or upwelling of subsurface shelf water. Neither of these upwelling mechanisms can be responsible for the reported outgassing because (1) the shelf-break current and its associated density fronts act as an effective barrier to cross-shelf exchange inhibiting the onwelling of slope water (*Beardsley and Boicourt*, 1981; *Loder et al.*, 1998; *Fratantoni and Pickart*, 2007; *Rutherford and Fennel*, 2018), and (2) coastal upwelling events, while frequently occurring on the Scotian Shelf (*Petrie et al.*, 1987; *Shan et al.*, 2016), are temporarily lowering surface-ocean $pCO_2$ and are too short-lived to impact the annually integrated flux (*Rutherford et al.*, 2021).

Here, we put forward a mechanistic explanation for the observed mid-latitude outgassing, provide a framework for testing this mechanism in other continental shelf regions, and suggest an explanation for why this outgassing was missed in many previous studies. We posit that carbon-rich subpolar North Atlantic water, which enters the shelf north of Newfoundland and travels along the shelf across the Grand Banks to the Scotian Shelf, the Gulf of Maine, and onward to the Middle Atlantic Bight as a distinctive water mass, becomes oversaturated with $CO_2$ as it warms along its southwestward journey. We provide results from a high-resolution biogeochemical model of the northwest North Atlantic shelves that includes passive dye tracers for water mass tracking. Our approach accounts for the inherently 3D nature of coastal transport processes which is key to the proposed mechanism and is applicable to other shelf regions around the globe.

## 4.3 Study region

The Scotian Shelf, located at the eastern coast of Canada, is approximately 700 km long, varies in width between 120 and 240 km, and takes up an area of approximately 1.3 x $10^5$ $km^2$. The Grand Banks to the north of the Scotian Shelf, and the semi-enclosed Gulf of Maine, located to the southwest of the Scotian Shelf, take up areas of 3.4 x $10^5$ $km^2$ and 1.8 x $10^5$ $km^2$, respectively (Figure 4.1).

These three shelf regions are strongly influenced by the Labrador Current System (LCS *Loder et al.*, 1998; *Fratantoni and Pickart*, 2007; *Rutherford and Fennel*, 2018). The LCS originates in the Labrador Sea and carries cool, carbon-rich water southward along the shelf and the shelf break in several distinct branches. The Labrador Current (LC) is the shelf-break branch of LCS. After turning around the tip of the Grand Banks and while moving southwestward along the Scotian Shelf, the LC is simply referred to as the shelf-break current (Figure 4.1). An inner branch of this large-scale current system with its own water mass signature can be traced southward to the Middle Atlantic Bight and Cape Hatteras (*Chapman and Beardsley*, 1989; *Mountain*, 1991).

Active shelf-ocean exchange between the Labrador Sea and Labrador Shelf (ENS in Figure 4.1) sets the initial properties of shelf waters north of Newfoundland. Properties are then modified as shelf water moves in a generally southwestward direction along the Scotian Shelf and Gulf of Maine, but retain a signature that is distinct from the adjacent open ocean because the shelf-break current is effectively inhibiting cross-shelf exchange (*Beardsley and Boicourt*, 1981; *Loder et al.*, 1998; *Fratantoni and Pickart*, 2007; *Rutherford and Fennel*, 2018). Some modification of shelf-water along its path occurs because of freshwater supplied from the St. Lawrence River and inflows of warm, salty water from the slope region via deep channels, e.g. the Laurentian Channel and the Northeast Channel (*Dever et al.*, 2016).

## 4.4 Methods

### 4.4.1 Model description

The biogeochemical model is based on ROMS v3.5, a terrain-following, free-surface, primitive-equation ocean model (*Haidvogel et al.*, 2008). The model grid has 30 vertical levels, has approximately 10 km horizontal resolution, and includes the Gulf of Maine,

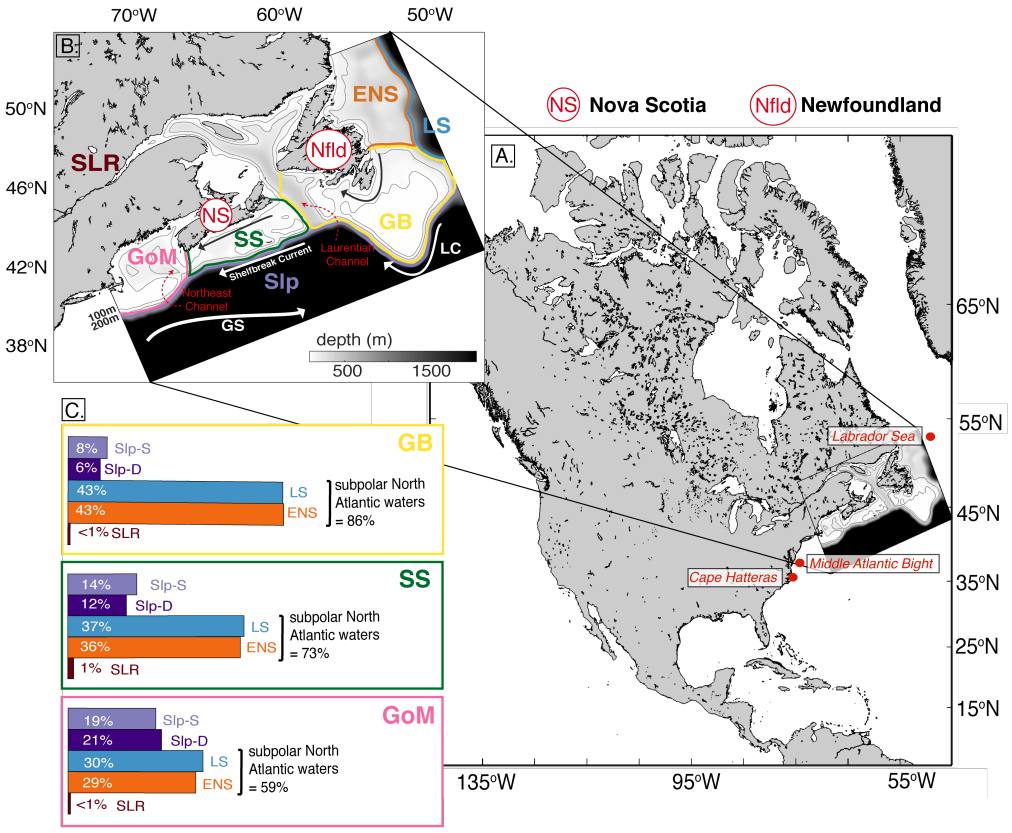


Figure 4.1: A) Map of North America with location of the model domain. B) Model domain and bathymetry. The domain is divided into different subregions indicated by colored outlines: East Newfoundland Shelf (ENS; orange), Labrador Sea (LS; blue), Grand Banks (GB; yellow), St. Lawrence River (SLR; red), Slope-Shallow and -Deep (Slp-S Slp-D, respectively; purple), Scotian Shelf (SS; green) and Gulf of Maine (GoM; pink). C) Endmember water mass fractions making up the GB, SS, and GoM waters when considering Slp-S, Slp-D, LS, ENS and SLR as distinct endmembers, defined using passive dye tracers.

Scotian Shelf, East Newfoundland Shelf, and Grand Banks (Figure 4.1). The physical model setup and validation are described in detail in *Brennan et al.* (2016) and *Rutherford and Fennel* (2018), who have shown it to realistically represent observed circulation patterns. The biogeochemical model is of medium complexity, based on the nitrogen cycle model with inorganic carbon chemistry of *Fennel et al.* (2006, 2008), but was expanded to include two phytoplankton and two zooplankton groups by *Laurent et al.* (2021). Detailed descriptions of the biological and inorganic carbon component in the current model version are given in *Laurent et al.* (2021) and *Rutherford et al.* (2021), respectively. Also used here are passive dye tracers (see Figure 4.1 for dye tracer source regions) for the calculation of

water mass fractions in the three shelf regions of interest (Scotian Shelf, Grand Banks and Gulf of Maine) similar to *Rutherford and Fennel* (2018). The model ran for 16 years from 1999 to 2014, where the first year is considered model spin-up. Here, we focus on years 2006 to 2014. Daily 3D snapshots of biogeochemical properties, dye tracers, salinity and temperature were saved.

### 4.4.2 Carbon disequilibrium

Similar to Apparent Oxygen Utilization (AOU), carbon disequilibrium was calculated as the difference between the model-simulated dissolved inorganic carbon (DIC) and an equilibrium value ($DIC_{eq}$). The equilibrium value $DIC_{eq}$ was calculated from the model-simulated temperature and salinity, assuming a constant atmospheric $pCO_2$ of 390 $\mu$atm, using the Matlab version 1.1 of CO2SYS (*Lewis and Wallace*, 1998). Unlike $pCO_2$, DIC is a conservative property, therefore the deviation of simulated DIC from its equilibrium value (DIC – $DIC_{eq}$) is a better metric of carbon disequilibrium.

### 4.4.3 Predicting properties from endmember concentrations and water mass fractions

For each of the three shelf regions of interest (Grand Banks, GB; Scotian Shelf, SS; and Gulf of Maine, GoM), we calculated what temperature (T), salinity (S), and DIC would be if the endmember properties of their source regions were unchanged during transport and conservatively mixed. This calculation uses the dye tracer mass fractions of five endmembers: Labrador Sea (LS), East Newfoundland Shelf (ENS), St. Lawrence River (SLR), and slope water (Slp-S and Slp-D; see Figure 4.1B). The predicted values are calculated as a weighted mean, as follows

$$reg_{pred} = \sum_{n=1}^{N} X_{reg,n} reg_n \tag{4.1}$$

where $reg_{pred}$ is the predicted value of T, S, and DIC for each shelf subregion; $X_{reg,n}$ is the mass fraction for each endmember $n$; and $reg_n$ is the average value throughout the water column of T, S, and DIC of endmember $n$ for a total of $N$ endmembers. The difference between the predicted and simulated shelf values is due to transformations during transit of water masses from their source regions.

Model values for T, S, and DIC were compared to observed values for each subregion from the GLODAPv2.2020 database (*Olsen et al.*, 2020). All available data were averaged

in time and space for each subregion. There were insufficient observations for the Grand Banks, so this region was omitted in the comparison.

## 4.5 Results

### 4.5.1 Simulated, predicted, and observed water mass properties

The mass fractions of five source-water regions (see Figure 4.1C) in the three shelf regions of interest (the Grand Banks, GB, the Scotian Shelf, SS, and the Gulf of Maine, GoM) were used to calculate a weighted mean DIC, S, and T (Equation 4.1; Table C.1), which we consider as predicted values when assuming conservative mixing of endmember properties. Discrepancies between the model-simulated values and their corresponding predicted values indicate what property modifications have occurred as waters travelled.

The simulated (filled circles) and predicted (open circles) values are shown in Figure 4.2 and lie within the polygon created by the end-members. The two main endmembers for the SS are subpolar waters from the ENS and LS (making up 36% and 37% respectively of SS waters; Figure 4.1C), both rich in DIC, resulting in a high predicted DIC for the SS. Simulated SS water is warmer and fresher than the corresponding predicted values (Figure 4.2, Table C.1) because a positive net heat flux from the atmosphere, freshening from the inflow of over 20 rivers, and net precipitation modified shelf waters during their transit along the shelf (none of these modifications are accounted for by the simple mixing calculation for predicted values). Likewise, simulated DIC on the SS is lower than its predicted value because outgassing occurred as the water travelled and biological activity converted inorganic carbon to organic carbon. Simulated SS water is on average 4$^{o}$C warmer and 30 mmol C m$^{-3}$ lower in DIC than on the ENS (black arrow in the left panel of Figure 4.2).

The GoM and GB show similar features as the SS. Simulated and predicted values of temperature and DIC for the GoM and GB are within the mixing polygon (Figure 4.2). Values for the GB lie between those of the ENS and SS (black arrow in Figure 4.2), whereas the GoM is more similar to Slp-S water. The higher slope water influence is also reflected in the mass fraction breakdown for the GoM (Figure 4.1C, Table S1) and is due to slope water mixing with shelf water in the GoM because of flow through the Northeast Channel (*Smith et al.*, 2001). Again, the simulated values for both GoM and GB are warmer, fresher, and lower in DIC compared to their respective predicted values.

The simulated values in each subregion are similar to the corresponding average observations (filled triangles) for all three properties (T, S, DIC). The largest difference between the observed and model-simulated values occurs in the GoM, where the model is approximately 4$^o$C cooler, possibly as a result of lower availability of winter observations in the GoM.

This analysis shows that the biogeochemical properties on the GB and SS are essentially set by the cold, carbon-rich subpolar waters from the LS and ENS, while a stronger influence of slope water is present in the GoM. The differences between the predicted and simulated values and the gradient in T and DIC values from the northernmost to the southernmost shelf region (ENS to GoM; Figure 4.2) illustrate that shelf waters are warming and losing inorganic carbon as they travel southwestward from the ENS, via both the GB and the SS, to the GoM.

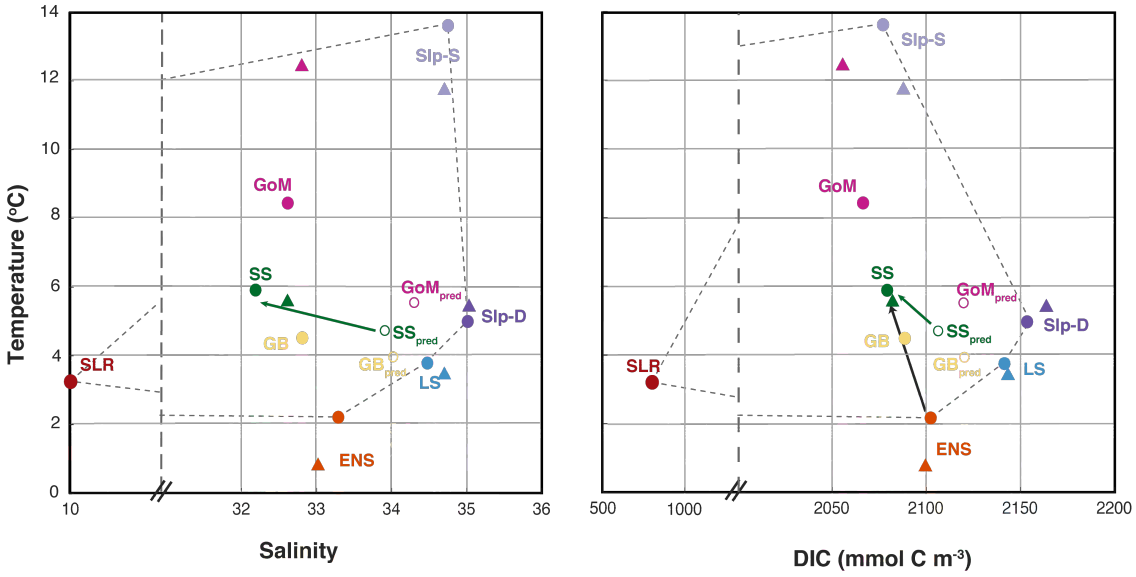


Figure 4.2: Points indicate the average T, S, and DIC throughout the water column for the different oceanic endmembers(ENS, LS, Slp-S, Slp-D), and the shelf regions (SS, GB, GoM). Predicted values are compared to simulated values for the shelf regions. Solid circles are model values, open circles are predicted values, and triangles are averaged observations. Observations for the GB were omitted because of low spatial and temporal coverage. Dashed lines indicate the mixing polygon.

### 4.5.2 Modifications in carbon saturation during southwestward transport

The modification of shelf-water properties during transit is analyzed further, focusing on three main properties in each of the shelf subregions: DIC, T, and the DIC disequilibrium DIC - $DIC_{eq}$. First, the model results were averaged in both time and space to obtain one mean profile for each of the regions (Figure 4.3).

LS water (blue) has higher DIC concentrations (by 50 to 75 mmol C $m^{-3}$) and colder water (by 5-10 $^{o}$C) in the upper 100 m compared to Slp water (purple), illustrating again the role of the LS as a cold, carbon-rich endmember. In the four shelf regions, DIC in the upper 60 m decreases in southwestward direction (from the ENS in orange to the GB in yellow to the SS in green and the GoM in pink) while DIC values below 60 m are very similar in the four shelf regions. This creates an increasing vertical gradient in DIC, which is likely a combination of outgassing of $CO_2$ at the surface and higher biological activity on the more southern shelf regions (i.e. biological drawdown of DIC in the surface, subsequent sinking of organic matter, and remineralization of DIC at depth).

The temperature profiles of the ENS, GB, and SS are all similar to the LS endmember, whereas the GoM is warmer throughout the water column. The ENS is the coldest region; it is about 2$^{o}$C cooler than the LS throughout most of the upper 100 m. Moving southward, the top 70 to 80 m are warming from the ENS to the GB, and the upper 100 m are warming when moving farther southward to the SS. These profiles of average temperature and DIC show again that shelf waters are warming and losing carbon at the surface as shelf water travels southwestward, consistent with the results in section 4.5.1 and Figure 4.2.

The profiles of carbon disequilibrium (DIC - $DIC_{eq}$, Figure 4.3) indicate over- or under-saturation of DIC with respect to equilibrium. The ENS and LS are both undersaturated, the ENS more so than the LS by about 10 to 15 mmol C $m^{-3}$, and mimicking the difference in temperature profiles between the ENS and LS (middle panel). Moving southward to the GB, water becomes less undersaturated with DIC - $DIC_{eq}$ ranging from 0 to about –25 mmol C $m^{-3}$. The change in saturation moving from ENS to GB is qualitatively similar to the change in temperature between the ENS and GB. The dashed yellow line shows the carbon disequilibrium on the GB if the water had not warmed during transit from the ENS to the GB (it was calculated using the ENS temperature profile and the GB DIC profile); it is more undersaturated and similar to the ENS disequilibrium. This analysis

shows that warming during transit shifts the water column closer to carbon equilibrium. Moving farther southward to the SS, the entire water column becomes oversaturated by 5-10 mmol C $m^{-3}$, again qualitatively similar to the changes in temperature that occurred as the water moved southward and consistent with the Scotian Shelf acting as a net source of $CO_2$. The green dashed line shows the carbon disequilibrium on the SS when using the ENS temperature profile. When removing the warming effect, water on the SS would be undersaturated, thus the oversaturation is the result of warming during transit. The GoM is near equilibrium (ranging from about –5 to 0 mmol C $m^{-3}$) throughout the water column.

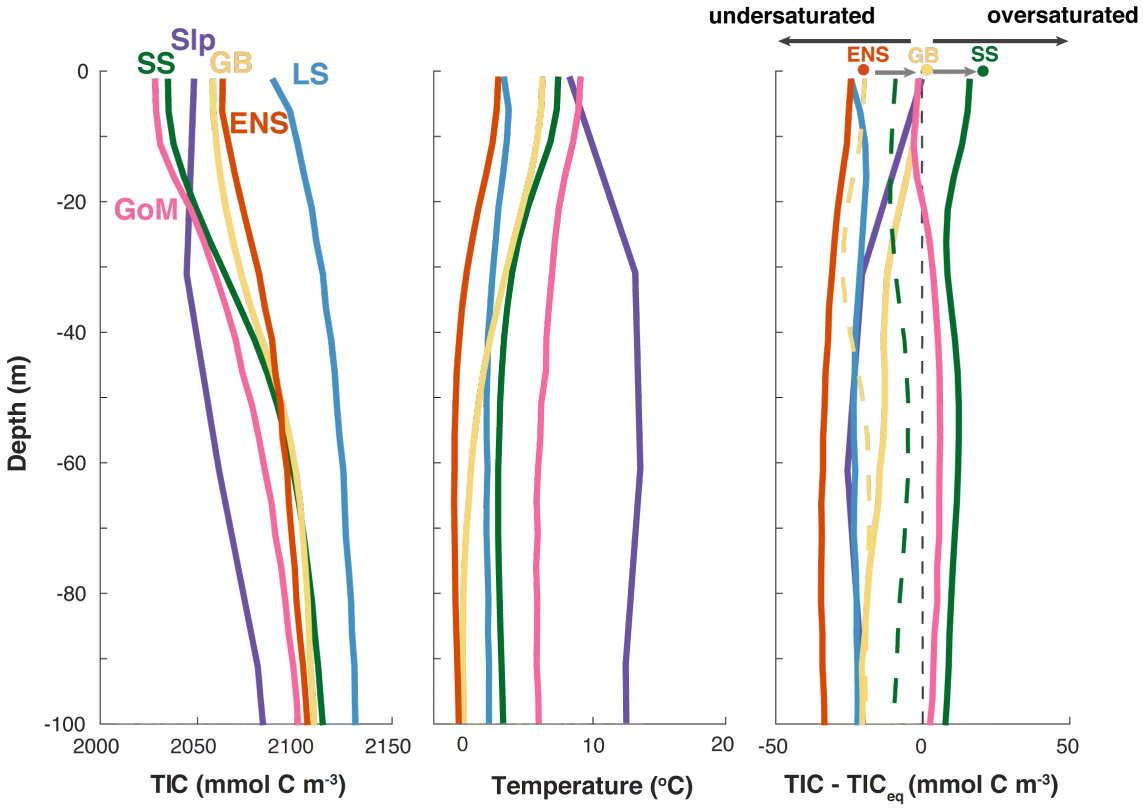


Figure 4.3: Horizontally and temporally averaged profiles of simulated (left to right) DIC (mmol C $m^{-3}$), temperature ($^o$C) and DIC – $DIC_{eq}$ (mmol C $m^{-3}$) in the six model subregions representing the two ocean end members (Slp and LS) and for the four shelf regions (ENS, GB, SS and GoM)are shown by the solid line. Dashed lines are DIC - $DIC_{eq}$ calculated using ENS temperature.

These analyses show that in the model, the GB is undersaturated with respect to carbon throughout the year and water column, and acts as a net sink of $CO_2$, the SS is oversaturated throughout the water column for most of the year and thus acts as a net source of $CO_2$ to the atmosphere, and the GoM is close to equilibrium throughout the water column with a

tendency towards undersaturation and acting as a weak net sink of $CO_2$.

## 4.6 Discussion and conclusion

The main objectives of this study were to resolve conflicting reports about the sign of the air-sea flux on the Scotian Shelf and to elucidate the transport and transformation processes that explain why this region behaves as a source of $CO_2$ (*Shadwick et al.*, 2010, 2011; *Shadwick and Thomas*, 2014) and deviates from the global pattern (*Laruelle et al.*, 2013; *Roobaert et al.*, 2019). We hypothesized that the cold, carbon-rich subpolar North Atlantic waters that move onto the East Newfoundland Shelf from the Labrador Sea and continue southwestward in along-shelf direction across the Grand Banks to the Scotian Shelf and Gulf of Maine (*Rutherford and Fennel*, 2018) become oversaturated with $CO_2$ as they travel due to warming. This hypothesis can be broken into two testable parts: (1) that these cold, carbon-rich subpolar North Atlantic waters are the main contributor to Scotian Shelf water, and (2) that the shelf waters warm as they travel and subsequently become oversaturated with DIC.

The first part is addressed using passive dye tracers in our regional model. An analysis of simulated dye tracer mass fractions on the Scotian Shelf shows that subpolar waters from the East Newfoundland Shelf and the Labrador Sea are present in high proportions on the Scotian Shelf (73%; Figure 4.1). We showed that the temperature, DIC, and salinity signatures of the Scotian Shelf can largely be explained by the mixing of these dominant endmembers (Figure 4.2 and 4.3).

Of course, modifications are occurring as the water travels southwestward, which is the second part of our hypothesis. These modifications are evident in our endmember analysis of simulated and observed properties. Specifically, the model-simulated temperature and DIC for the Scotian Shelf are lower than the predicted values (Figure 4.2) which indicates that loss of inorganic carbon due outgassing and/or biological activity and warming must have occurred during transit. These modifications are also evident in the DIC decrease of 30 mmol C $m^{-3}$ and warming of $4^{o}$C between the East Newfoundland Shelf and Scotian Shelf profiles (Figure 4.2). In the model, the cold, carbon-rich subpolar waters warm throughout the water column as they transit to the Scotian Shelf (Figures 4.3). Biological production strengthens the vertical DIC gradient compared to shelf regions upstream of the Scotian Shelf, enhancing DIC at depth. This leads to oversaturation of carbon and

drives the observed outgassing throughout much of the year on the Scotian Shelf (see Supporting Information, Figure C.3). It is important to note that the model has been thoroughly validated and found to represent observed features reasonably well (*Brennan et al.*, 2016; *Laurent et al.*, 2021; *Rutherford et al.*, 2021) and that the present study results are backed by observations. We believe these model results can therefore be extended to make inferences about the real system and that the evidence presented confirms our hypothesis, which we henceforth refer to as a mechanism.

Central to this mechanism explaining the observed mid-latitude outgassing is the location of the Scotian Shelf downstream of the carbon-rich Labrador Sea, the relative isolation of shelf waters from the adjacent open ocean by the shelf-break current, and the warming as water travels southwestward on the shelf. The outgassing of $CO_2$ on the Scotian Shelf makes it an outlier not only in the global pattern, but even compared to its neighbouring shelf regions. Water on the more northern Grand Banks does not experience enough warming to become oversaturated, whereas the Gulf of Maine is more heavily influenced by Gulf Stream water and thus weakly undersaturated. The air-sea flux both on the Grand Banks and in the Gulf of Maine is similar to other mid- and high-latitude shelves (see Supporting Information, Figure C.4).

Our model simulates outgassing of $CO_2$ of $+1.7\pm0.2$ mol C $m^{-2}$ $yr^{-1}$ for the Scotian Shelf in a marked deviation from the global $CO_2$ flux pattern (Figure C.4), reported to be in the range of $-1$ to $-3\pm0.2$ mol C $m^{-2}$ in *Roobaert et al.* (2019) for similar latitudes. The discrepancy is partly explained by the fact that Previous estimates for the Scotian Shelf (e.g. *Laruelle et al.*, 2014; *Roobaert et al.*, 2019) used SOCAT database versions that did not include high-resolution observations for the Scotian Shelf from a CARIOCA buoy (*Shadwick et al.*, 2011; *Shadwick and Thomas*, 2014) and a volunteer observing vessel (*Rutherford et al.*, 2021). Without the inclusion of such high-resolution observations, the estimates from these global studies come with large uncertainty (*Gruber*, 2015), and the Scotian Shelf is merely one example of this.

Global models often do not resolve the circulation structure that drives the Scotian Shelf outgassing, therefore misrepresenting its air-sea $CO_2$ flux. Typical model resolutions in global models (for example, $\sim$38 km in *Bourgeois et al.*, 2016, vs. $\sim$10 km in our model) are insufficient to accurately represent small-scale coastal dynamics including the shelf-break current. As a result, residence times in the region can be underestimated;

compare, for example, 12-36 days in *Bourgeois et al.* (2016) to 3 to 6 months in our model (see *Rutherford and Fennel*, 2018) for the same region. This likely applies to all models of similar resolution and might be an argument for parameterizing these processes in coarser-resolution models to more accurately represent coastal air-sea $CO_2$ fluxes.

Although each shelf region is unique in its location and specific geometry, there may be other subpolar or subantarctic shelves that behave similar to the Scotian Shelf if supplied with cold, carbon-rich polar or subpolar water, for example, the Patagonian Shelf in the southwestern South Atlantic Ocean. The Patagonian Shelf is wide (120 to 300 km) and located at the confluence of the subtropical Brazil Current and subantarctic Malvinas Current, which is a branch of the Circumpolar Current (*Liu et al.*, 2010). The physical and chemical properties of the shelf can be fully explained by subantarctic water masses derived from the Malvinas Current, which is nutrient rich (*Liu et al.*, 2010). Temperature ranges from 7 to 20$^o$C seasonally and spatially, only slightly less pronounced than the seasonal cycle on the Scotian Shelf (*Liu et al.*, 2010). There are only few $pCO_2$ observations in SOCAT for the Patagonian Shelf, hence another large $CO_2$ source to the atmosphere might be missed.

We have presented a novel approach for addressing the 3D nature of coastal processes affecting air-sea carbon flux. The approach utilizes passive dye tracers in a regional biogeochemical model to trace the pathways and mixing ratios of water masses in connection with their temperature, salinity, and inorganic carbon properties and allows one to analyze how regional circulation in connection with modification of water properties along their transit pathways affects the source or sink behaviour of a continental shelf region. By applying this approach to the northwest North Atlantic we have provided, for the first time, a plausible mechanism that explains why the Scotian Shelf acts as a large source of $CO_2$. We advocate for this approach to be applied to all shelf regions to better understand their respective source-sink behaviours. A high-latitude shelf region that deserves particular attention is the Patagonian shelf because it shares the major characteristics that make the Scotian Shelf a large source of $CO_2$ and is fairly underrepresented in the SOCAT data set.

# CHAPTER 5

# SHIFTING CIRCULATION UNDER A CHANGING CLIMATE: BIOGEOCHEMICAL IMPACTS IN THE NORTHWEST NORTH ATLANTIC

## 5.1 Introduction

The northwest North Atlantic shelf at the eastern Canadian seaboard has recently been experiencing warming that exceeds the global trend (*Pershing et al.*, 2015; *Brickman et al.*, 2018; *Alexander et al.*, 2020; *Neto et al.*, 2021) and projections of the region have shown that it will potentially continue to warm at a rate that is three times the global average over the next century (*Saba et al.*, 2016). In addition to the rapid warming, the biogeochemistry of the region is also evolving quickly. Declining oxygen has already been reported on the Scotian Shelf and in the Gulf of St. Lawrence (*Gilbert et al.*, 2010; *Lavoie et al.*, 2019), at rates of –1.19 $\pm$0.45 $\mu$ M yr$^{-1}$ and –0.51 $\pm$ 0.24 $\mu$ M yr$^{-1}$, respectively (*Claret et al.*, 2018). pH has also already declined by approximately 0.2-0.3 units both on the Scotian Shelf and into the Gulf of St. Lawrence Estuary (*Curran and Azetsu-Scott*, 2012; *Mucci et al.*, 2011).

It has been speculated that some of these changes are linked to changes in the regional circulation structure. Here, the subpolar and subtropical gyres of the North Atlantic converge (Figure 5.1), strongly influencing the adjacent continental shelf (*Loder et al.*, 1997; *Hannah et al.*, 2001). North of Cape Hatteras the shelf is primarily influenced by the Labrador Current System (LCS), which carries cold, oxygen- and carbon-rich subpolar

North Atlantic waters southwestward (*Loder et al.*, 1998; *Fratantoni and Pickart*, 2007) and limits cross-shelf exchange (*Loder et al.*, 2003; *Hannah et al.*, 1996; *Rutherford and Fennel*, 2018). The outer branch of the LCS traverses along the shelf break and is forced to turn southwestward at the Tail of the Grand Banks to form the shelf-break current along the Scotian Shelf, separating shelf water from warm and salty slope waters (*Beardsley and Boicourt*, 1981; *Loder et al.*, 1998; *Fratantoni and Pickart*, 2007). The slope water is a mixture of water masses but retains a strong signature from the northeastward transiting Gulf Stream. The recent warming on the Scotian Shelf is often linked to increased inflow of these warm, salty slope waters (e.g. *Brickman et al.*, 2018; *Neto et al.*, 2021). In fact, the projections reported in *Saba et al.* (2016) indicate there could be a decline in the transport of the LCS over the next century, which would lead to an even larger influence of warm, salty slope waters on the shelf and enhanced warming. The effect of increased slope water inflow is not just observed in temperature changes. Studies have also speculated that recent deoxygenation on the shelf could be linked to a stronger influence of oxygen-poor Gulf Stream water, versus oxygen-rich subpolar North Atlantic waters (*Gilbert et al.*, 2005; *Sherwood et al.*, 2011). *Claret et al.* (2018) additionally suggested that there could be a large decline in the influence of the LCS on the shelf over the next century, which would be tied to a weaker shelf-break current, increases of warm, salty water on the shelves, and subsequent deoxygenation.

The link between any future changes to the regional circulation and the shelf-wide carbonate chemistry, however, does not seem to be well established yet. At present, the Scotian Shelf is tightly tied to the delivery of carbon-rich subpolar North Atlantic waters that are traveling southwestward along the shelf (*Rutherford and Fennel*, subm.), with little modification from cross-shelf exchange due to the dominant shelf-break current (*Rutherford and Fennel*, 2018). This system results in a unique air-sea $CO_2$ flux signal on the Scotian Shelf, which deviates from the global latitudinal flux trend (for example *Laruelle et al.*, 2014; *Roobaert et al.*, 2019) by acting as a large net source of $CO_2$ (*Shadwick et al.*, 2010; *Shadwick and Thomas*, 2014; *Rutherford et al.*, 2021). It is thus reasonable to assume that any future change in the shelf-break current, leading to increased inflow of warm, salty slope water, would have a large impact on the carbonate chemistry. Recently, *Salisbury and Jönsson* (2018) decomposed the pH signal in the Gulf of Maine, specifically in relation to increasing warm and salty water on the shelf region. They found

that the higher temperature and salinity were essentially mitigating the long-term ocean acidification signal in the Gulf. These results imply that perhaps increased warm, salty inflow onto the shelf are not solely tied to negative impacts, as one might assume from only looking at the temperature and oxygen signals as in *Saba et al.* (2016) and *Claret et al.* (2018), respectively. The overarching goal of this work is therefore to address the question: what happens to the shelf-wide carbonate chemistry (including air-sea $CO_2$ flux and pH) if the shelf-break current vanishes under a climate change scenario?

There is a wide range in climate predictions for the northwest North Atlantic. For example, the high-resolution Geophysical Fluid Dynamics Lab (GFDL) CM2.6 climate model has been reported to predict large declines in the amount of subpolar North Atlantic waters transiting southwestward via the LCS and an almost complete disappearance of the Scotian Shelf's shelf-break current, leading to increased contributions of slope water onto the shelves (see for example *Saba et al.*, 2016). Conversely, Canada's Department of Fisheries and Oceans (DFO) presents a large-scale model of the North Atlantic that predicts minimal changes to the system's circulation (see *Brickman*, 2016, for model details). Although these are only two examples, they encapsulate the range of possible outcomes for the region (i.e. nearly a complete disappearance of the shelf-break current versus essentially present-day conditions) and we can use them as two extreme cases to compare and contrast to answer the overarching question of this study. It is important to use regional models for future projections, especially in dynamic regions with complex circulation features, as they are better able to capture the small-scale features. Specifically for the northwest North Atlantic, regional models such as ours have been shown to better capture the placement and strength of the Labrador Current (e.g. *Rutherford and Fennel* 2018 vs. *Bourgeois et al.* 2016) and more accurately represent the biology compared to global models (*Laurent et al.*, 2021) under present-day conditions. We therefore downscale the two large-scale models to our high-resolution regional model of the northwest North Atlantic to best approach the goals of this study.

At present, inflow of warm, salty slope water only transits onto the shelf through deep basins and channels, for example through the Northeast Channel into the Gulf of Maine and into the Gulf of St. Lawrence through the Laurentian Channel (*Smith et al.*, 2001; *Rutherford and Fennel*, 2018; *Mountain*, 2012). As a result, the more southern shelf regions (i.e. Gulf of Maine) are more strongly influenced by warm, salty slope water

than their more northern counterparts (i.e. Grand Banks, Scotian Shelf; *Rutherford and Fennel*, 2018). Recently observed increases of slope water inflow onto the Scotian Shelf tend to be focused on the central and southwestern portions of the shelf. For example, in 2011-2012, it was reported that warm, salty inflow created warm anomalies ($\sim$4-6$^o$C in bottom waters) on the southwestern Scotian Shelf (*Gawarkiewicz et al.*, 2012), impacting the snow crab population and commercial fishery (*Zisserson and Cook*, 2017). *Claret et al.* (2018) also focus on the central Scotian Shelf as a region with large deoxygenation potentially tied to inflow of warm, salty slope water. We therefore hypothesize that under a future scenario with a complete removal of the shelf-break current, there will be large inflow of slope water onto the southwestern half of the Scotian Shelf and that the Scotian Shelf as a whole will biogeochemically behave more similarly to the Gulf of Maine, and less like the Grand Banks and East Newfoundland Shelf, as it does at present day. Based on *Salisbury and Jönsson* (2018), we also expect regions with more warm, salty inflow to have less acidification and regions with cool, fresh water to have higher acidification.

To test these hypotheses, we apply the same biological future changes (from GFDL CM2.6) to both of the downscaled scenarios. This allows us to contrast how the different circulation features in the two scenarios affect the carbonate chemistry. We downscale the GFDL and DFO scenarios using the same regional model for mid-century time slices ($\sim$2075) and compare the resulting two future states to the present-day conditions reported in *Brennan et al.* (2016a); *Laurent et al.* (2021); *Rutherford and Fennel* (2018); *Rutherford et al.* (2021), and *Rutherford and Fennel* (subm.). More specifically, in this study we: (1) calculate differences in along-shelf transport; (2) implement passive dye tracers, as in *Rutherford and Fennel* (2018), to quantify changes in water mass composition; (3) estimate the effects of circulation-only changes via endmember mixing, as in *Rutherford and Fennel* (subm.); (4) compare DIC, pH, and air-sea $CO_2$ flux between the scenarios; and (5) compare acidification in regions with higher contributions of warm, salty slope water versus those with higher subpolar North Atlantic water contribution.

## 5.2 Methods

### 5.2.1 Regional model description

We employ a regional biogeochemical model of the northwest North Atlantic that has 30 vertical levels, $\sim$10 km horizontal resolution, and is based on ROMS v3.5, which is a

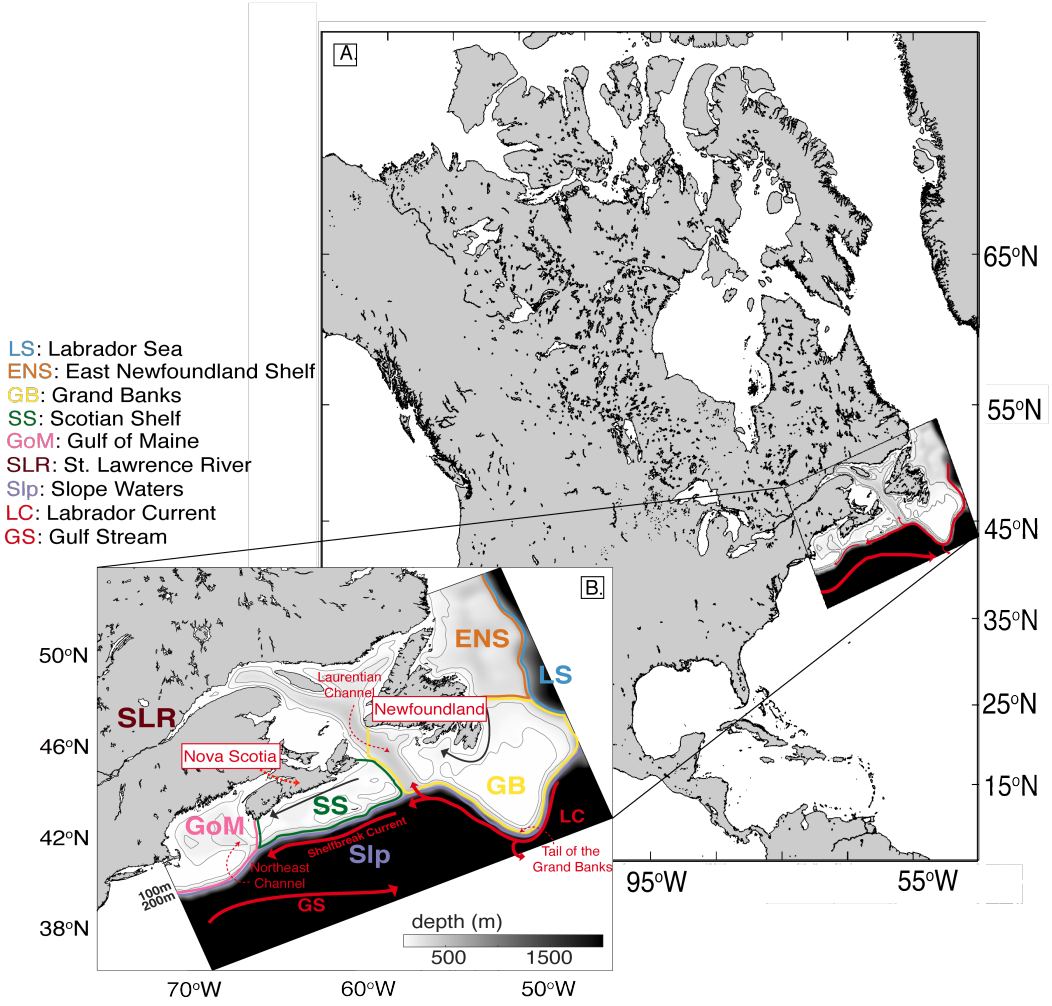


Figure 5.1: (A) Map of North America with the location of the regional model indicated. (B) Regional model domain with shelf regions and dye tracer initialization regions indicated.

terrain-following, free-surface, primitive equation ocean model (*Haidvogel et al.*, 2008). The model domain includes the Gulf of Maine, Scotian Shelf, Grand Banks, and East Newfoundland Shelf (Figure 4.1). *Brennan et al.* (2016a) and *Rutherford and Fennel* (2018) describe the physical model setup and validation, and have shown that the model represents present-day circulation patterns reasonably well. The biogeochemical model is of medium complexity, including two phytoplankton and two zooplankton groups, and is fully described in *Laurent et al.* (2021) and is based on the model described in *Fennel et al.* (2006, 2008). Descriptions and validation of the biological and inorganic carbon component are given in *Laurent et al.* (2021) and *Rutherford et al.* (2021), who show that

the model represents the present-day biological seasonality well. The present-day model ran for 16 years from 1999 to 2014, where the first year is considered model spin-up. We focus on model years 2006 to 2014 in the present study.

### 5.2.2 Downscaling of larger scale models

Two large-scale models were downscaled to our regional model in alternative future scenarios: the Geophysical Fluid Dynamics Lab (GFDL) global climate model CM2.6 (*Delworth et al.*, 2012; *Winton et al.*, 2014; *Dufour et al.*, 2015), and the Department of Fisheries and Oceans NEMO model (BNAM) of the North Atlantic (*Brickman*, 2016; *Brickman et al.*, 2018; *Wang et al.*, 2019; *Brickman et al.*, 2021). A 16-year future time slice, representing mid-century conditions ($\sim$2075), was run for each model. Both models were initialized in 2065 by adding deltas (2065 minus 1999 conditions) to the 1999 conditions for temperature (T), salinity (S), horizontal momentum (U, V), sea-surface height (SSH), dissolved inorganic carbon (DIC), nitrate ($NO_3$), and oxygen ($O_2$). More specific details about each model and the corresponding downscaling techniques are given below. The last 8 years of each future time slice are analyzed, allowing for 8 years of spin-up. Daily 3D model output of biogeochemical properties, dye tracers, salinity, and temperature was saved.

The GFDL CM2.6 climate model is a coupled atmosphere-ocean-ice model, which is fully described in *Delworth et al.* (2012), *Winton et al.* (2014) and *Dufour et al.* (2015), whose ocean component (MOM5) has $1/10^o$ resolution and 50 vertical levels. GFDL performed 2 different simulations: (1) a pre-industrial control scenario, which is an 80-year simulation with atmospheric $CO_2$ held constant at pre-industrial concentrations; and (2) a warming scenario with $CO_2$ doubling where $CO_2$ is increased at an annual rate of 1% until it is doubled (model year 70), at which point atmospheric $CO_2$ is held constant for an additional 10 years. During the doubling period, atmospheric $CO_2$ roughly follows RCP 6 conditions (see *Claret et al.*, 2018).

From the GFDL warming scenario, monthly output of all physical variables (T, S, U, V, SSH) and atmospheric forcing were interpolated to the regional model grid using objective analysis. After interpolation, the mean annual cycle was calculated over the 80-year simulation at each grid cell for both the oceanic and atmospheric variables and was removed, leaving de-seasoned gridded data. The time dimension of this de-seasoned data was then stretched so that the doubling trajectory of atmospheric $CO_2$ closely resembles

that of the RCP 6 scenario (following *Claret et al.*, 2018). This results in CM2.6 time being stretched by a factor of 1.903 ($t_{rcp6} = 1.903t_{cm26} + 1947.5$) to equal RCP 6 time. The initial file for the time slice was calculated from the de-seasoned monthly means and temporally stretched gridded data by adding the difference between 2065 and 1999 for each of the physical variables to the 1999 initial file and the model was run for 16 years starting in 2065.

The DFO BNAM ocean model was developed to better resolve the intraction of the Gulf Stream and Labrador Current at the Tail of the Grand Banks and is fully described in *Brickman* (2016), *Brickman et al.* (2018), *Wang et al.* (2019), and *Brickman et al.* (2021). The BNAM model is based on NEMO-OPA code (*Madec*, 2008) and covers 7-75$^o$N latitude and 100$^o$W-25$^o$E with 1/12-degree resolution and 50 z-levels (*Brickman et al.*, 2021). Details of their future simulations and methods are given in *Brickman* (2016) and *Brickman et al.* (2021), which describes how they used six CMIP5 ESMs to simulate various future periods using the delta method. Used here are the climatological difference from the 2066-2085 period minus 1999 from their RCP 8.5 simulation. These differences were supplied from the BNAM model at the boundaries of our domain for all physical variables (T, S, SSH, U, V) and for surface forcings (air temperature and precipitation). These differences were interpolated to the regional model grid and added to the present day (1999 conditions) for all physical variables and surface forcings. The initial file was calculated by averaging the difference between the 2066-2085 period minus 1999 from all of the boundary point profiles for each variable, which were then added to the 1999 present-day initial file. The model was run for 16 years, simulating the average conditions between 2066-2085 in the larger model, which is a similar period to the GFDL model time slice.

The same biological initial and boundary conditions were applied to both future scenarios. These biological conditions were taken from the GFDL CM2.6 biogeochemical model (miniBLING, see *Galbraith et al.*, 2015; *Dufour et al.*, 2015) output which is only available for the last 20 years of both the control and $CO_2$ doubling experiment (model years 60-80, which is approximately equal to RCP 6 years 2060-2100) as 3D annual means. The variables DIC, $O_2$, and $PO_4$, the latter of which was converted to $NO_3$ using the Redfield Ratio, were interpolated to the regional model grid through objective analysis. The difference between the $CO_2$ doubling experiment and the control simulation over

model years 61-70 (equal to years 2065-2080 in RCP6 years) was calculated at every grid cell and averaged throughout that time period to get one biological delta, essentially estimating the difference between the 2065-2080 period and 1999. The average difference over this period was added to the 1999 initial file and boundary conditions in both scenarios. This approach assumes that the bulk of the biological changes between the control and $CO_2$ doubling experiment occur after 1999, and could therefore slightly overestimate any biogeochemical changes. In both simulations, atmospheric $pCO_2$ was set to follow RCP 6 conditions with the present-day seasonal cycle imposed (see Supporting Information in *Rutherford et al.*, 2021, for the present-day seasonal cycle).

Henceforth, the BNAM scenario, which still has the shelf-break current (SC) in tact, will be referred to as "Case 1: strong SC". The GFDL CM2.6 scenario, with near disappearance of the shelf-break current, will be referred to as "Case 2: weak SC".

### 5.2.3 Dye tracer implementation

We additionally implemented passive dye tracers in each of the time slices, the setup of which is described in detail in *Rutherford and Fennel* (2018); the dye tracer source regions are shown in Figure 5.1. As in *Rutherford and Fennel* (2018), two types of dye tracer simulations were performed: (1) dye tracers were initialized once after model spin-up and allowed to advect and diffuse throughout the model domain, and used to visualize and quantify changes to dye tracer pathways; and (2) dye tracers were constantly reinitialized in their source region as a constant supply of the dye tracers, used to calculate dye tracer mass fractions on each of the shelves of interest (Grand Banks, Scotian Shelf, and Gulf of Maine). Dye tracer mass fractions were used to calculate predicted values of temperature, salinity, and DIC for each of the shelf regions, as in *Rutherford and Fennel* (subm.). These predicted values indicate shelf properties if only simple mixing was occurring and are calculated as a simple weighted mean. Two types of predicted values were calculated in the present study using the future scenario mass fraction composition: firstly, the "true" future predicted value, which uses the future scenario mass fractions with the future scenario endmember values, and secondly, a predicted value that uses the future scenario mass fraction composition with the present-day endmember values. This second type of predicted value tells us the effect of mixing without any atmospheric inputs affecting the endmember values. In other words, it hints how just circulation changes would impact the continental shelves here.

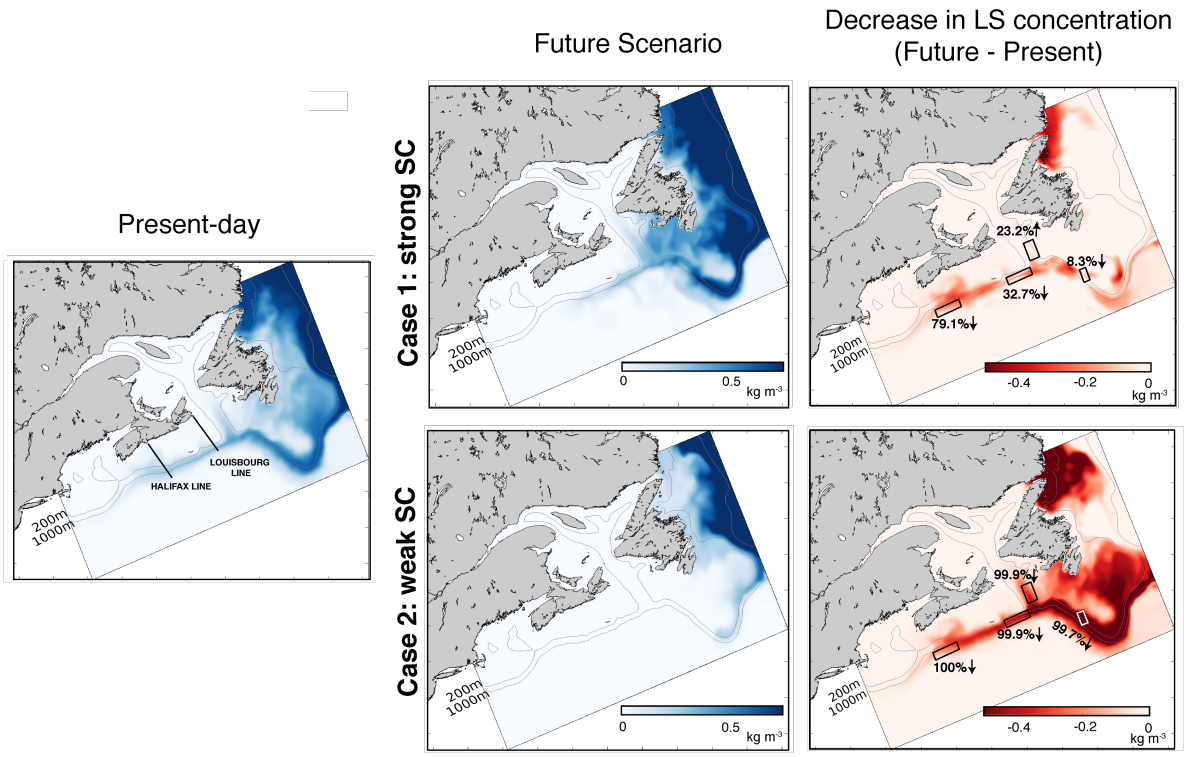


Figure 5.2: Time slices of vertically averaged concentration of LS dye in present day (left panel) versus two future (middle panels) scenarios at about 9 months after dye tracer initialization. Right panels show the decrease in vertical mean LS dye concentration between future and present day. Four boxes indicate regions of interest with the average % decrease in water-column-averaged LS dye.

## 5.3 Results

### 5.3.1 Projected changes to along-shelf transport and water-mass composition

Simulation of passive dye tracers in the different time slices allows us to visualize and quantify changes in the circulation under the different future scenarios. Of particular interest are any changes to the Labrador Current System and its southwestward transport along the shelf. Figure 5.2 shows the distribution of Labrador Sea (LS) dye, which best marks the shelf-break current, about 9 months after dye initialization in the present and two future scenarios (Case 1 with a strong SC vs. Case 2 with a weak SC). In the present-day simulation (Figure 5.2a), the shelf-break current is intact, following the shelf edge from the Grand Banks southwestward along the Scotian Shelf. In both future scenarios, the amount of LS dye moving along the shelf break declines. In Case 1 (strong SC), there is a

~33% decrease in the northern portion and ~79% decrease in the southern portion of the shelf break (Figure 5.2). In the Case 2 (weak SC), LS dye disappears entirely along the Scotian Shelf, at the Tail of the Grand Banks, and in the Laurentian Channel (Figure 5.2f).

The along-shelf volume transport is shown in Figure 5.3 for the present day (both from the model and observations from *Loder et al.*, 1998) and the two future scenarios. Transport in the present day and Case 1 is similar with only a 20% decrease in transport at the tip of Grand Banks (GB2 section), and 19% and 15% decreases in transport along Scotian Shelf sections SF1 and SF2, respectively, in the future. In Case 2, along-shelf transport at the SF1 and SF2 sections is drastically reduced (by 92% and 87%, respectively) with a smaller reduction of 12% at GB2. The drastic reduction in southwestward along-shelf volume transport is consistent with the disappearance of LS dye along the Scotian Shelf in the Case 2 (weak SC) scenario (Figure 5.2).

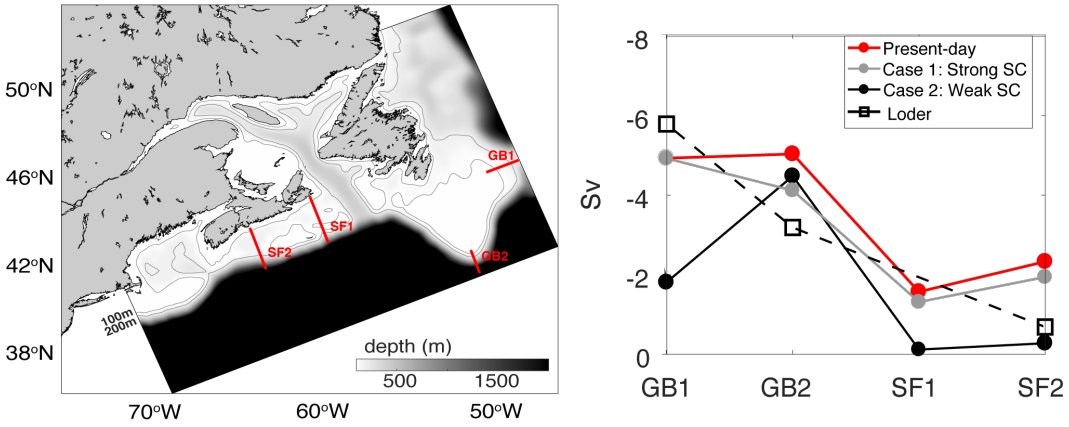


Figure 5.3: Volume transport (Sv) along the shelf of the northwest North Atlantic. Left panel indicates the locations the transport was calculated. The right panel compares the average volume transport at 4 different locations along the shelf between present day (red), Case 1 (strong SC) future scenario (grey) and Case 2 (weak SC) future scenario (black). Open squares indicate observations from *Loder et al.* (1998).

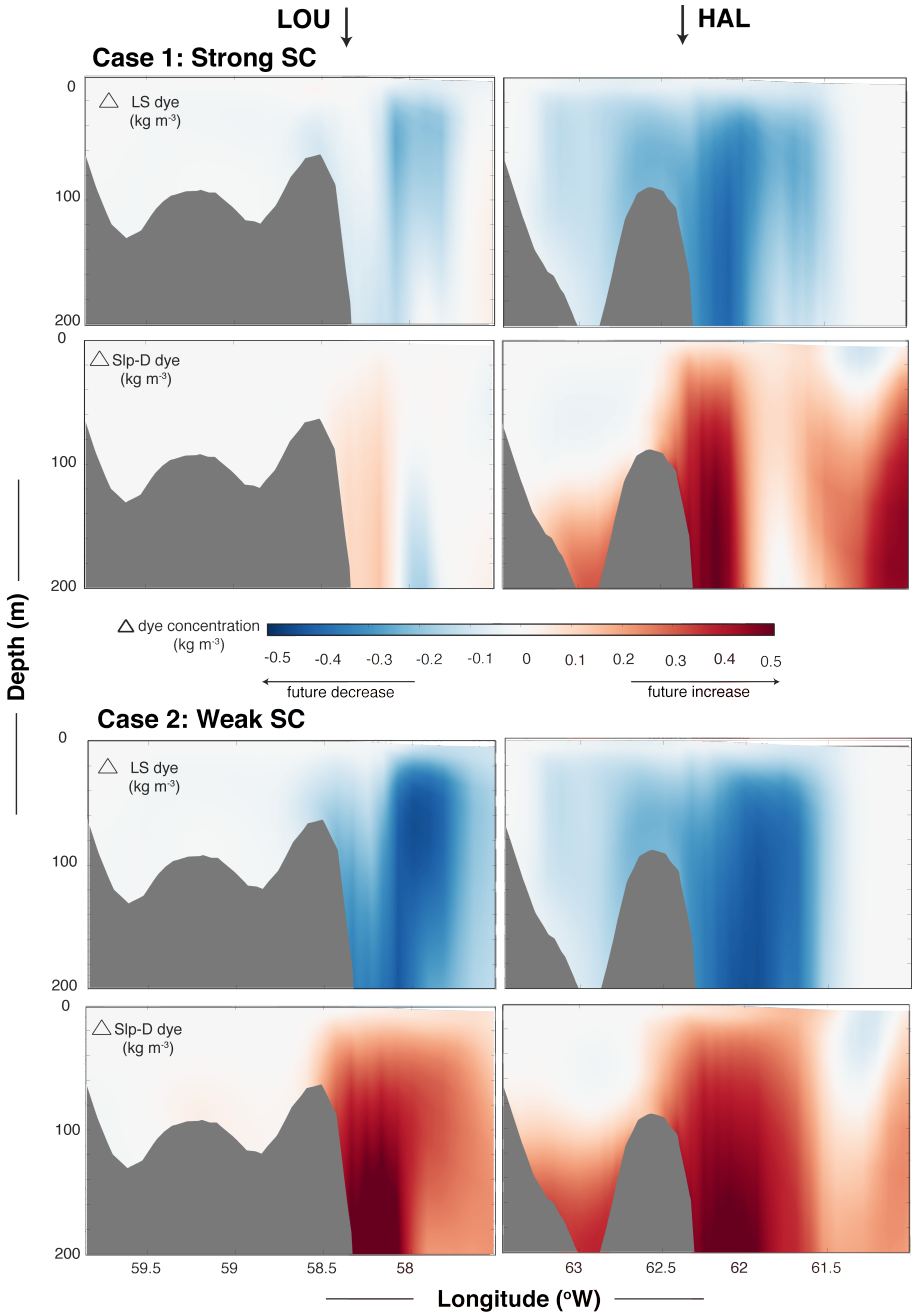


Figure 5.4: Changes in LS and Slp-D dye concentration in 2 transects (indicated in Figure 5.2) along the Scotian Shelf. Negative values (red for LS, green for Slp-D) indicate a decrease and positive (blue for LS, purple for Slp-D) values indicate an increase in LS dye concentrations in the future. Top panels are Case 1 (strong SC scenario) and bottom panels are Case 2 (weak SC scenario).

With less LS dye moving southwestward in both scenarios, the presence of deep-slope water (Slp-D) dye increases on the Scotian Shelf, particularly in the deep basins, and along the shelf break (Figure 5.4), especially on the Halifax (HAL) transect. This is more pronounced in Case 2 (weak SC), where a larger fraction of LS dye is replaced by Slp-D dye on the Scotian Shelf and along the shelf break. This replacement is also reflected in the dye tracer mass fractions, which provide more comprehensive information about the changes in composition of shelf waters (Table D.1 and Figure 5.5). In Case 1 (strong SC), the composition of water on the shelf is similar to present day with only modest changes in the ratio of Slp water to LS and Eastern Newfoundland Shelf (ENS) water throughout the shelf region and slight increases in the fraction of Slp water on the Grand Banks (roughly 1:6 ratio of Slp:LS+ENS at present vs. roughly 1:5 at 2075) and the Scotian Shelf (1:3 ratio of Slp:LS+ENS at present vs. between 1:2 and 1:3 at 2075). In the Case 2 (weak SC), the ratio of Slp water to LS+ENS water increases markedly on both the Scotian Shelf (1:3 of Slp:LS+ENS at present vs. roughly 1:1 at 2075) and in the Gulf of Maine (2:3 of Slp:LS+ENS at present vs. 2:1 at 2075), with less Slp water increases on the Grand Banks (1:6 of Slp:LS+ENS at present vs. 1:3 at 2075).

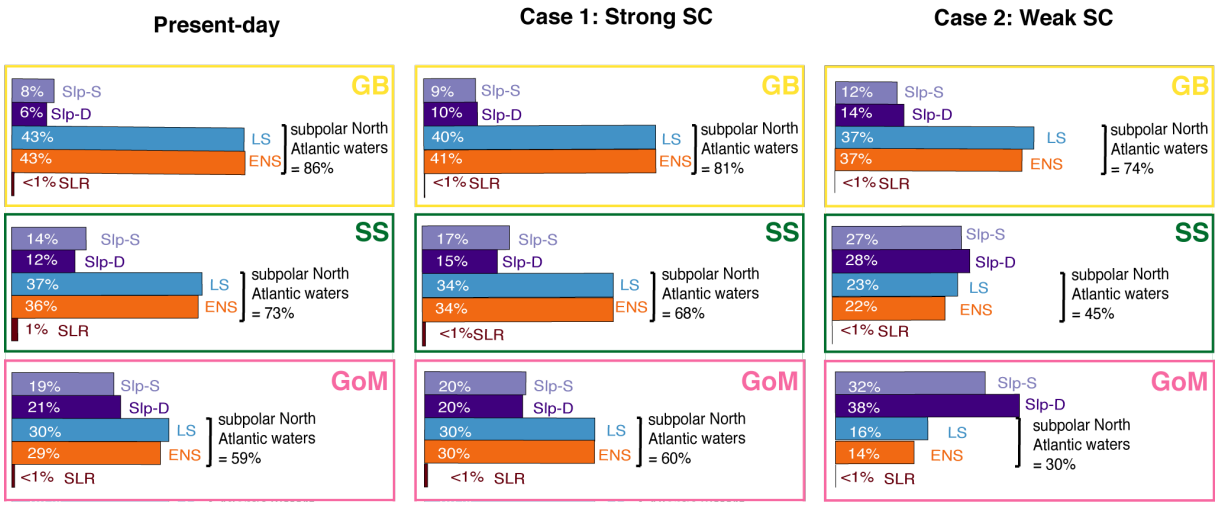


Figure 5.5: Mass fractions for (top to bottom) Grand Banks (GB), Scotian Shelf (SS), and Gulf of Maine (GoM) in each time slice: (left to right) present day, Case 1 (strong SC future scenario) and Case 2 (weak SC future scenario). Endmembers and shelf locations are indicated in Figure 5.1.

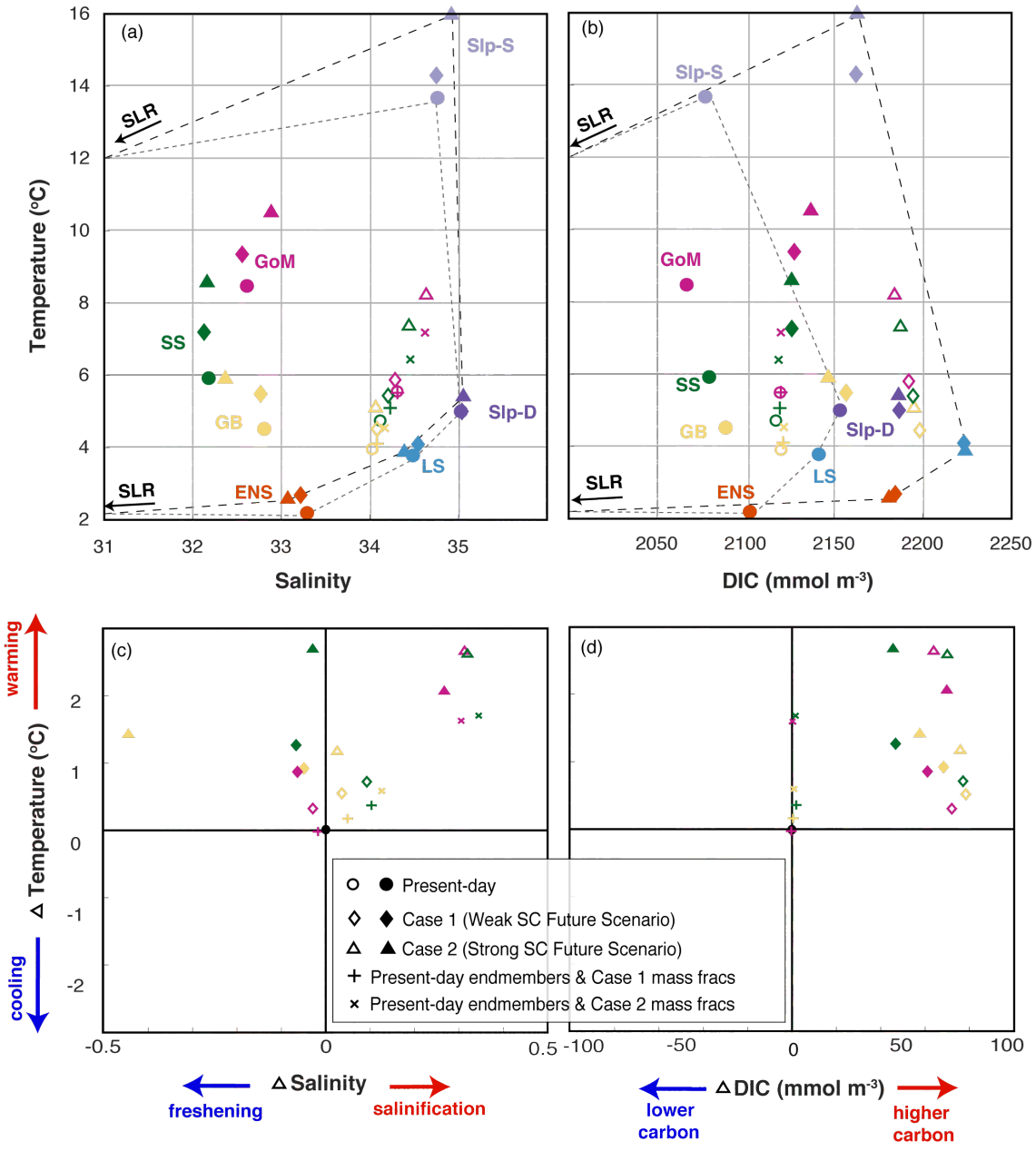


Figure 5.6: (a) T-S and (b) T-DIC diagrams, with different symbols indicating different simulations (circles = present day; diamonds = Case 1; triangles = Case 2). Open symbols indicate predicted values and filled symbols indicate actual simulated values. Panels (c) and (d) indicate changes in temperature, salinity and dissolved inorganic carbon (DIC) between the future and present-day values (future minus present).

The left panel in Figure 5.6 shows the resulting average changes (throughout space and time) to temperature (T) and salinity (S) in the subregions defined in Figure 5.1 for both future scenarios. Although every ocean end member warmed, the most notable warming is in Slp-S ($\sim$+2$^o$C) and ENS (+0.75$^o$C); the latter also became slightly fresher (by $\sim$ 0.2). The other end members (LS, Slp-D) warmed by $<$0.5$^o$C and $<$0.1 salinity units on average. As a result, the mixing polygon is similar between the present and future. The shelves (GB, SS, GoM) all have larger changes in T and S compared to the end members, particularly in terms of warming. GB has fewer differences between the scenarios, with similar warming (by about 1 to 1.5$^o$C) but larger salinity changes in Case 2 with decreases of about 0.45 in Case 2 (weak SC) vs 0.05 in Case 1 (strong SC). The SS and GoM are both warmer by 1$^o$C in Case 1 and 2 to 2.5$^o$C in Case 2. The mean changes in SS salinity are the same in both scenarios (decreasing by about 0.05; Figure 5.6) but the GoM becomes saltier in Case 2 by 0.25 versus fresher in Case 1 by about 0.05 to 0.1.

Average changes to surface temperature were relatively similar between the scenarios, with slightly more warming in Case 1 with a strong SC (by 2.7, 2.1, and 1.8$^o$C on the Scotian Shelf, Grand Banks, and Gulf of Maine, respectively) versus in Case 2 with a weak SC (by 2.2, 1.3, and 1.6$^o$C, on the Scotian Shelf, Grand Banks, and Gulf of Maine, respectively). Average changes to surface salinity were similar for the Scotian Shelf between the two scenarios (–0.15 in Case 1 vs. –0.19 in Case 2) but diverged for Gulf of Maine (–0.13 for Case 1 vs. +0.27 for Case 2) and Grand Banks (–0.11 for Case 1 vs –0.58 for Case 2), similar to the results shown in Figure 5.6. The differences between the two scenarios are perhaps most obvious when considering bottom waters (Figure 5.7) and illustrate the effects of the changes in circulation and water mass composition shown in Figures 5.2-5.5. There is increased warming in bottom waters throughout the shelf in Case 2 (on average by 2.8, 2.2, and 1.3$^o$C for the Scotian Shelf, Gulf of Maine, and Grand Banks, respectively). Warming is particularly high in the southern portion of the Scotian Shelf (by 3.5$^o$C on average with maxima of up to 5$^o$C). This warming is in contrast to the minimal temperature increases in Case 1 (on average by 0.2, 0.4, and 0.1$^o$C on the Scotian Shelf, Gulf of Maine, and Grand Banks, respectively). Changes to salinity are similar. In Case 1 (strong SC), there is almost no change to bottom salinity (small average decreases of 0.01, 0.02, and 0.01 on the Scotian Shelf, Gulf of Maine, and Grand Banks). In contrast, in Case 2 (weak SC) the southern portion of the Scotian Shelf, the Gulf of

Maine, and the Laurentian Channel shows pronounced salinification whereas the Grand Banks and the northern portion of the Scotian Shelf are considerably fresher. The average bottom water salinity in Case 2 increases by 0.2 and 0.28 on the Scotian Shelf and Gulf of Maine but decreases by 0.20 on the Grand Banks. These large differences in bottom water properties between the two scenarios are a result of diminished transport of cool, fresh water southwestward along the shelf break in Case 2, leading to warmer, saltier water replacing it on the southern portion of the shelf and in the Gulf of Maine, particularly in the deep basins (see LS vs Slp-D dye; Figure 5.4).

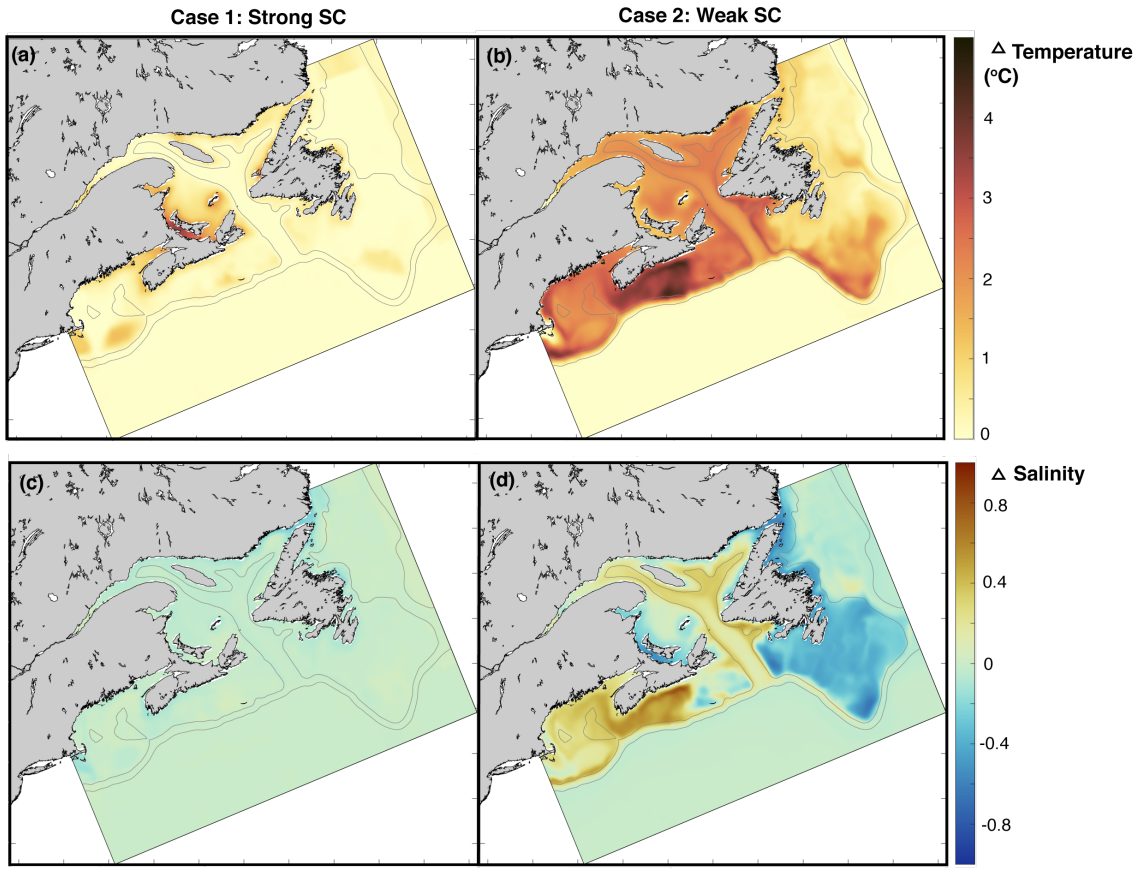


Figure 5.7: Bottom average changes (future minus present) in temperature (top) and salinity (bottom). Left panel is Case 1 (strong SC) and right panel is Case 2 (weak SC).

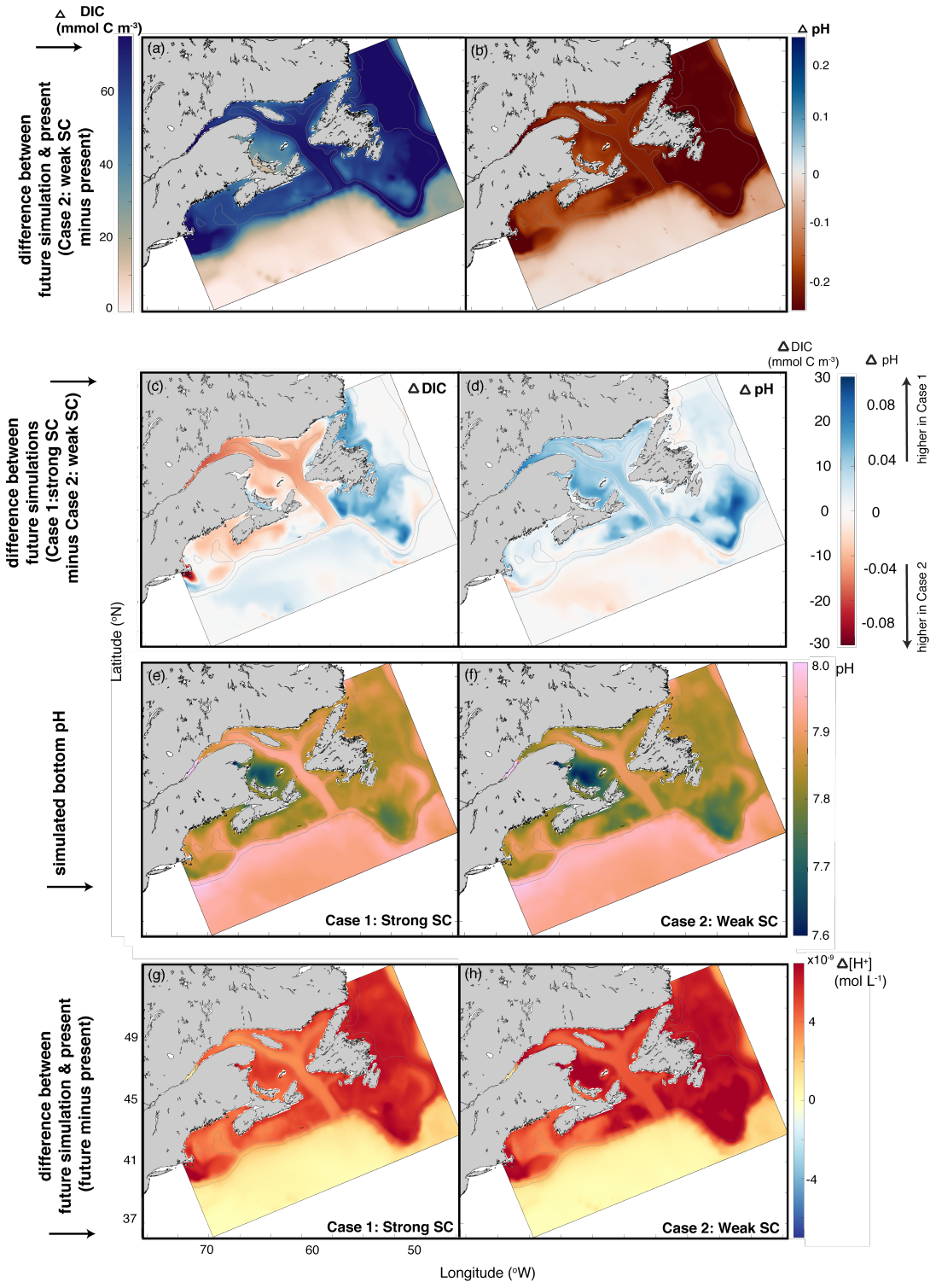


Figure 5.8: Panels a-b: Difference between future scenario (Case 2, weak SC) and present-day bottom DIC (right) and bottom pH (left). Panels c-d: Difference between two future scenarios (Case 1 minus Case 2) for bottom dissolved inorganic carbon (DIC; left) and pH (right). Panels e-f: Bottom pH in two future scenarios: Case 1 (strong SC; left) and Case 2 (weak SC; right). Panels g-h: Changes in bottom [H+] in two future scenarios: Case 1 (strong SC; left) and Case 2 (weak SC; right).

### 5.3.2 Projected changes to carbon properties

Now, we analyze how carbon properties (DIC, pH, and air-sea $CO_2$ flux) change on the shelf in these future scenarios. The right panel in Figure 5.6 shows average DIC in relation to temperature in both the present and future time slices for the different subregions. All regions (end members and shelf regions) have increased DIC concentrations in both future scenarios, with the largest endmember increase occurring in LS and Slp-S (by about 90 mmol C $m^{-3}$, Figure 5.6b). DIC concentration on the shelf increases by about 50-75 mmol C $m^{-3}$ in both the scenarios (Figure 5.6b,d), despite large differences in their circulation regime (Figure 5.2-5.5) and water mass composition (Figure 5.6).

Surface air-sea $CO_2$ fluxes increase throughout the region so that under both future scenarios, all of the shelves are acting as large net sources of $CO_2$. There is a gradient from stronger net outgassing on Grand Banks to less net outgassing in the Gulf of Maine in both scenarios. In Case 1 (strong SC), Grand Banks outgasses at 4.2 $\pm$ 0.6 mol C $m^{-2}$ $yr^{-1}$; Scotian Shelf outgasses at 3.6 $\pm$ 0.4 mol C $m^{-2}$ $yr^{-1}$, and Gulf of Maine outgasses at 2.6 $\pm$ 0.4 mol C $m^{-2}$ $yr^{-1}$. The fluxes are larger in Case 2 (weak SC): Grand Banks outgasses at 5.4 $\pm$ 0.2 mol C $m^{-2}$ $yr^{-1}$; Scotian Shelf outgasses at 3.8 $\pm$ 0.2 mol C $m^{-2}$ $yr^{-1}$, and Gulf of Maine outgasses at 3.1 $\pm$ 0.2 mol C $m^{-2}$ $yr^{-1}$. For comparison, in the present-day scenario, air-sea fluxes are: Scotian Shelf + 1.7 $\pm$ 0.2 mol C $m^{-2}$ $yr^{-1}$, Gulf of Maine -0.5 $\pm$ 0.2 mol C $m^{-2}$ $yr^{-1}$, and uptake in Grand Banks -1.3 $\pm$ 0.3 mol C $m^{-2}$ $yr^{-1}$.

Changes in bottom DIC concentrations are relatively similar between the two scenarios with increases of 69, 59, and 65 mmol C $m^{-3}$ in the Case 2 and 74, 56, and 61 mmol C $m^{-3}$ in the Case 1 for Grand Banks, Scotian Shelf, and Gulf of Maine, respectively. Figure 5.8 (top panels) shows the differences in bottom DIC and pH between the two future scenarios. Case 1 (strong SC) has larger DIC concentrations on the East Newfoundland Shelf and Grand Banks, whereas Case 2 (weak SC) has larger DIC concentrations in the Laurentian Channel, Gulf of St. Lawrence, and southern portion of the Scotian Shelf. Changes in bottom pH are also similar between the scenarios, with slightly larger acidification (more acidic by 0.03-0.05 pH units in some locations) in Case 2, particularly on the Grand Banks and on the more northern portion of the Scotian Shelf. Figure 5.8 (bottom panel) shows the actual bottom pH values in the two future scenarios to highlight the most acidified regions, which are the tip of Grand Banks, coastal areas in the Gulf of St. Lawrence, Gulf of Maine, and the more northern portion of the Scotian Shelf. In general, these regions

are more acidified in Case 2 (weak SC), reaching minimum pH values of 7.7 pH units (e.g. GB, northeastern Scotian Shelf) compared to 7.8 pH units in Case 1 (strong SC). The lowest pH values are reached in the Gulf of St. Lawrence (7.6 in Case 2; 7.7 in Case 1). Like bottom salinity and temperature, bottom pH in Case 1 (strong SC) is more uniform than in Case 2 (weak SC), where a stronger north to south gradient in pH (more acidic to less acidic) is present (Grand Banks and northeastern Scotian Shelf vs. southwestern Scotian Shelf and Gulf of Maine).

### 5.3.3 Identifying the effects of different circulation regimes

To distinguish between future changes in shelf properties that are due to circulation changes versus local air-sea exchange, we calculated predicted T, S, and DIC values, which indicate the effects of only simple mixing. These are calculated as a weighted mean using the endmember T, S, and DIC values combined with the water mass fractions (Figure 5.6). By using the present-day endmembers with the future scenario water mass compositions, we can quantify the changes to T, S, and DIC if there was only a shift in circulation but no changes to water mass properties in the endmember regions. The difference between these "circulation-only" predicted values and the "true" future simulated values indicates how much of the property changes on the shelf can be attributed to circulation changes (Figure 5.6c,d). In the Case 2 (weak SC), circulation changes account for up to 50-60% of the changes in temperature for all shelves versus 10-20% in Case 1 (strong SC). For both scenarios, circulation changes account for nearly all of the salinity changes in the Gulf of Maine. In the Scotian Shelf and Grand Banks, however, there is net freshening occurring in the actual simulated future values that is not accounted for in the circulation-only predicted values (e.g., caused by increased net precipitation), indicating that only circulation changes would cause net salinification in these two regions. For DIC, however, the predicted values show no significant changes occurring to the DIC concentrations from just circulation effects.

Perhaps the largest impacts of the different circulation regimes on the carbonate chemistry are tied to spatial variability. In Case 2, with larger changes to the circulation, the divide between the northern and southern portions of the Scotian Shelf is large, with almost 1 unit of salinity and 2.5$^o$C difference between the regions versus 0.5 unit difference in salinity and 2$^o$C difference between the regions at present and in Case 1. Under Case 2, the southern portion of the shelf is biogeochemically behaving more similarly to the warmer

and saltier Gulf of Maine, with strong influence of Slp water and less acidification. The more northern portion biogeochemically behaves more similarly to the slightly cooler and fresher Grand Banks, where there is still larger influence of LS+ENS waters and higher acidification. This trend is reflected in the surface air-sea $CO_2$ fluxes as well, with larger difference in flux between the northern and southern sections of the Scotian Shelf in Case 2 (northeastern Scotian Shelf at $4.2 \pm 0.2$ mol C $m^{-2}$ $yr^{-1}$ vs. southwestern Scotian Shelf $3.6 \pm 0.1$ mol C $m^{-2}$ $yr^{-1}$ in Case 2; northeastern Scotian Shelf at $3.8 \pm 0.4$ mol C $m^{-2}$ $yr^{-1}$ vs. southwestern Scotian Shelf $3.5 \pm 0.4$ mol C $m^{-2}$ $yr^{-1}$ in Case 1).

## 5.4 Discussion

This study addressed the question: what happens to the carbonate chemistry on the northwest North Atlantic shelf under a future scenario where the shelf-break current vanishes? To answer this question, we analyzed two potential future states by downscaling larger scale models (Case 1 with a strong SC, and Case 2 with a weak SC) to our medium-complexity biogeochemical regional model, one of which predicts modest changes to the circulation structure and the other large declines in the strength of the shelf-break current. We quantified potential changes to the circulation, and any subsequent changes to the endmember contribution on the continental shelves by mid-century ($\sim$ 2075). The goals of this work were accomplished by implementing passive dye tracers in the regional model and analyzing changes in shelf-break transport. We then analyzed resulting changes to the carbonate chemistry on the continental shelf. We will discuss the results in relation to the hypotheses proposed in the introduction, that under the scenario with weak shelf-break current transport: (1) there would be increased slope water inflow on the southwestern half of the Scotian Shelf; (2) the Scotian Shelf will biogeochemically behave more similarly to the Gulf of Maine; and (3) slope water inflow will be associated with less acidification.

The two future scenarios projected varying degrees of modification to the circulation structure, as anticipated. The Case 1 has more modest changes to the southwestward volume transport (Figure 5.3) and delivery of LS dye to the Scotian Shelf (Figure 5.2). This results in very similar proportions of Slp:LS+ENS waters on the shelves compared to present-day values. Conversely, Case 2 has a drastic decrease in volume transport along the Scotian Shelf (Figure 5.3) and in the amount of LS dye traveling southwestward past Grand Banks towards the Scotian Shelf (Figure 5.2). The decreased southwestward transport

results in a larger increase of Slp water (Figure 5.4) and a shift in the Slp:LS+ENS ratio on the shelves (Figure 5.5). These results establish the two future scenarios as representative examples of two extreme cases for the future of the shelf-break current.

Despite the large difference in the strength of the shelf-break current and water mass composition, under both future scenarios the shelves all act as large net sources of $CO_2$. These results suggest that regardless of the circulation changes in the system, air-sea flux will be determined by increased warming and increased DIC concentrations. Furthermore, the air-sea flux behaviour of the shelf now follows a north-south gradient with the largest outgassing occurring on Grand Banks and the smallest outgassing in the Gulf of Maine. This is in contrast to the present-day system where Grand Banks is a sink of $CO_2$, the Scotian Shelf is a large source of $CO_2$, and the Gulf of Maine is a weak net sink (*Rutherford et al.*, 2021; *Rutherford and Fennel*, subm.). The regional model does tend to slightly overestimate surface $pCO_2$ at present day (see *Rutherford et al.*, 2021) and the DIC deltas were calculated in such a way that might overestimate future DIC concentrations (see Section 5.2.2), therefore the magnitude of outgassing is potentially larger than we would expect in the future but the overall finding that atmospheric forcing is the dominant control on setting future air-sea fluxes is a robust result.

Surface temperature and salinity, particularly on the Scotian Shelf, were also similar between the scenarios and further indicative that the shelf-break current strength is less of a control on setting surface values. However, despite these strong similarities at the surface, the bottom waters illustrate a stark contrast between the scenarios (Figure 5.7). These waters are mainly set by the circulation, with a permanent density stratification on the shelf insulating bottom waters from atmospheric inputs to some extent. In Case 1, where the shelf-break current is intact, there are little changes to temperature and salinity in the shelf bottom waters, in this scenario. Conversely, in Case 2 with the shelf-break current nearly vanishing, there is extensive bottom water warming on the shelves, some locations reaching $+5^{o}$C. Perhaps more interesting are the bottom water salinity changes in Case 2, which can be a better tracer of water mass change than temperature. In the Gulf of St. Lawrence, the southern portion of the Scotian Shelf, and in the Gulf of Maine, there are large salinity increases under Case 2. The regions with higher salinity align with regions that already see higher portions of slope water inflow at present day (*Smith et al.*, 2001; *Rutherford and Fennel*, 2018) and where there are larger increases in Slp-D water which

have replaced LS water (Figure 5.4).

The increasing presence of slope water inflow create a distinct north-south gradient in shelf biogeochemistry. At present day, due to the decreasing transport of the Labrador Current as it transits southwestward (Loder et al. 1998; Figure 5.3), the northeastern half of the Scotian Shelf is heavily influenced by the subpolar North Atlantic water and the southwestern part of the Scotian Shelf can experience more inflow of Slp water, similar to the Gulf of Maine (*Rutherford and Fennel*, 2018), creating a weak division in the behaviour of the northeastern and southwestern portions of the Scotian Shelf. Under Case 2, the weak shelf-break current promotes significant inflow of slope water and creates an even larger disconnect between the southwestern and northeastern part of the Scotian Shelf than what is currently present. The southwestern portion of the Scotian Shelf and the Gulf of Maine are the most impacted by the lack of shelf-break current and inflow of slope water, associated with some of the largest salinification and warming in the bottom waters in Case 2 (Figure 5.7). Overall, this inflow causes the southwestern portion of the Scotian Shelf to biogeochemically behave more similarly to the Gulf of Maine, and the northeastern portion biogeochemically behaves more similarly to Grand Banks and the East Newfoundland Shelf. Although we hypothesized that there would be larger inflow of slope water on the southwestern portion of the Scotian Shelf, we did not anticipate that such a strong division would occur as a result, and instead predicted the entire Scotian Shelf would biogeochemically behave like the Gulf of Maine.

The resulting divide on the Scotian Shelf in Case 2 (weak SC) creates localized regions of higher acidification whereas under Case 1 (strong SC), the acidification is more uniform across the shelf. The regions that are more highly affected by Slp-D water (central Gulf of Maine, southwestern Scotian Shelf) tend to experience higher warming but less acidification than regions with larger subpolar North Atlantic water influence. These results align with our initial hypothesis and the results from *Salisbury and Jönsson* (2018). With the absence of a shelf-break current, the shelves here are divided into either regions that are warmer, saltier, and less acidic (southwestern shelves) or regions that are cooler, fresher, and more acidic (northeastern shelves). This would have many implications on species in the region. For example, on the northeastern Scotian Shelf where acidification is high, we would expect to see more impacts on American lobster growth rates, and decreases in the calcification rates of oysters and soft-shell clams (*Brennan et al.*, 2016). On the

southwestern Scotian Shelf where temperatures are highest, there would be more effects on species such as snow crab, adult Northern shrimp, and adult Greenland halibut (*Brennan et al.*, 2016). These are just some examples of species that would be critically affected and does not account for the overlap of acidified waters with either deoxygenated waters and/or waters with temperatures exceeding threshold values. A more robust analysis, combining temperature, oxygen, and pH levels should be performed to see the overall effect on regional species and fisheries.

The validity of each of these future scenarios is of course difficult to comment on and we instead view these two cases as bookends for a wide range of possible outcomes for the region. Atmospheric inputs will likely be the largest factor controlling the future of the regional carbonate chemistry, regardless of the future state of the circulation structure. Any changes to the circulation will likely have a higher impact for localized regions than the entire shelf system as a whole. Future work will include analysis of a long projection from 2000-2100 rather than time slices to better understand how these potential changes progress over the century; for example, when pH and aragonite saturation reach threshold values. It would additionally be useful to look at extreme, shorter-term events in both pH and temperature since we only looked at average changes – there are likely events in both scenarios where temperature and acidification are much larger than reported.

## 5.5 Conclusions

In this study, we downscaled two larger scale models to our regional model of the northwest North Atlantic to analyze two potential future scenarios for the continental shelves along eastern Canada to quantify how potential future circulation changes would impact the carbonate chemistry. Overall, we found that atmospheric inputs overwhelmingly control the regional carbonate system under both future scenarios, which is particularly evident in the large outgassing of $CO_2$ present in both future scenarios. The different circulation regimes do, however, impact bottom temperature and salinity on the shelves, creating contrasting spatial variability of bottom water pH. Decreasing southwestward transport of cold subpolar North Atlantic waters creates increased slope water inflow on the southwestern half of the Scotian Shelf and into the Gulf of Maine. As a result, the southwestern half of the Scotian Shelf biogeochemically behaves more similarly to the Gulf of Maine under such a circulation regime, whereas the northeastern half biogeochemically behaves more

similarly to the Grand Banks. The regions with higher slope water inflow tend towards less acidification on average compared to regions with higher influence from subpolar North Atlantic waters.

# CHAPTER 6

# CONCLUSIONS

Continental shelves play an important role in the discussion of air-sea $CO_2$ fluxes as they disproportionately contribute to global fluxes (*Laruelle et al.*, 2010) and experience the effects of climate change on much shorter timescales than the open ocean (*Cai et al.*, 2010). It is, however, difficult to constrain fluxes on shelves because of their high spatial and temporal variability and the relatively low resolution of observations, which make it difficult to fully capture the intricate dynamics (*Gruber*, 2015). The Scotian Shelf in particular has various conflicting estimates of its air-sea $CO_2$ flux, perhaps indicative of some large variability underlying the $CO_2$ dynamics here. For this reason, my thesis has focused on understanding the processes underlying the air-sea $CO_2$ fluxes on the Scotian Shelf, both now and under potential future states. I expanded and validated a regional biogeochemical ROMS model of the northwest North Atlantic to achieve my thesis goals, which included calculating mean residence times, water ages, regional air-sea $CO_2$ flux estimates, and a measure of carbon saturation (DIC-DIC$_{eq}$ or DIC disequilibrium). Overall, my thesis objectives were to:

1. better understand the main transport mechanisms, residence times, and transport timescales in the region that could be driving air-sea $CO_2$ fluxes,

2. explore the seasonality and spatial variability of $pCO_2$ on the Scotian Shelf, and estimate the fluxes in the region,

3. track how the carbonate chemistry of water changes as it travels to the Scotian Shelf to better understand how the transport mechanisms were affecting the flux estimates and causing the Scotian Shelf to deviate from the global trend in air-sea $CO_2$ fluxes,

and

4. explore how a changing climate will affect the Scotian Shelf carbonate chemistry.

In the first chapter of my thesis, I implemented passive dye tracers in the regional model, and found that residence times in the region are relatively short ($\sim$3 months for the Scotian Shelf, $\sim$3 months for Grand Banks, $\sim$6 months for the Gulf of Maine and $\sim$12 months for the Gulf of St. Lawrence) and along-shelf southwestward transport is the dominant transit pathway under present-day conditions. Dye tracer mass fractions illustrate that most of the water on the Scotian Shelf comes from the Gulf of St. Lawrence or from the more northern regions of the continental shelf (East Newfoundland Shelf, Grand Banks). The dominant shelf-break current along the Scotian Shelf, an extension of the Labrador Current, acts like a wall inhibiting transport of water across the Scotian Shelf shelf break, either onto or off the shelf. Neither the Continental Shelf Pump nor upwelling across the shelf break are dominantly occurring here.

In the second chapter of my thesis, I presented a composite of high-resolution observations and regional model output to better understand the processes underlying the temporal and spatial variability of $CO_2$ on the Scotian Shelf. $pCO_2$ here undergoes a strong seasonal cycle, associated with a large biological drawdown in DIC during the spring bloom and temperatures ranging from $0^oC$ in winter to $20^oC$ in summer. Throughout the summer, persistent coastal upwelling acts to lower $pCO_2$ nearshore but does not have a significant effect on shelf-wide fluxes. I found the Scotian Shelf to act as a large net source of $CO_2$, in agreement with *Shadwick et al.* (2010, 2011), whereas the adjacent shelves of the Gulf of Maine and Grand Banks act as a weak net sink and large net sink, respectively. The latter two regions act in agreement with the global trend in continental shelf air-sea $CO_2$ fluxes, whereas the Scotian Shelf deviates from the trend. Overall, I found that the Scotian shelf has relatively homogenous surface $pCO_2$ and that the CARIOCA buoy observations did a good job at representing the shelf-wide $CO_2$ fluxes.

My third chapter combines the dye tracers from Chapter 1 and the results from the validated carbonate model from Chapter 2 to investigate why the Scotian Shelf deviates from the global trend in $CO_2$ fluxes. I tracked the carbon saturation on the water's transit pathway from the Labrador Sea to the Scotian Shelf and found that the Scotian Shelf is heavily influenced by subpolar North Atlantic waters, which are cold and carbon-rich. These waters warm on their transit to the Scotian Shelf, leading to oversaturation of carbon

throughout the water column, and net outgassing on the Scotian Shelf.

My fourth chapter considers two potential future states of the regional circulation and determines how a weaker shelf-break current and an altered water mass composition might impact the carbonate chemistry of the shelf along eastern Canada. I again used the dye tracers from Chapter 1, which allowed me to visualize and quantify changes to shelf-wide endmember compositions, and combined these results with an analysis of the future state of air-sea $CO_2$ flux and pH. I found that any potential changes in the regional circulation that might shift the balance between warm, salty slope water and the cold subpolar North Atlantic waters would not play a dominant control on setting the carbonate chemistry in the region, and that atmospheric inputs would be the largest factor to consider. Increasing intrusions of warm, salty slope water, particularly onto the southwestern portion of the shelf, will however promote a larger divide between the northeastern and southwestern shelves in the region. These slope water intrusions may also help alleviate some of the acidification that is expected to occur here.

Overall, I implemented and validated passive dye tracers and the carbonate chemistry module in our model of Atlantic Canada, which is the basis of many significant scientific outcomes of my thesis work. My thesis includes one of the first regional studies to estimate mean residence times and water ages for the continental shelves off of eastern Canada. My work contributed some of the first regional model estimates for air-sea $CO_2$ flux for the shelves off of eastern Canada, and added to the discussion of the source or sink status of the Scotian Shelf. I introduced a methodological framework for understanding how water end members can be contributing to setting air-sea $CO_2$ fluxes on continental shelves. I specifically used this framework for the Scotian Shelf, and connected the circulation structure here with air-sea $CO_2$ fluxes, emphasizing the importance of subpolar North Atlantic waters in setting the biogeochemical properties on the shelves off of eastern North America. Furthermore, the tie between the Scotian Shelf being oversaturated with $CO_2$ and the delivery of cold, carbon-rich subpolar North Atlantic waters via the inner and outer branches of the southwestward transit emphasizes the importance of modeling the circulation structure in this region well. Many global models struggle to capture the placement of the circulation here, which could be, in part, the reason why other modeling studies have not found the Scotian Shelf to act as a net source of $CO_2$. My work illustrated which factors may impact future changes in shelf-wide pH and air-sea $CO_2$ fluxes over the

coming century, identifying which regional changes we can expect regardless of the future circulation structure and which changes are more uncertain. These findings contribute to the important discussion of regional climate change effects, which currently predicts quite widespread results.

There are, of course, questions remaining from my thesis. One of the largest remaining questions relates to the bloom-related decline in $pCO_2$. In the observations from the moored CARIOCA buoy and Atlantic Condor transect, there is a large and rapid decline in $pCO_2$ associated with the drawdown of DIC during the spring bloom. The model was not able to capture the magnitude of the drawdown in $pCO_2$ and could not consistently capture the timing of the spring bloom drawdown either. From the interannual variability in the model simulation, it can be seen that there are larger declines in $pCO_2$ in years where the chlorophyll peaks earlier. This leaves the question of what dynamics underlie the earlier spring bloom peak? And if decoupling the phytoplankton and zooplankton could more accurately represent the biology during the spring bloom here? Additionally, following the bloom, the model overestimates $pCO_2$ throughout the summer. More work should be done to better understand this model bias – is it related to not drawing down enough DIC during the bloom or are the other biological dynamics during the summer, such as remineralization, not well captured in the model? Although we already know that biological models have a long ways to go in terms of accurately representing the true biological dynamics in the ocean, my thesis work illustrates that perhaps unconventional datasets, such as long time series of surface $pCO_2$, can be used to evaluate biological models, pinpoint weaknesses, and maybe even diagnose ways to improve the models. I believe future work should be aimed at better understanding the tie between the phytoplankton-zooplankton dynamics, and the $pCO_2$ seasonal cycle on the Scotian Shelf.

The first three chapters of my thesis looked at the Scotian Shelf on a seasonal timescale for the early 2000s and neglected the documented warming that occurs in the region between 2005-2010 (see for example *Brickman et al.*, 2018). Although understanding the seasonality at present day is important, future work should look at the recent warming on the shelves here and if there have been recent changes in the carbonate chemistry. This could additionally address questions related to why earlier SOCAT versions did not capture the outgassing on the Scotian Shelf. Specifically, is it truly a simple matter of low observation resolution in SOCAT v1.5 and v2 that lead to previous studies (e.g. *Signorini*

*et al.*, 2013; *Laruelle et al.*, 2014, 2015) estimating the Scotian Shelf to act as a net sink of $CO_2$? Or, was there a shift in the carbonate chemistry here after the reported warming that would be represented in the CARIOCA observations (recorded from 2007-2014) and Atlantic Condor observations (2018-2019), but not in earlier samples reported in the SOCAT database?

My last chapter poses perhaps some of the most difficult to answer questions and can be viewed as a starting point for future work. For example, analyzing a long simulation from 2000 to 2100 rather than time slices will be an important next step, answering questions such as when the shelves along eastern Canada start behaving as overwhelming sources of $CO_2$ or when temperature, pH, and oxygen reach threshold values for certain species. This chapter also only looked at average future changes. Future work should include looking at extreme values since averaging changes does not necessarily capture times when key variables exceed threshold values for potentially significant periods of time throughout the year. Additionally, a more complete analysis of the overlap of highly warmed, deoxygenated, and acidic waters should be completed, particularly identifying regions that will be most impacted and how these regions might overlap with important habitats and fisheries.

# APPENDIX A

# SUPPLEMENTARY INFORMATION FOR *Diagnosing transit times on the northwestern North Atlantic continental shelf*

## A.1 Introduction

The following supplementary information is divided into three parts.

A.2 includes time series of subregion-averaged mean age, illustrating the spin-up period needed to reach a dynamic steady state in each of the 9 subregions.

A.3 includes an overview of the model validation performed, following *Brennan et al.* (2016).

A.4 includes dye and age maps from the model simulations that include an outline of the initial dye region.

## A.2 Mean age time series

Figures A.1, A.2 and A.3 show time series of area-averaged mean age in the Gulf of St. Lawrence, on the Scotian Shelf and in the Gulf of Maine, respectively.

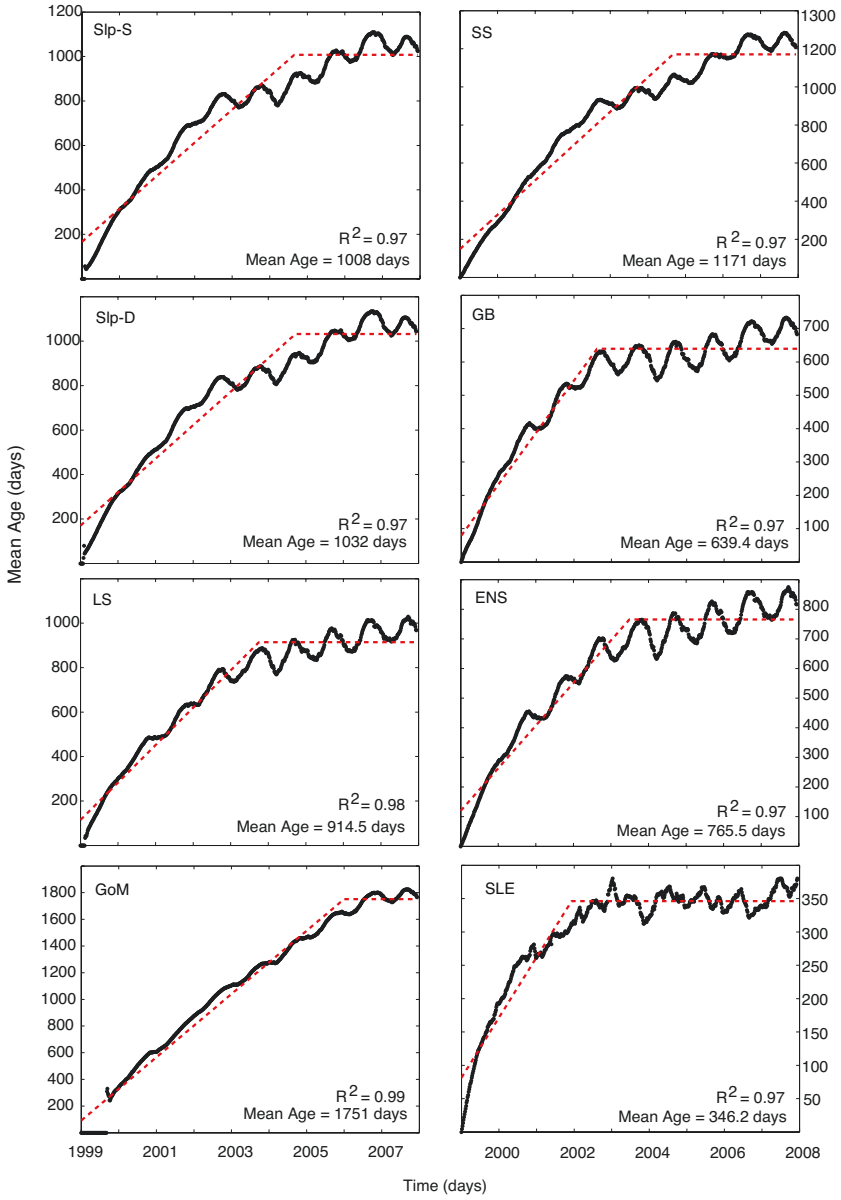


Figure A.1: Time series of age averaged within Gulf of St. Lawrence for each dye (black) and bilinear fit (red) used to determine the mean age of each dye in Gulf of St. Lawrence.

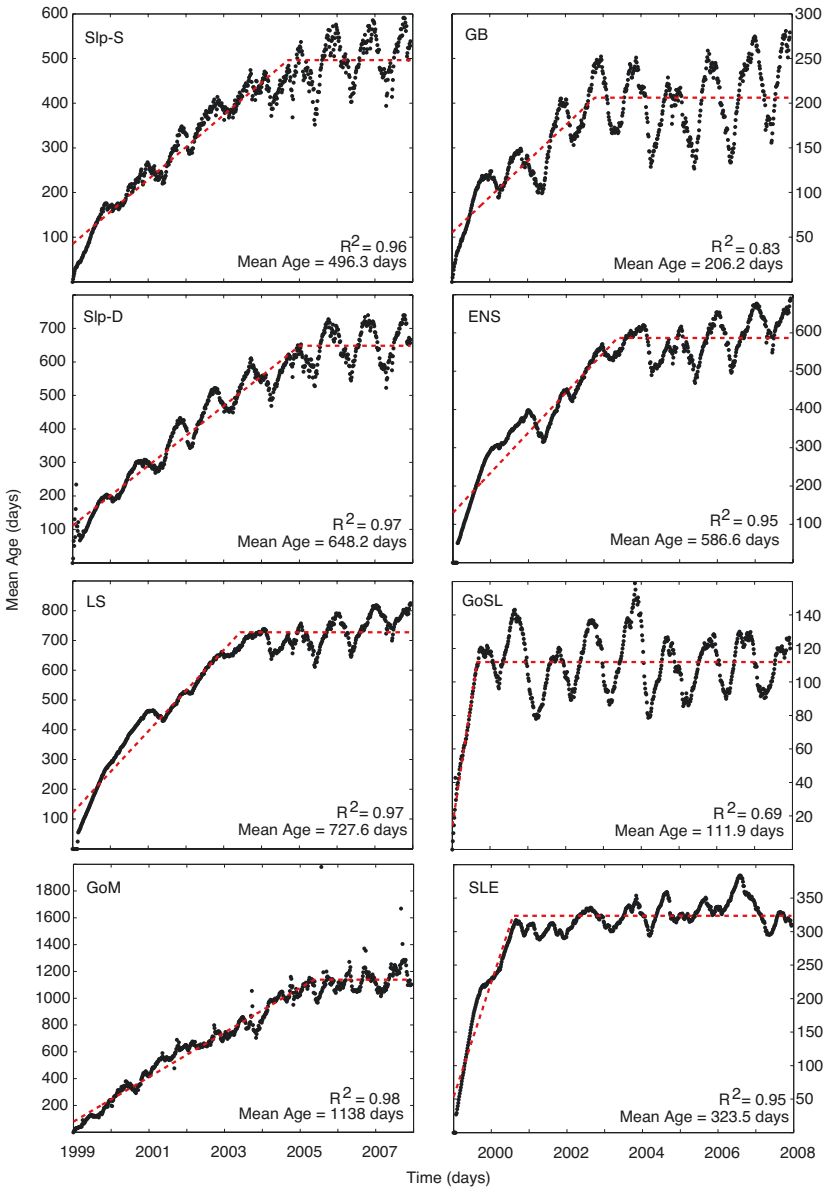


Figure A.2: Time series of mean age averaged on Scotian Shelf for each dye (black) and bilinear fit (red) used to determine the steady state or mean age of each dye on the Scotian Shelf.

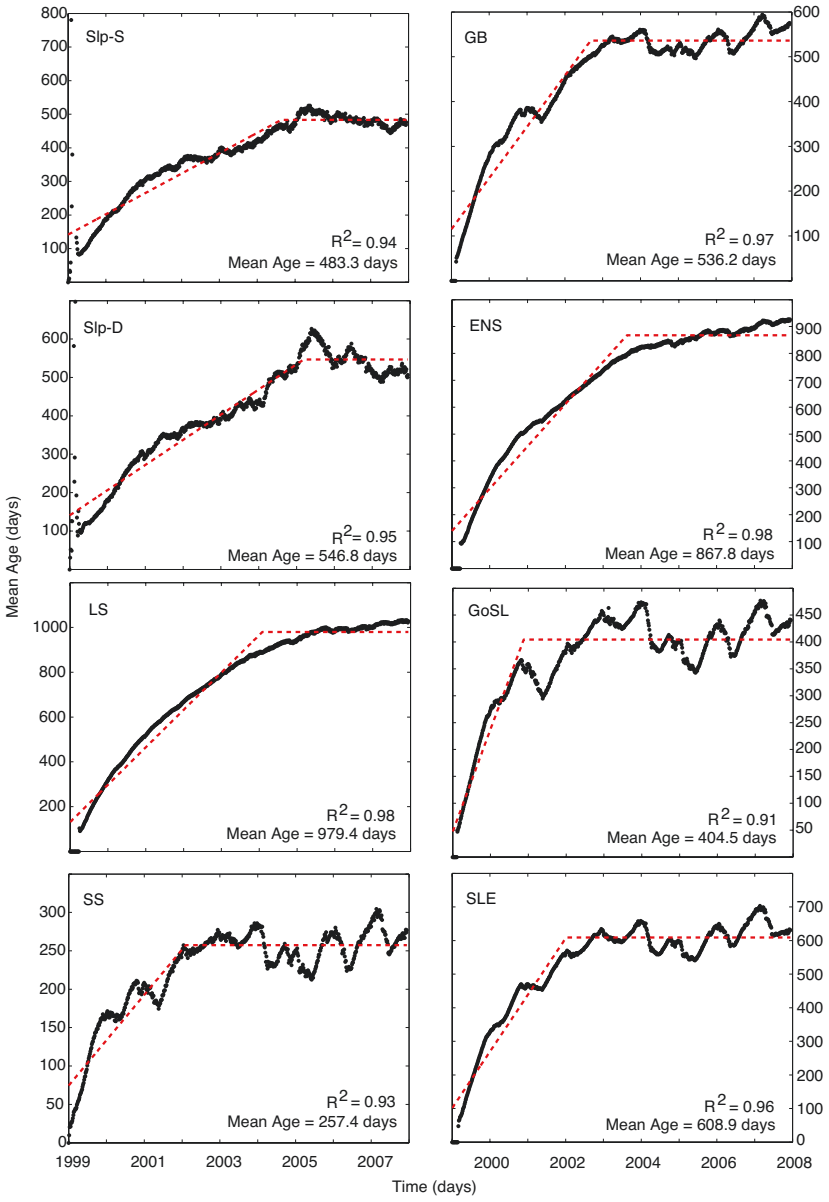


Figure A.3: Time series of mean age averaged within the Gulf of Maine for each dye (black) and bilinear fit (red) used to determine the steady state or mean age of each dye in the Gulf of Maine.

## A.3 Model validation

The model was extensively validated in *Brennan et al.* (2016). Here, we repeat a few key aspects of that validation for our simulation.

Figure A.5 and Figure A.6 compare model output to Atlantic Zone Monitoring Program (AZMP) observations along two transects on the Scotian Shelf: the Halifax and Louisbourg Lines (locations shown in Figure A.4). These transects show that the model is able to capture the vertical structure on the shelf well, specifically in the deeper basins.

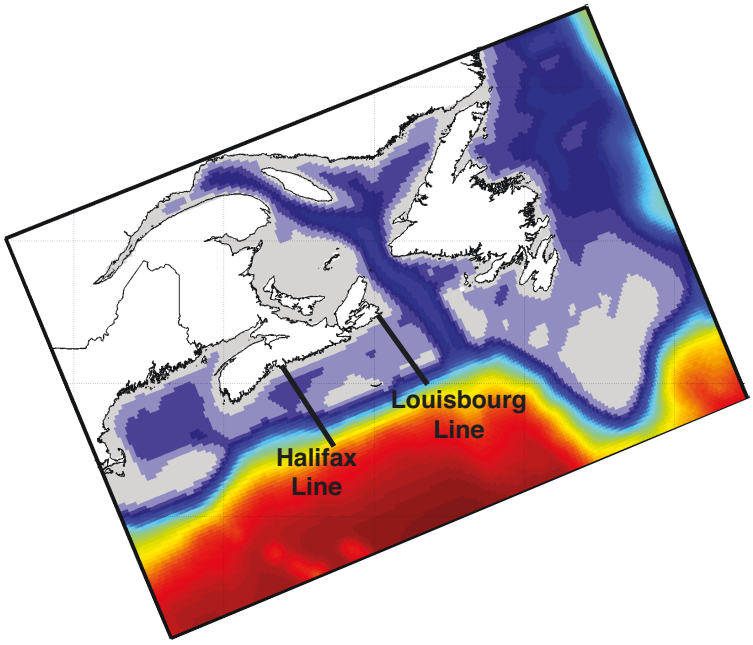


Figure A.4: Location of AZMP monitoring transects: Louisbourg and Halifax Lines.

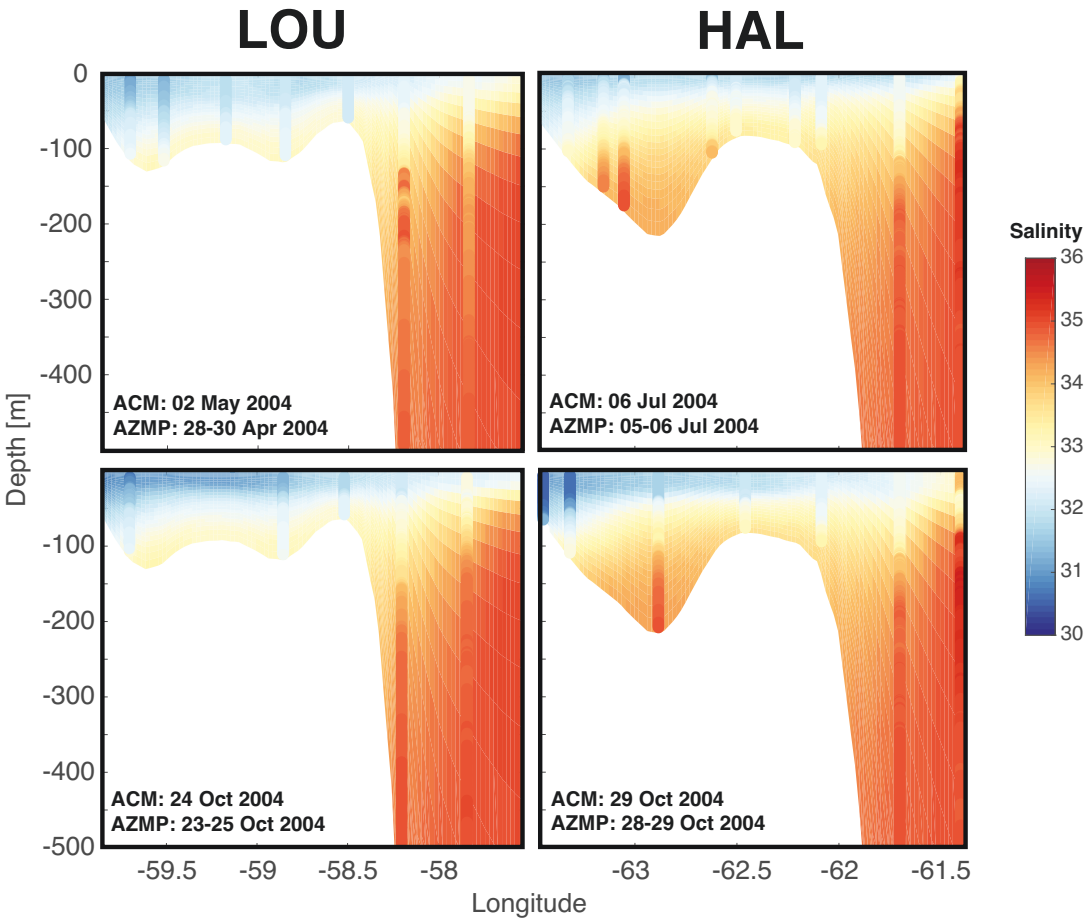


Figure A.5: Model salinity along the Louisbourg Line (left panels) and Halifax Line (right panels) transects overlain by AZMP observations.

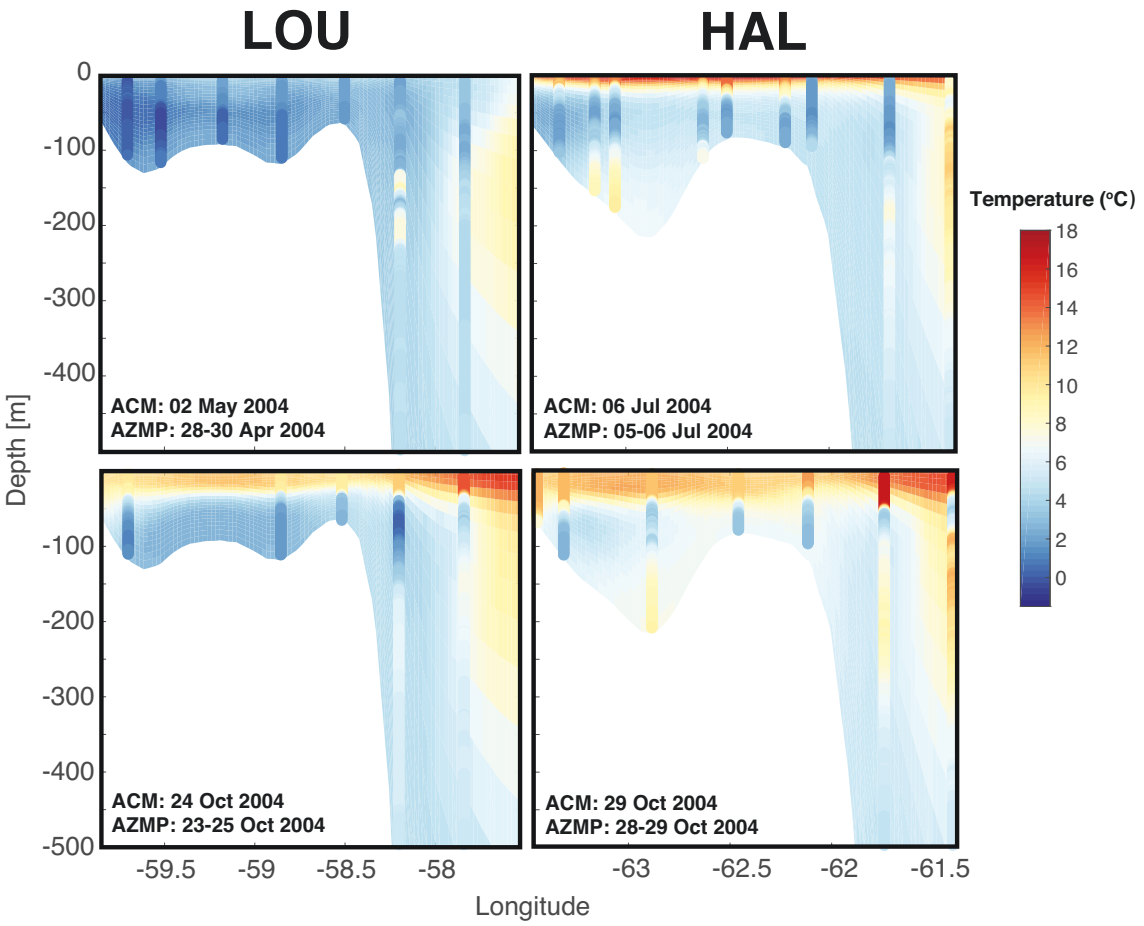


Figure A.6: Model temperature along the Louisbourg Line (left panels) and Halifax Line (right panels) transects overlain by AZMP observations.

Further to these transects, Figure A.7 compares the model SST and SSS to climatology (*Geshelin et al.*, 1999) and output from a larger regional model (*Urrego-Blanco and Sheng*, 2012) in a time series averaged over the Scotian Shelf. The model captures the seasonal cycle of both surface temperature and salinity well.

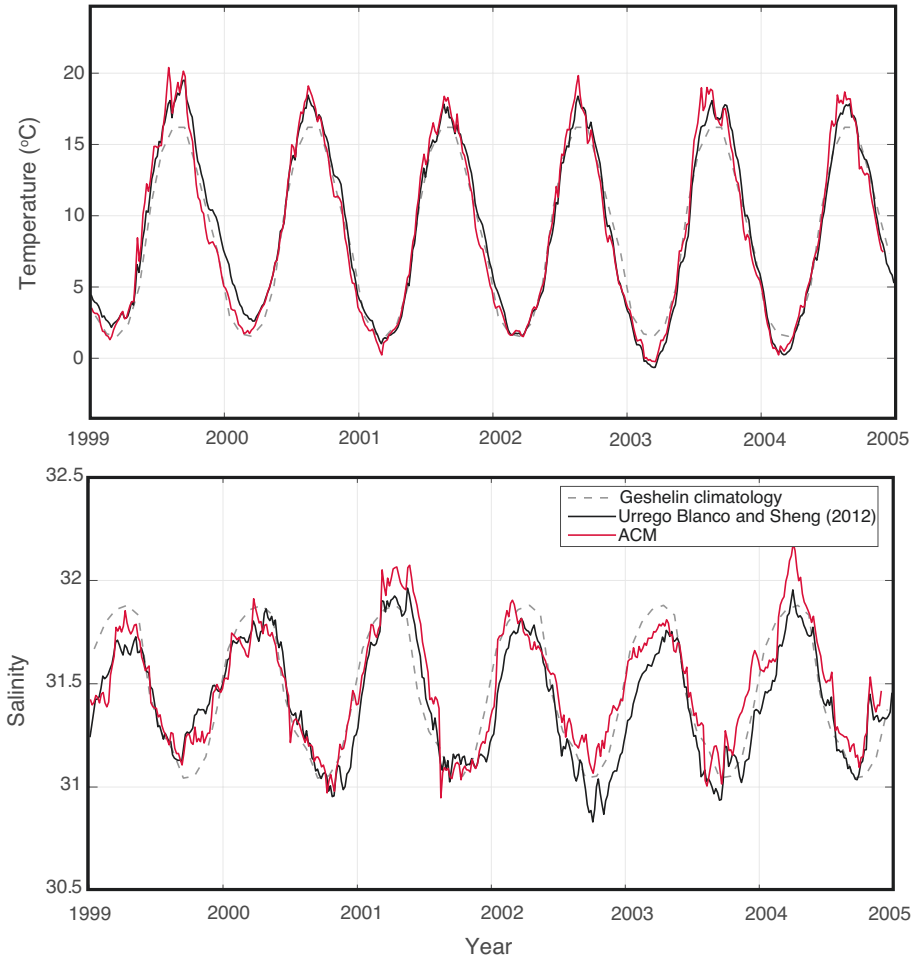


Figure A.7: Time series of area-averaged Scotian Shelf temperature (top) and salinity (bottom) at the sea surface.

Figure A.8 compares the model mean volume transport to those reported in *Loder et al.* (1998) along different sections on the continental shelves, illustrating that our model reasonably captures the volume transport throughout the region.

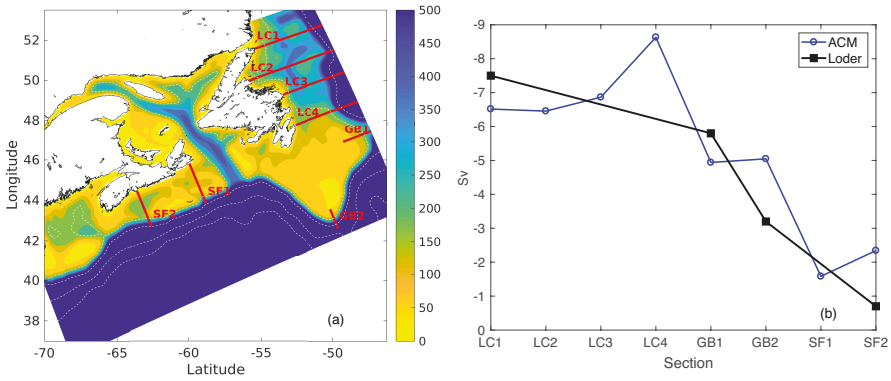


Figure A.8: (a) Section locations for model long-term mean volume transport comparison to estimated mean annual transport listed by *Loder et al.* (1998). LC1, GB1, GB2, and SF2 are the same as their Hamilton Bank, Flemish Pass, Tail of Grand Banks, and Halifax Section, respectively. (b) Long-term mean volume transport (Sv) from model simulation compared to the estimate transport from *Loder et al.* (1998).

Figure A.9 shows SST snapshots from June 29 and August 3, 2004. These plots of surface temperature illustrate the ability of the model to resolve mesoscale features, such as tendrils of cool water off of Newfoundland and finer-scale circulation features throughout the Gulf of St. Lawrence and Scotian Shelf. Additionally, Figure A.9 shows a thin band of cool water along the southern coast of Nova Scotia that is consistent with previous reports of coastal upwelling within 10 km of the coast (*Petrie et al.*, 1987; *Shan et al.*, 2016).

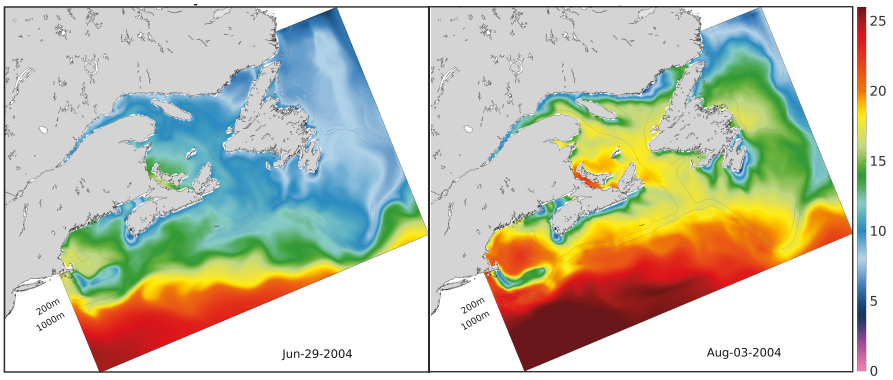


Figure A.9: Sea surface temperature snapshots from the model simulation taken on June 29, 2004 (left) and August 3, 2004 (right).

## A.4 Dye tracer & age distributions

Figure A.10 and Figure A.11 respectively show maps of vertically averaged dye concentrations and surface ages with the dye initialization areas overlain on top.

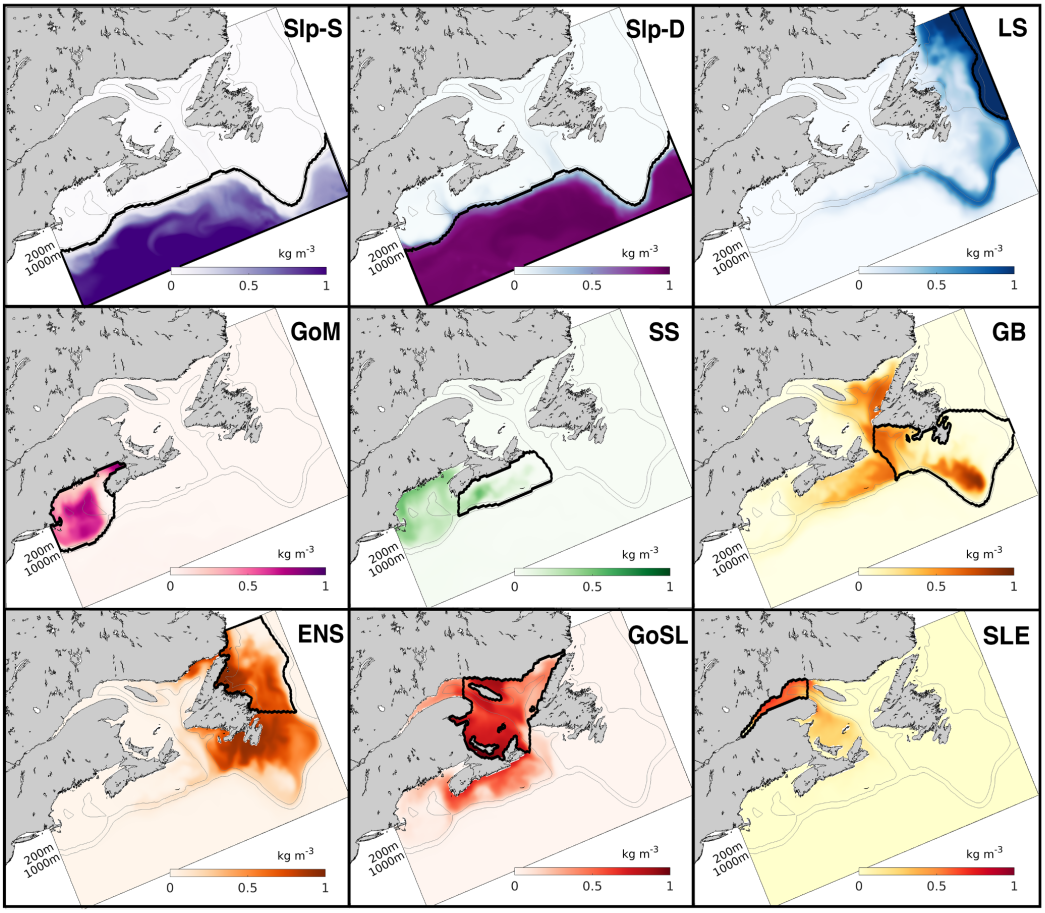


Figure A.10: Maps of vertical mean dye concentrations on June 16, 1999 (6 months into the TRANS simulation). Thick black line indicates location of dye initialization.

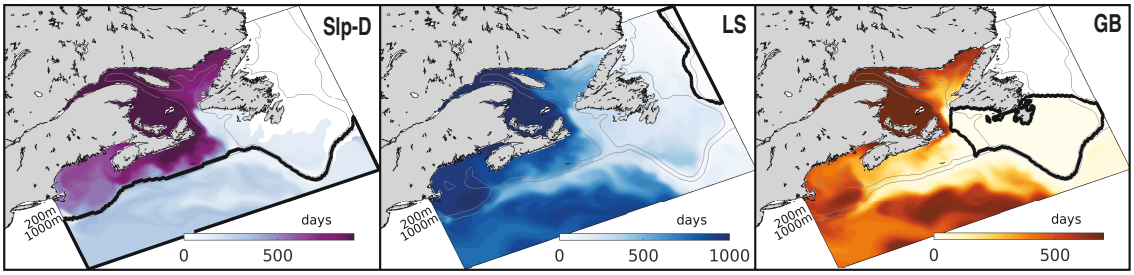


Figure A.11: Surface age (days) as determined from the AGE experiment. Snapshot from last year of 6 year simulation (June 10, 2004). White areas are regions where dye concentrations $< 0.001$ kg m$^{-}3$. Thick black line indicates location of dye initialization.

# APPENDIX B

# SUPPLEMENTARY INFORMATION FOR *A modeling study of temporal and spatial $pCO_2$ variability on the biologically active and temperature dominated Scotian Shelf*

## B.1 Introduction

The following supplementary information is divided into six parts.

B.2 includes a table outlining the location (latitude, longitude) and year/month of sampling of the observational datasets used.

B.3 includes details about the long-term trend in atmospheric $p\mathrm{CO}_2$ and the regression used in ROMS.

B.4 includes figures comparing the seasonal cycle of $p\mathrm{CO}_2$ in each year of the model simulation at different locations in the model.

B.5 includes model validation of Dissolved Inorganic Carbon (DIC) and Total Alkalinity (TA).

B.6 includes further comparison of $p\mathrm{CO}_2$ and temperature in the Halifax Harbour bin versus the Deep Panuke/Shelfbreak bin along the Atlantic Condor transect.

B.7 includes further figures describing the upwelling event of July 3, 2006 in the model.

## B.2 Observational datasets

Table B.1 indicates the location (latitude, longitude) and years/months of sampling of $p\mathrm{CO}_2$ at the CARIOCA buoy and from the Atlantic Condor Transect.

Table B.1: Summary of observational datasets, including latitude, longitude location and month/year of sampling.

| **Observational Dataset** | **Location** | **Year & month of sampling** |
|---|---|---|
| CARIOCA Buoy | 4.3$^o$N, 63.3$^o$W | **2007**: May, Jun, July, Aug, Sept, Oct<br><br>**2008**: Jan, Feb, Mar, Apr, May, Jul, Aug, Sept, Oct, Dec<br><br>**2009**: Sept, Oct, Nov, Dec<br><br>**2010**: Jan, Apr, May, Jun, Jul, Aug, Sept<br><br>**2011**: Jul, Aug, Sept, Oct, Nov, Dec<br><br>**2012**: Jan, Feb, Mar, Apr, May<br><br>**2014**: Feb, Mar, Apr, May, Jun, Jul, Aug, Sept, Oct, Nov Dec |
| Atlantic Condor Transect | $43.8^oN, 60.6\mathrm{o}W$ to $44.6\mathrm{o}N, 63.5\mathrm{o}W$ | **2018**: Feb, Mar, Apr, May, Jun, Jul, Sept, Oct, Nov<br><br>**2019**: Jun, Jul, Oct, Nov |

## B.3 Atmospheric $p\mathrm{CO}_2$

Figure B.1 illustrates the secular and seasonal cycle in atmospheric $p\mathrm{CO}_2$. The black points are observations taken at Sable Island and the red line is the regression used in ROMS:

$$\begin{aligned} pCO_{2,atm} = 273.9904 + 1.9738t + 5.3132\cos 2\pi t + 4.0601\sin 2\pi t - \\ 0.5814\cos 4\pi t - 2.1740\sin 4\pi t - 0.5009\cos 6\pi t + 0.5904\sin 6\pi t \end{aligned} \tag{B.1}$$

where $t = year – 1951 + yearday/365$.

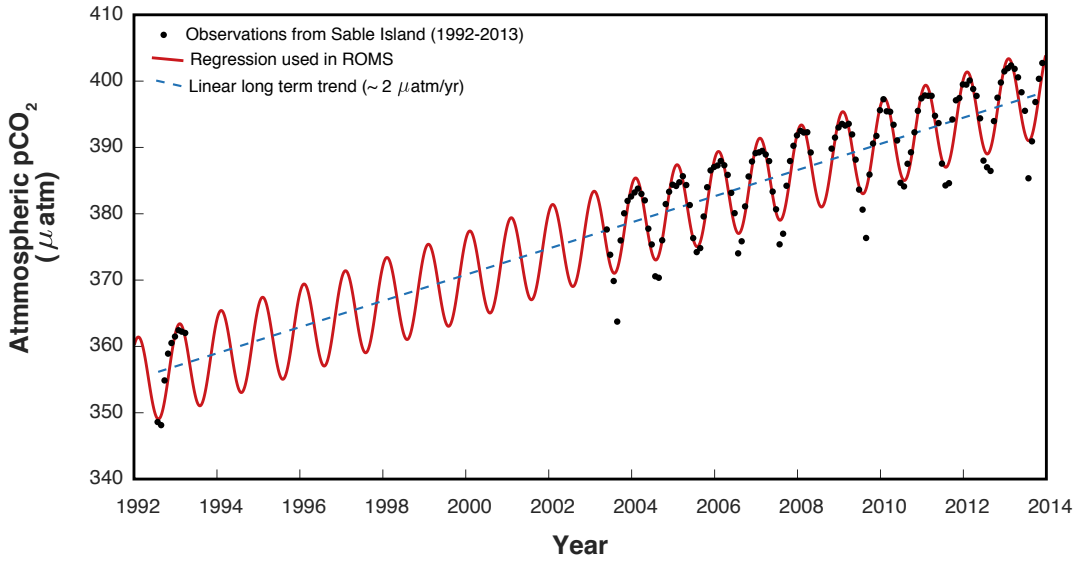


Figure B.1: Atmospheric $p\mathrm{CO}_2$ observations (black points) taken on the Scotian Shelf and fit to a regression (red line) used in ROMS and a linear long term fit (blue dashed line) for mapping surface ocean $p\mathrm{CO}_2$ onto the same year.

The blue dashed line is the long term linear fit of $+2\mu$atm yr$^{-1}$ used to map model years and observations onto the same year for comparison.

## B.4 Interannaul variability of surface water $p\mathrm{CO}_2$

Figures B.2 – B.5 illustrate $p\mathrm{CO}_2$ at the CARIOCA buoy, and averaged on the Scotian Shelf, Grand Banks and Gulf of Maine, respectively, throughout the model simulation (excluding the spin-up year). Each panel in these figures compares year 2000 to each subsequent year in the model simulation. Years 2001-2014 are mapped to year 2000 using the linear atmospheric trend $2\ \mu$atm yr$^{-1}$ to eliminate the long term trend in $p\mathrm{CO}_2$.

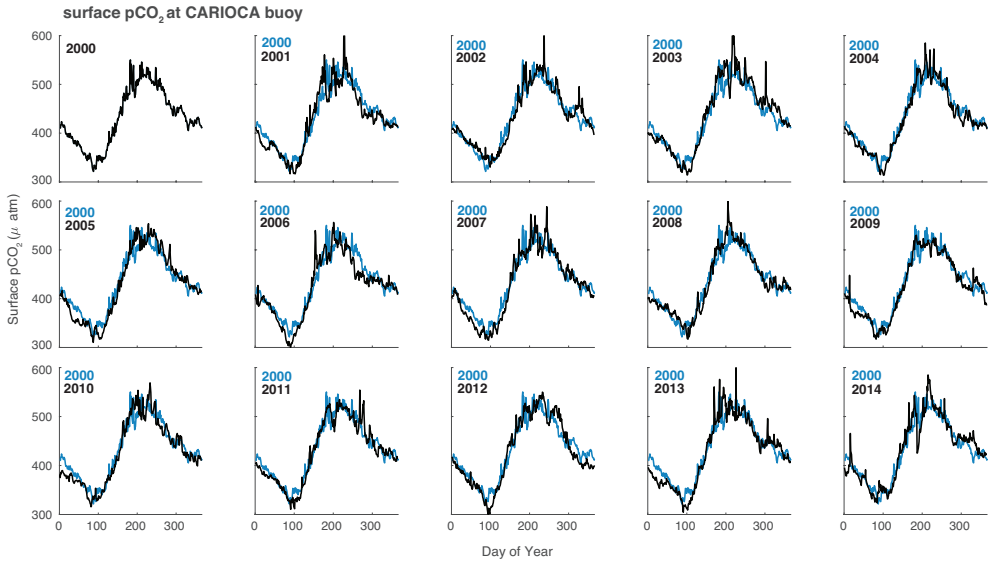


Figure B.2: Surface $pCO_2$ at the CARIOCA buoy (see Figure 1) comparing year 2000 with each subsequent year. Years 2001 to 2014 were mapped onto year 2000 using the longterm linear trend in atmospheric $pCO_2$.

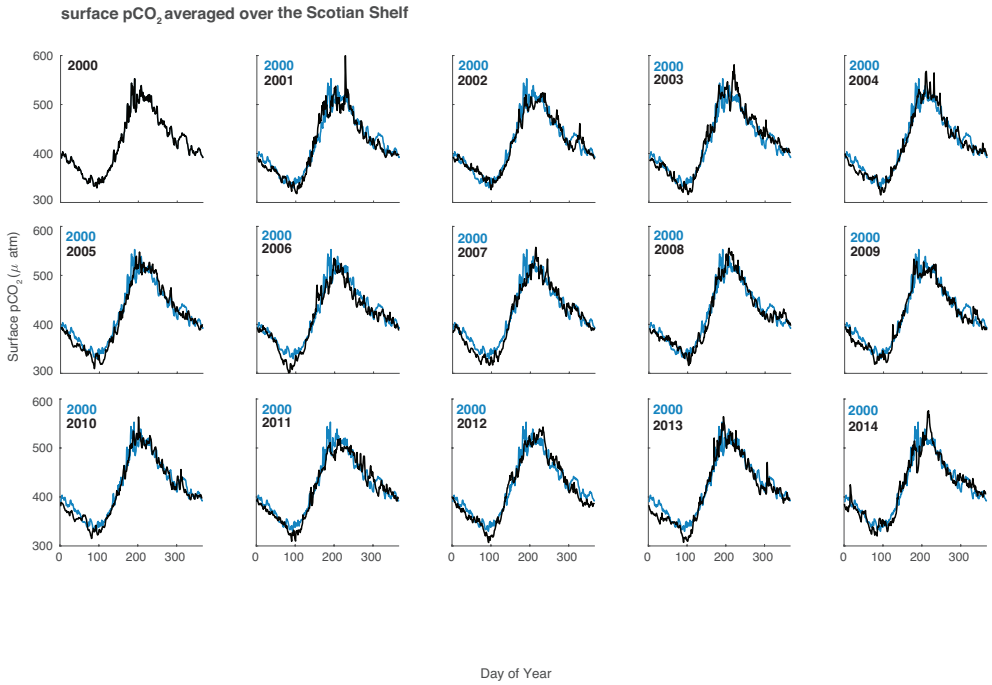


Figure B.3: Surface $pCO_2$ averaged over the Scotian Shelf comparing year 2000 with each subsequent year. Years 2001 to 2014 were mapped onto year 2000 using the longterm linear trend in atmospheric $pCO_2$.

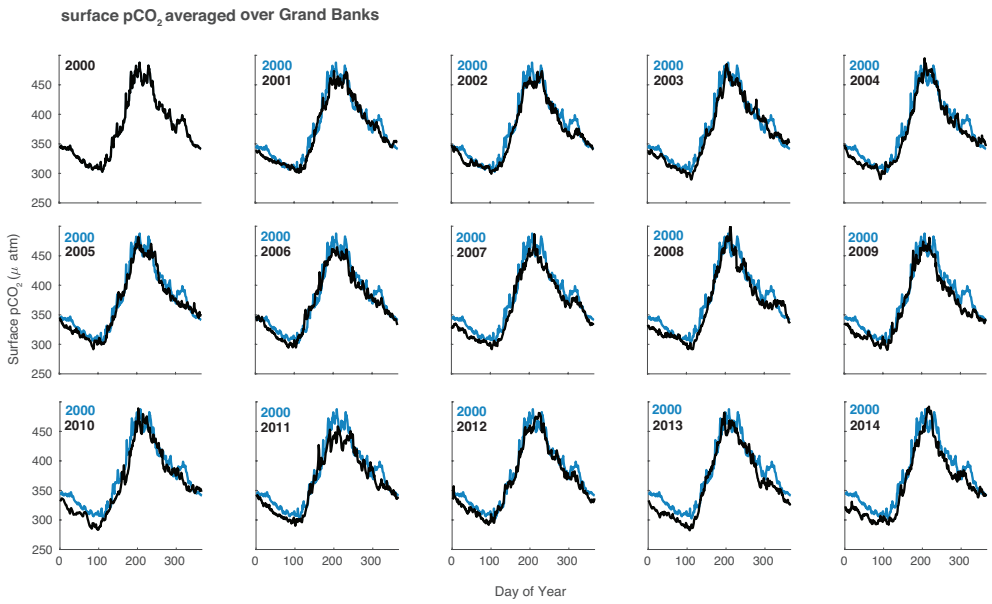


Figure B.4: Surface $pCO_2$ averaged over the Grand Banks comparing year 2000 with each subsequent year. Years 2001 to 2014 were mapped onto year 2000 using the longterm linear trend in atmospheric $pCO_2$.

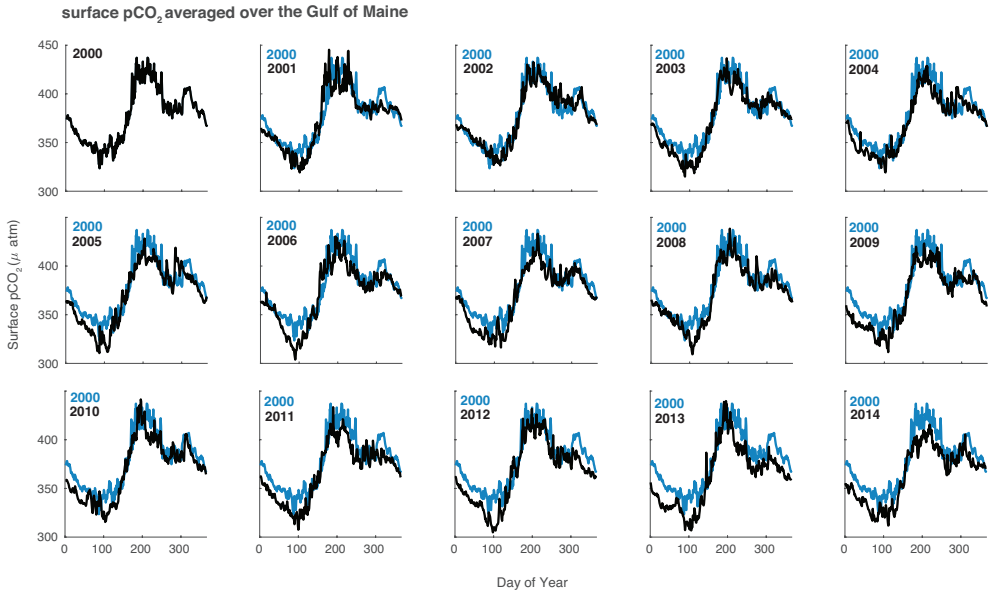


Figure B.5: Surface $pCO_2$ averaged over the Gulf of Maine comparing year 2000 with each subsequent year. Years 2001 to 2014 were mapped onto year 2000 using the longterm linear trend in atmospheric $pCO_2$.

## B.5 Model validation

Figure B.7 compares the model (year 2006) to DFO's AZMP cruise data (see Methods) at the CARIOCA buoy (location indicated in Figure 3.1, Table B.2 and Figure B.6). In Dissolved Inorganic Carbon (DIC), there is a similar model-observation comparison as in $pCO_2$. Mainly, during the bloom (April), surface DIC is overestimated in the model, indicating that the model does not quite capture the magnitude of the bloom and therefore does not capture the magnitude of the associated DIC drawdown. There is subsequently overestimation throughout the year in the model in the surface waters, similar to $pCO_2$ and likely as a result of the low bloom-related drawdown. In total alkalinity (TA), there is relatively good agreement with some overestimation later in the year, mainly in the surface waters. Figure B.8 shows further comparison of the model to AZMP cruise data along the Halifax Line (see Figure B.6 for location) for different months. There is relatively good qualitative agreement between the model and observations.

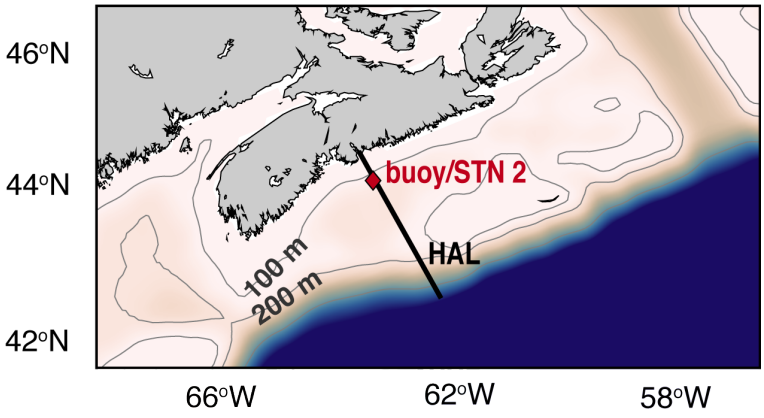


Figure B.6: Map of the Scotian Shelf with 100 m and 200 m isobaths. The Halifax Line (HAL; from AZMP cruises) in indicated by the black line and the CARIOCA buoy (Station 2 along the Halifax Line) is indicated by the red diamond.

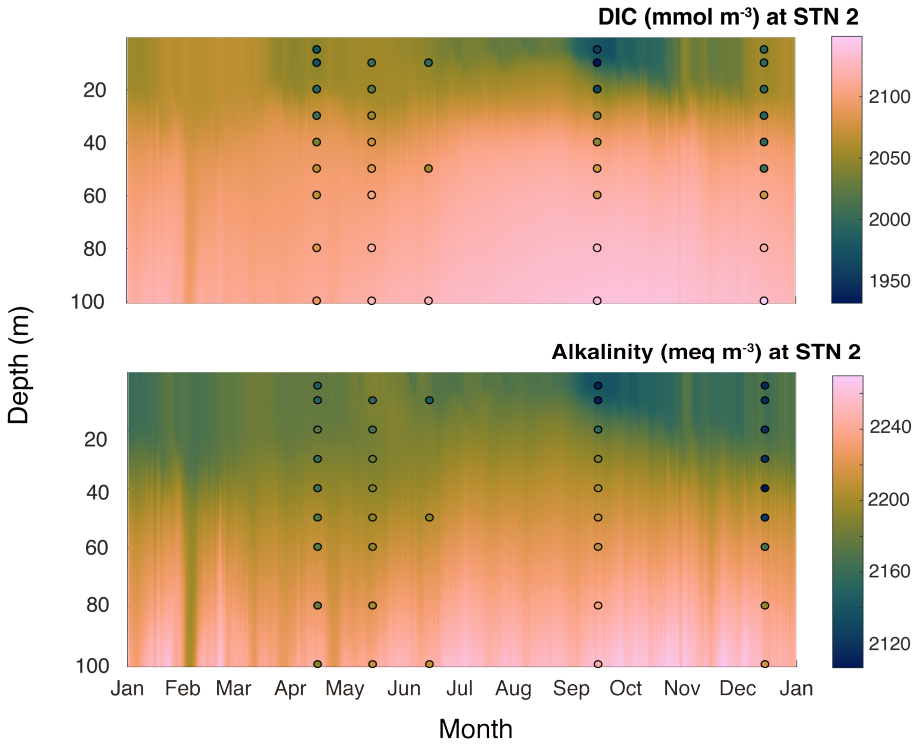


Figure B.7: Dissolved Inorganic Carbon (DIC; top panel) and Alkalinity (bottom panel) at the CARIOCA Buoy (Station 2 in the Halifax Line, for location see Figure 3.1 and Figure B.6). Background colour is year 2006 of model simulation. Points are averaged DIC and TA at each depth for each available month from the AZMP cruises.

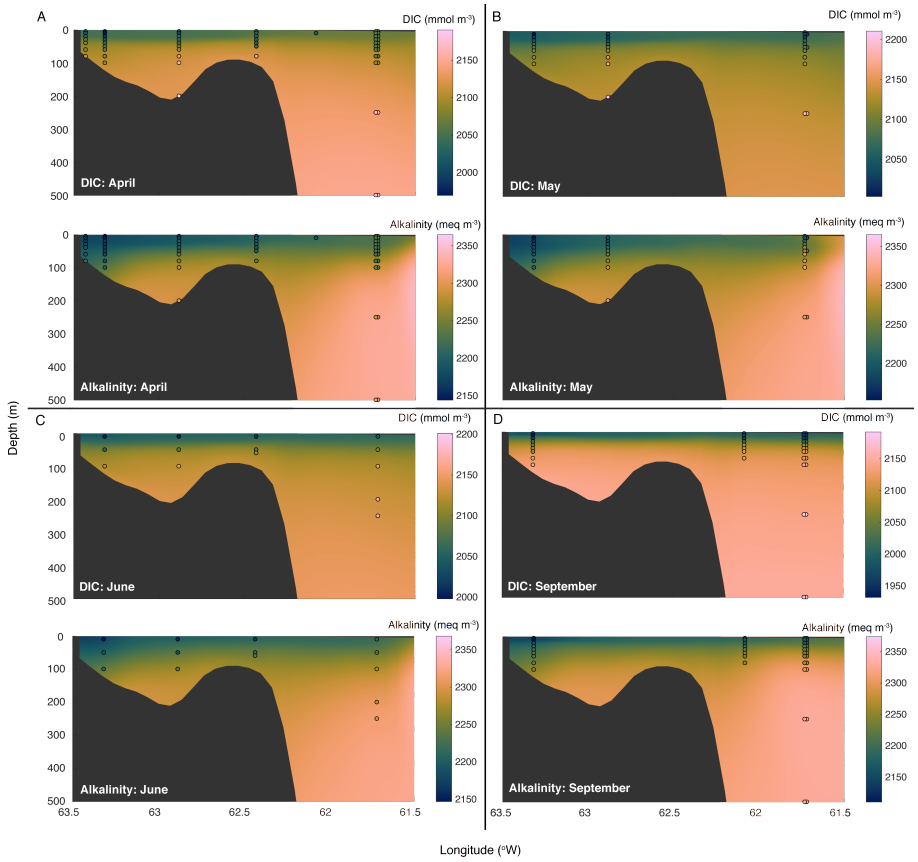


Figure B.8: Dissolved Inorganic Carbon (DIC) and Total Alkalinity (TA) at the CARIOCA Buoy along the Halifax Line (HAL; for location see Figure B.6) for (A) April, (B) May, (C) June, and (D) September. Background colour is monthly average DIC or TA for year 2006 of model simulation. Points are averaged DIC and TA at each depth for each available month from the AZMP cruises.

## B.6 Condor transect $pCO_2$

Figure S9 shows the full seasonal cycle of $pCO_2$ in two bins along the Atlantic Condor transect, both in the model and in the observations (panel a). Panels b through d illustrate the differences in $pCO_2$ and panels e through g illustrate temperature in the two bins during three time slices (A-C).

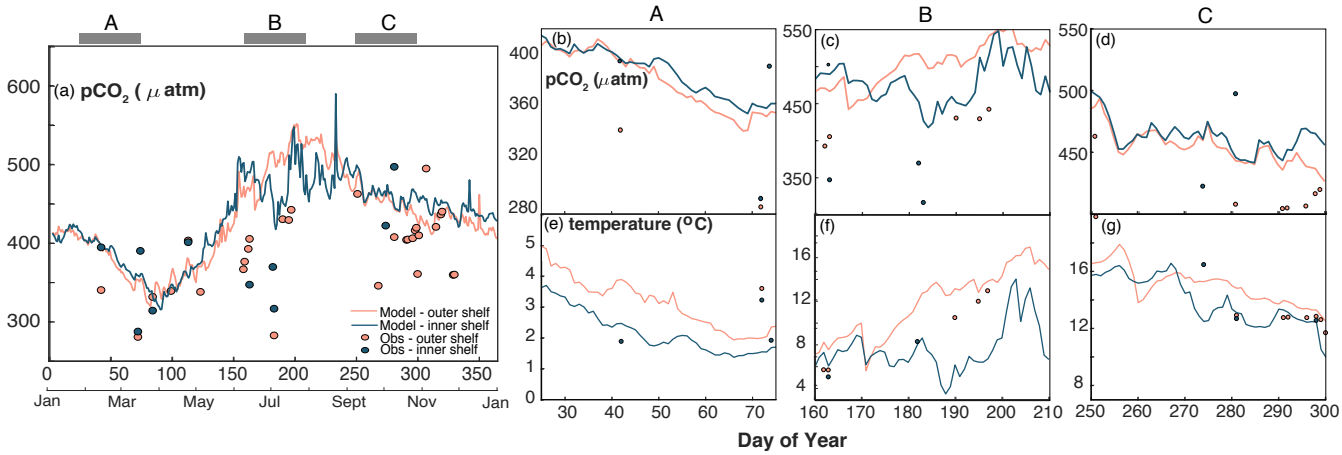


Figure B.9: Panel (a) indicates the full seasonal cycle of surface $pCO_2$ in two bins along the Atlantic Condor transect: Halifax Harbour bin (blue) and Deep Panuke/Shelfbreak bin (pink). See Figure 3.1 for the bin locations. Panels (b-d) indicate $pCO_2$ in these bins at three different time slices (A, B and C) which are indicated in panel (a). Panels (e-g) indicate temperature in these bins at the same time slices. The lines indicate the model year 2006 and the points indicate the Atlantic Condor observations.

## B.7 Upwelling transects

Figure B.10 shows additional variables along the Condor transect during the July 3, 2006 upwelling event in addition to the variables in Figure 3.6 in the main text.

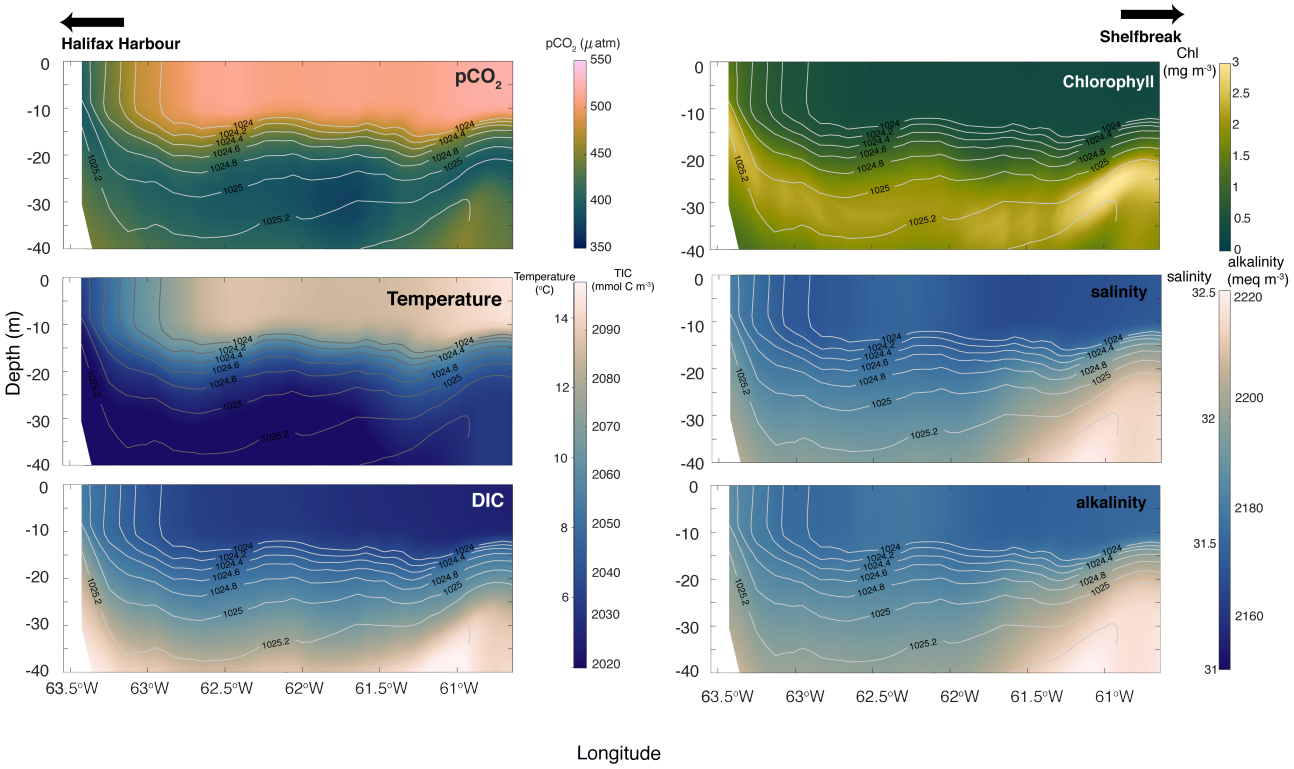


Figure B.10: Additional variables along the Atlantic Condor transect during the July 3, 2006 upwelling event. Left panels include (top to bottom): $p\mathrm{CO}_2$, temperature and dissolved inorganic carbon (DIC). Right panels include (top to bottom): chlorophyll, salinity, alkalinity. Contours on each panel indicate density. See Figure 1 for the location of the Atlantic Condor transect.

Figure B.11 illustrates the complete Taylor decomposition from Figure 3.7, including the effects of alkalinity ($\Delta\ p\mathrm{CO}_{2,TA}$) and salinity ($\Delta\ p\mathrm{CO}_{2,S}$).

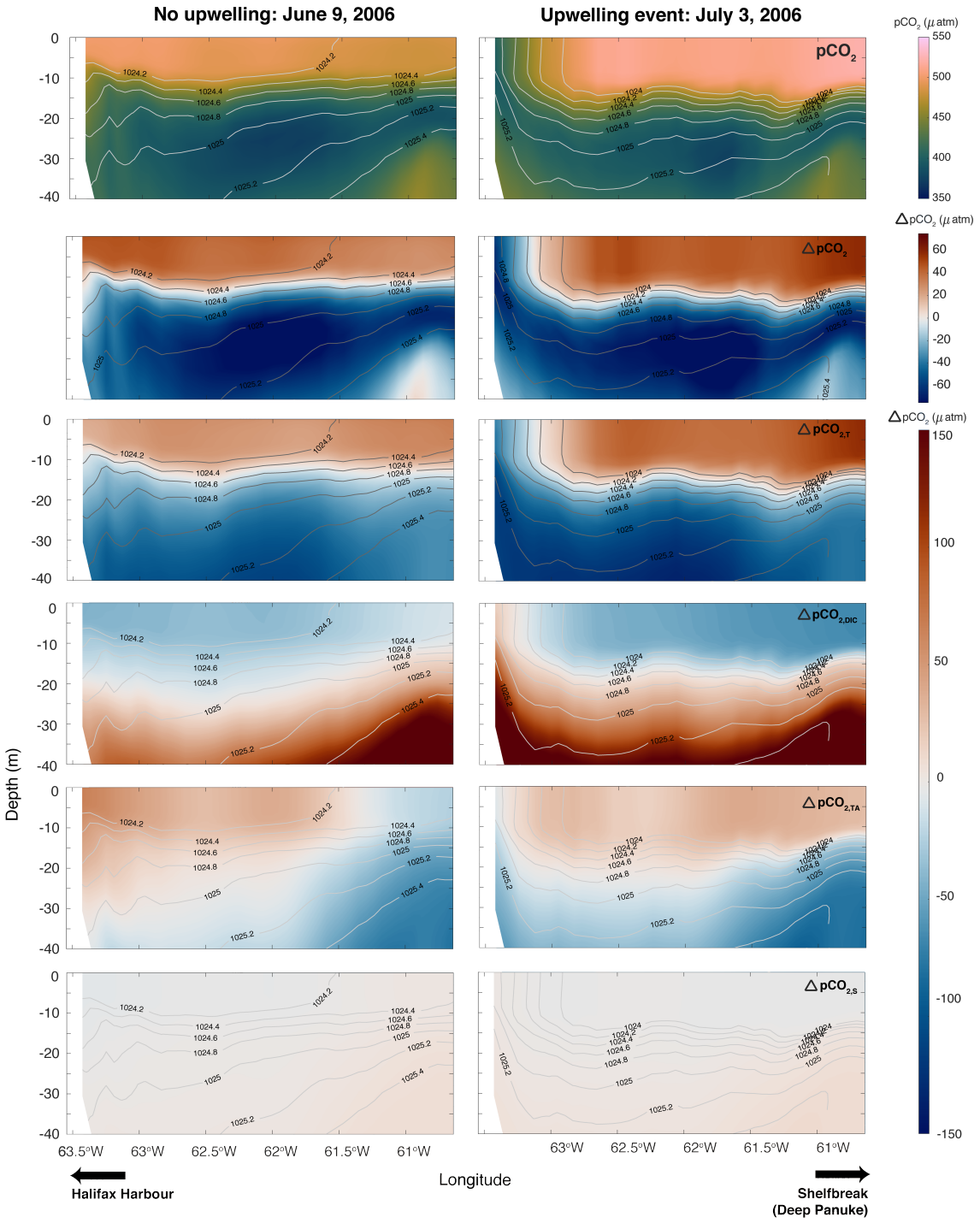


Figure B.11: The full Taylor decomposition of June 9, 2006 (left) versus July 3, 2006 (right). From top to bottom: (a) $pCO_2$, (b) overall anomaly in pCO2 ($\Delta$ $pCO_2$) from the mean $pCO_2$ in the upper 40 m, (c) anomaly in $pCO_2$ due to temperature changes ($\Delta$ $pCO_{2,T}$), (d) anomaly in $pCO_2$ due to DIC changes ($\Delta$ $pCO_{2,DIC}$), (e) anomaly in $pCO_2$ due to alkalinity changes ($\Delta$ $pCO_{2,TA}$), and (f) anomaly in $pCO_2$ due to salinity changes ($\Delta$ $pCO_{2,S}$).

# APPENDIX C

# SUPPLEMENTARY INFORMATION FOR *Elucidating coastal ocean carbon transport processes: A novel approach applied to the northwest North Atlantic shelf*

**Contents of this file**

1. Seasonal cycle of carbon disequilibrium (Section C.2 and Figure C.3)
2. Table C.1: Summary of endmember analysis
3. Figure C.2: Latitudinal trends in air-sea $CO_2$ flux including our regional model estimates
4. Section C.3: Further discussion of shelves that could behave similarly to the Scotian Shelf

## C.1 Introduction

The following supporting information includes: (1) extended depth profiles to incude the Gulf of St. Lawrence and total alkalinity, and a decomposition of DIC - $DIC_{eq}$; (2) of a table summary of the endmember analysis performed further to Figure 4.2 in the main text (see Table C.1); (3) an overview of the seasonal cycle of carbon disequilibrium (DIC - $DIC_{eq}$) on each of the continental shelves along eastern Canada (see section C.4, Figure

C.3); (4) a comparison of the model estimated air-sea $CO_2$ flux for the Grand Banks, Scotian Shelf and Gulf of Maine to the global synthesis of *Roobaert et al.* (2019) (see Figure C.4); and (5) an extended discussion of other shelves that could behave similarly to the Scotian Shelf.

## C.2 Extended depth profiles

Figure C.1 shows the spatially and temporally averaged depth profiles in each subregion, including the Gulf of St. Lawrence. The profiles for the Gulf of St. Lawrence illustrate its effect on the Scotian Shelf, which is particularly evident in the alkalinity profiles: the low alkalinity in the Gulf of St. Lawrence drives the Scotian Shelf alkalinity lower than the other shelves in the region (e.g. Gulf of Maine, Grand Banks, East Newfoundland Shelf). The increased DIC at depth and lower alkalinity compared to the other shelves in the region is likely indicative of the accumulation of remineralization products at depth, which has been shown to dominantly occur in the region (see *Wang et al.*, 2017).

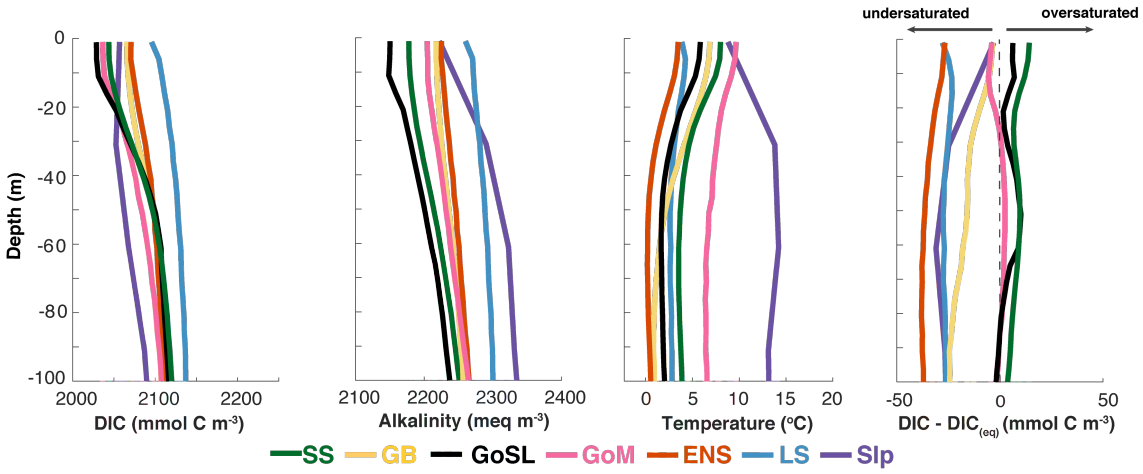


Figure C.1: Horizontally and temporally averaged profiles of simulated (left to right) DIC (mmol C $m^{-3}$), alkalinity (meq $^{-3}$), temperature ($^o$C) and DIC – $DIC_{eq}$ (mmol C $m^{-3}$) in the six model subregions representing the two ocean end members (Slp and LS) and for the four shelf regions (ENS, GB, SS and GoM)are shown by the solid line.

To further illustrate the effect of biological processing versus temperature on the carbonate chemistry in the region, we further decompose carbon disequilibrium (DIC - $DIC_{eq}$), which is calculated according to:

$$(DIC - DIC_{eq})_X = DIC_X - f(T_X, S_X, TA_X, pCO_{2,eq}) \tag{C.1}$$

where $X$ is the region of interest (Scotian Shelf, Gulf of Maine, Grand Banks, etc.) and $f$ is the CO2SYS function (*Lewis and Wallace*, 1998) based off of temperature (T), salinity (S), alkainity (TA), dissolved inorganic carbon (DIC), and an equilibrium $pCO_2$. We can substitute one by one DIC, T, S and TA from ENS to better understand how each variable is impacting the carbon disequilibrium in region X. To illustrate the effect of each variable most effectively, here we cumulatively add in the effect of T, S, TA and DIC to the Scotian Shelf and Grand Banks carbon disequilibrium to essentially reproduce the ENS carbon disequilibrium in Figure C.2. This decomposition shows that temperature accounts for 60-100% of the change in saturation from East Newfoundland Shelf to both Grand Banks and Scotian Shelf in the upper 30 m, with less of an effect below 30 m. The combined effect of alkainity and DIC, accounts for the remaining change in saturation.

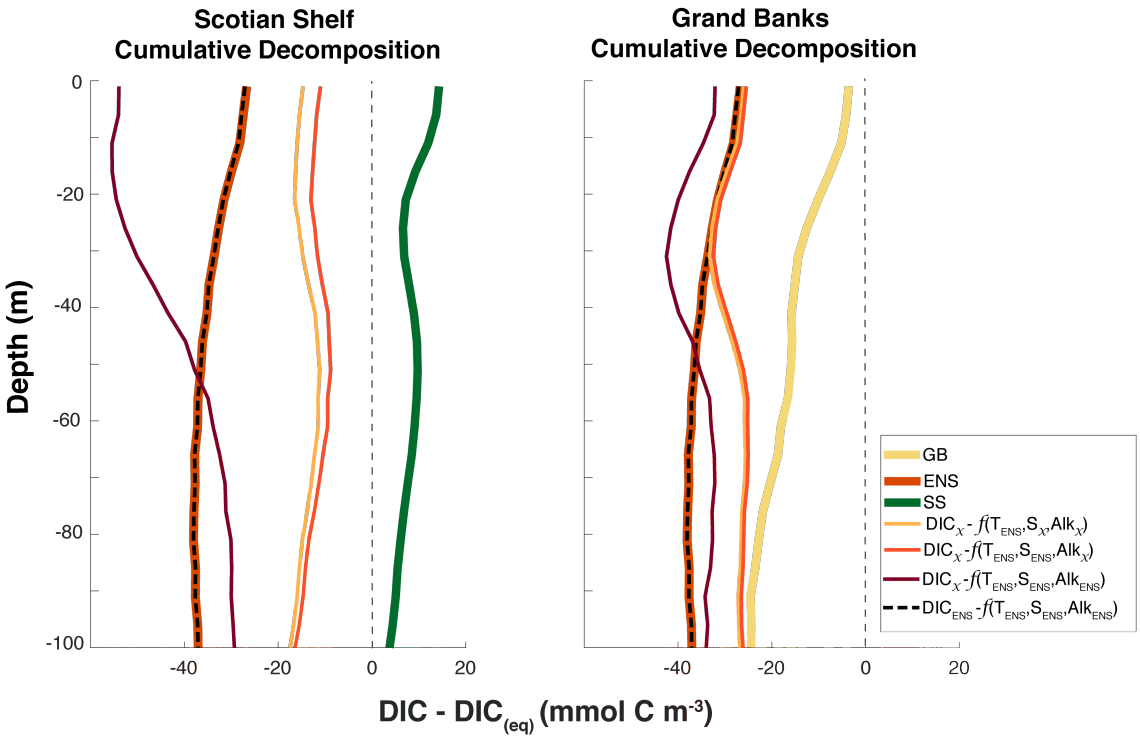


Figure C.2: Cumulatively replacing $T_X$, $S_X$, $TA_X$ and $DIC_X$ in equation C.1 with $T_{ENS}$, $S_{ENS}$, $TA_{ENS}$ and $DIC_{ENS}$ to decompose DIC – $DIC_{eq}$ (mmol C $m^{-3}$) for both Grand Banks (left) and Scotian Shelf (right).

## C.3 Table summary of endmember analysis

Table C.1: Dye mass fractions ($X_{reg}$), which sum to 1, and average DIC, T and S for each subregion. Combining the mass fractions and mean values in a simple weighted mean (see Equation 1 in main text) yields the predicted values for the Scotian Shelf ($SS_{pred}$), Grand Banks ($GB_{pred}$) and Gulf of Maine ($GoM_{pred}$).

| | **Dye Mass Fraction ($X_{reg}$)** | | | **DIC** | **Temperature** | |
|---|---|---|---|---|---|---|
| **Region** | **SS** | **GB** | **GoM** | **(mmol C m$^{-3}$)** | **($^o$C)** | **Salinity** |
| Slp-S | 0.14 | 0.08 | 0.19 | 2077.6 | 13.7 | 34.8 |
| Slp-D | 0.12 | 0.06 | 0.21 | 2153.7 | 5.0 | 35.0 |
| LS | 0.37 | 0.43 | 0.30 | 2141.7 | 3.8 | 34.5 |
| ENS | 0.36 | 0.43 | 0.29 | 2102.8 | 2.2 | 33.3 |
| SLR | 0.01 | <0.01 | <0.01 | 796.3 | 3.2 | 10.0 |
| **$SS_{pred}$** | – | – | – | 2106.7 | 4.7 | 33.9 |
| **$SS_{model}$** | – | – | – | 2079.8 | 5.9 | 32.2 |
| **$GB_{pred}$** | – | – | – | 2120.6 | 3.9 | 34.0 |
| **$GB_{model}$** | – | – | – | 2089.1 | 4.5 | 32.8 |
| **$GoM_{pred}$** | – | – | – | 2120.1 | 5.5 | 34.3 |
| **$GoM_{model}$** | – | – | – | 2067.1 | 5.9 | 32.2 |

## C.4 Seasonal cycle of carbon disequilibrium

The seasonal cycle of the carbon disequilibrium (DIC – $DIC_{eq}$) in the four shelf regions is shown in Figure C.3. The seasonal patterns of carbon disequilibrium are similar on the ENS and GB and remain undersaturated throughout most of the year. The minimum in undersaturation on the ENS and weak oversaturation on the GB occurs during the summer months in the top 20 to 30 m because of seasonal surface warming. The undersaturation is weaker on the GB as a result of warming as the water moved from the ENS to the GB. The pattern of seasonal carbon disequilibirum on the SS shows undersaturation only briefly during the spring bloom (March to May) while temperatures are lowest and photosynthetic carbon uptake is highest (*Rutherford et al.*, 2021) and marks the brief period when the SS acts as a sink of $CO_2$ (*Rutherford et al.*, 2021; *Shadwick et al.*, 2011). The SS is strongly oversaturated from June to January throughout the water column. This oversaturation is the direct result of warming that occurred while shelf water travelled from ENS to SS (Figure 3, main text). The GoM, where the influence of Gulf Stream waters is more pronounced and the fraction of ENS and LS waters reduced, is closer to equilibrium than the other

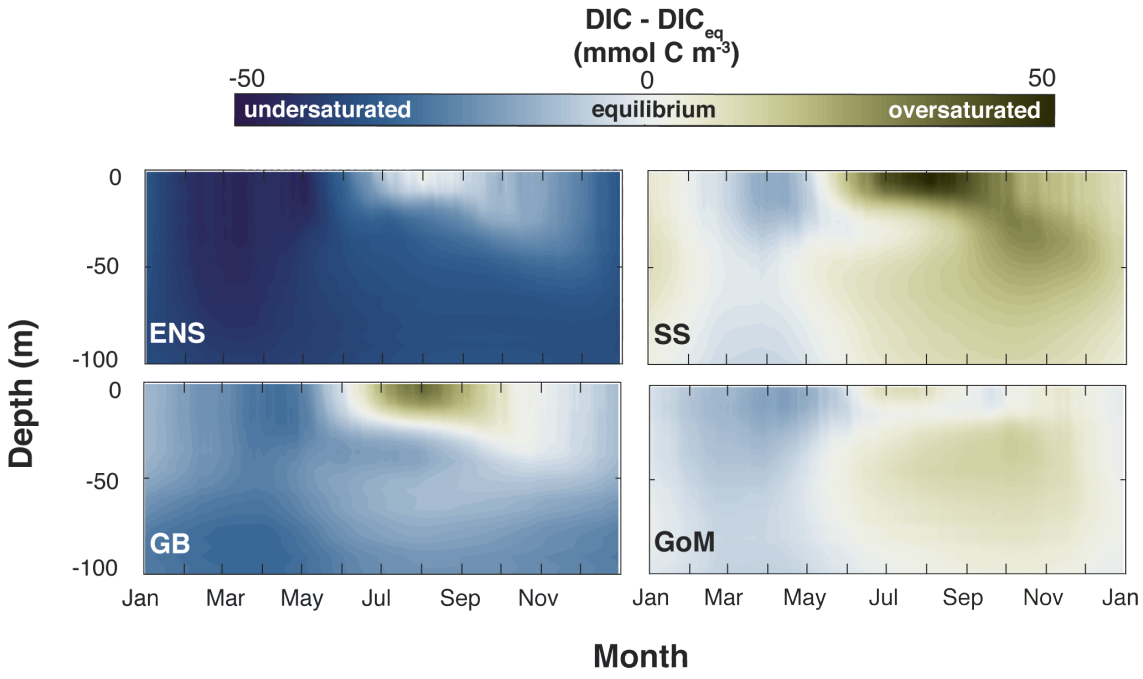


Figure C.3: Horizontally averaged profiles of DIC – DIC$_{eq}$ (mmol C m$^{-3}$) for each of the four shelf regions.

shelve regions. GoM has a long period of undersaturation from January to June throughout the entire water column, and is near equilibrium throughout the water column from July to December.

## C.5 Global latitudinal trends in air-sea $CO_2$ flux

Figure C.4 illustrates the latitudinal trend in air-sea $CO_2$ fluxes, and is adapted from *Roobaert et al.* (2019). The model simulated values from the present study are also included for comparison to the latitudinal trend.

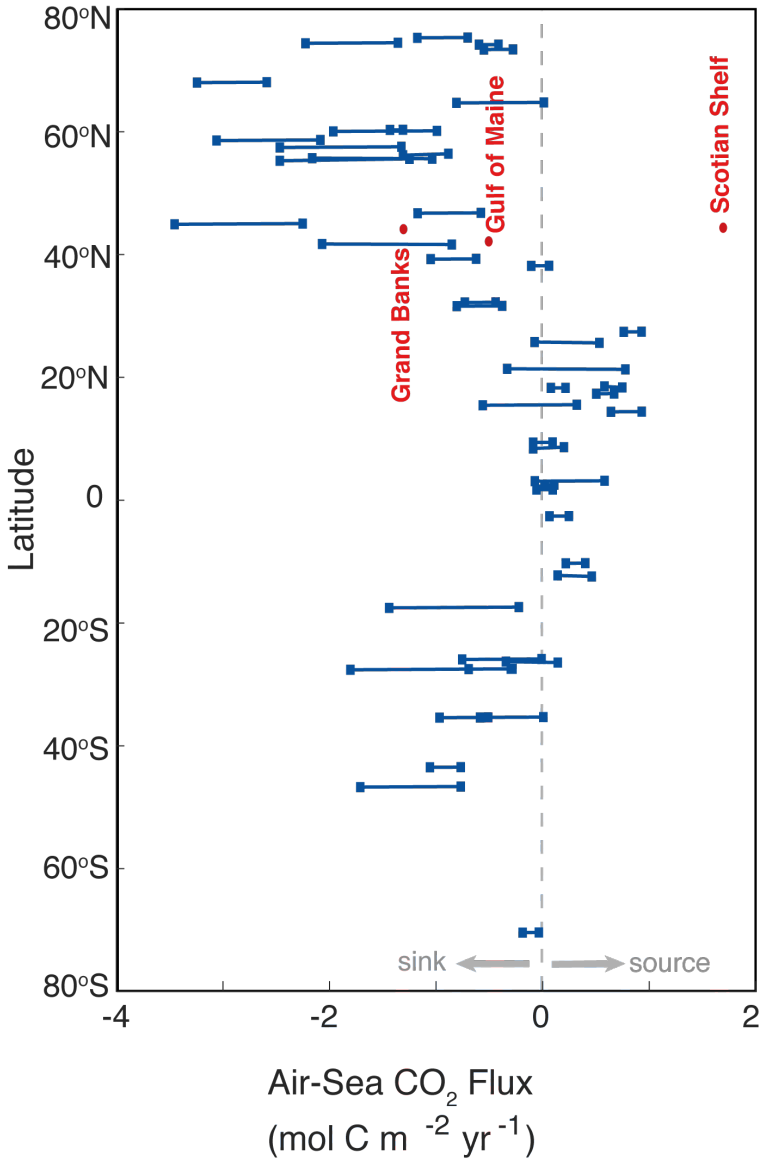


Figure C.4: Latitudinal trends in air-sea $CO_2$ flux. The blue lines indicate observational flux ranges and the red points indicate simulated values. The figure is adapted, and observational numbers taken, from *Roobaert et al.* (2019). The simulated values for the Scotian Shelf, Grand Banks, and Gulf of Maine are from the present study.

## C.6 Discussion of global continental shelves

In Section 4.6, we discuss how the Patagonian Shelf might behave similarly to the Scotian Shelf. This comparison is based on the following features: (1) shelf geometry (width of $\sim$120 to 300 km), (2) location at the confluence of a subtropical current (Brazil Current) and subantarctic current (Malvinas Current), (3) physical and chemical properties largely being explained by the nutrient rich subantarctic water masses, and (4) seasonal temperatures ranging from 7 to 20$^o$C (*Liu et al.*, 2010). There are other potential analogues that are worth discussing.

The eastern coast of New Zealand's south island is another subpolar shelf that could be explored. Its southernmost portion, the Otago shelf, is quite narrow (on the order of $\sim$40 km wide) and is bounded by the Southland Current along the shelf-break, which is thought to be mainly subtropical in origin rather than a subpolar or subantarctic originating current (*Liu et al.*, 2010; *Hawke*, 1989). North of the Otago Shelf is Pegasus Bay where the shelf is wider and more influenced by subantarctic waters (*Stevens et al.*, 2021). Seasonal temperature ranges here are large but slightly smaller than the Scotian Shelf and Patagonian shelf, ranging from $\sim$8 to 20 $^o$C (*Stevens et al.*, 2021). These comparisons indicate that potentially the northeastern coast of New Zealand's south island, where subantarctic waters dominate, could behave similarly to the Scotian Shelf.

The southeastern coast of Tasmania could potentially be another region of interest. It is complexly affected by two opposing currents: the East Australian Current, which carries warm and salty water southward along the eastern coast of Tasmania, and the relatively fresher and cooler Zeehan Current which flows southward along Tasmania's western coast and turns at the southern tip to travel slightly northward along the eastern shelf (*Oliver and Holbrook*, 2018). There is a distinct seasonality in the behaviour of these currents, whereby in summer, the East Australian Current dominates most of the eastern shelf of Tasmania and in winter the Zeehan Current affects most of the eastern shelf (*Ridgway*, 2007; *Oliver and Holbrook*, 2018). Overall, the complex circulation features indicate that potentially the most southern portion of the eastern shelf, which is affected more by the cool, fresh Zeehan Current throughout most of the year, could be a region behaving similarly to the Scotian Shelf. Surface temperature ranges here are, however, much smaller, on the order of $\sim$12-17$^o$C (*Ridgway*, 2007), making it less likely to behave similar to the Scotian Shelf.

# APPENDIX D

# SUPPLEMENTARY INFORMATION FOR *Shifting circulation under a changing climate: Biogeochemical impacts in the northwest North Atlantic*

Table D.1: Dye mass fractions comparing present-day water mass composition to two future scenarios, DFO-NEMO and GFDL, on each of the shelves (Grand Banks, GB; Scotian Shelf, SS; and Gulf of Maine, GoM).

| | Region | Slp-S | Slp-D | LS | ENS | SLR |
|---|---|---|---|---|---|---|
| Present | GB | 0.08 | 0.06 | 0.43 | 0.43 | <0.01 |
| | SS | 0.14 | 0.12 | 0.37 | 0.36 | <0.01 |
| | GoM | 0.19 | 0.21 | 0.30 | 0.29 | <0.01 |
| DFO-NEMO | GB | 0.09 | 0.10 | 0.40 | 0.41 | <0.01 |
| | SS | 0.17 | 0.15 | 0.34 | 0.34 | <0.01 |
| | GoM | 0.20 | 0.20 | 0.30 | 0.30 | <0.01 |
| GFDL | GB | 0.12 | 0.14 | 0.37 | 0.37 | <0.01 |
| | SS | 0.27 | 0.28 | 0.23 | 0.22 | <0.01 |
| | GoM | 0.32 | 0.38 | 0.16 | 0.14 | <0.01 |

# BIBLIOGRAPHY


Agmon, N., Residence times in diffusion processes, *Journal of Chemical Physics*, *81*, 3644–3647, 1984.

Alexander, M. A., S.-i. Shin, J. D. Scott, E. Curchitser, and C. Stock, The response of the northwest atlantic ocean to climate change, *Journal of Climate*, *33*, 405–428, 2020.

Arruda, R., D. Atamanchuk, M. Cronin, T. Steinhoff, and D. W. Wallace, At-sea intercomparison of three underway $pco_2$ systems, *Limnology and Oceanography: Methods*, *18*, 63–76, 2020.

Bakker, D. C., B. Pfeil, K. Smith, S. Hankin, A. Olsen, S. R. Alin, C. Cosca, S. Harasawa, A. Kozyr, Y. Nojiri, et al., An update to the surface ocean $CO_2$ atlas (SOCAT version 2), *Earth System Science Data*, *6*, 69–90, 2014.

Bakker, D. C., B. Pfeil, C. S. Landa, N. Metzl, K. M. O'brien, A. Olsen, K. Smith, C. Cosca, S. Harasawa, S. D. Jones, et al., A multi-decade record of high-quality $fCO_2$ data in version 3 of the Surface Ocean $CO_2$ Atlas (SOCAT), *Earth System Science Data*, *8*, 383–413, 2016.

Banas, N. S., and B. M. Hickey, Mapping exchange and residence time in a model of Willapa Bay, Washington, a branching, macrotidal estuary, *Journal of Geophysical Research: Oceans*, *110*, 1–20, 2005.

Banyte, D., M. Visbeck, T. Tanhua, T. Fischer, G. Krahmann, and J. Karstensen, Lateral diffusivity from tracer release experiments in the tropical North Atlantic thermocline, *Journal of Geophysical Research: Oceans*, *118*, 2719–2733, 2013.

Beardsley, R. C., and W. C. Boicourt, On Estuarine and Continental-Shelf Circulation in the Middle Atlantic Bight, in *Evolution of Physical Oceanography*, pp. 198–233, 1981.

Beining, P., and W. Roether, Temporal evolution of CFC 11 and CFC 12 concentrations in the ocean interior, *Journal of Geophysical Research: Oceans*, *101*, 16455–16464, 1996.

Berezhkovskii, A. M., V. Zaloj, and N. Agmon, Residence time distribusion of a Brownian particle, *Physics Review E*, *57*, 3937–3947, 1998.

Bianucci, L., K. Fennel, D. Chabot, N. Shackell, and D. Lavoie, Ocean biogeochemical models as management tools: a case study for Atlantic wolffish and declining oxygen, *ICES Journal of Marine Science*, *73*, 263–274, 2016.

Bourgeois, T., J. C. Orr, L. Resplandy, J. Terhaar, C. Ethé, M. Gehlen, and L. Bopp, Coastal-ocean uptake of anthropogenic carbon, *Biogeosciences*, *13*, 4167–4185, 2016.

Brennan, C. E., L. Bianucci, and K. Fennel, Sensitivity of northwest North Atlantic shelf circulation to surface and boundary forcing: A regional model assessment, *Atmosphere-Ocean*, *54*, 230–247, 2016.

Brennan, C. E., H. Blanchard, and K. Fennel, Putting temperature and oxygen thresholds of marine animals in context of environmental change: A regional perspective for the Scotian Shelf and Gulf of St. Lawrence, *PLoS ONE*, *11*, 1–27, 2016a.

Brickman, D., *High resolution future climate ocean model simulations for the northwest Atlantic shelf region*, Fisheries and Oceans Canada, 2016.

Brickman, D., D. Hebert, and Z. Wang, Mechanism for the recent ocean warming events on the Scotian Shelf of eastern Canada, *Continental Shelf Research*, *156*, 11–22, 2018.

Brickman, D., M. A. Alexander, A. Pershing, J. D. Scott, and Z. Wang, Projections of physical conditions in the Gulf of Maine in 2050, *Elem Sci Anth*, *9*, 00055, 2021.

Broecker, W. S., The great ocean conveyor, *Oceanography*, *4*, 79–89, 1991.

Bugden, G., B. Hargrave, M. Sinclair, C. Tang, J.-C. Therriault, and P. Yeats, Freshwater runoff effects in the marine environment: The Gulf of St. Lawrence example, *Canadian Technical Report of Fisheries and Aquatic Sciences*, 1982.

Burt, W. J., H. Thomas, and J. P. Auclair, Short-lived radium isotopes on the Scotian Shelf: Unique distribution and tracers of cross-shelf $CO_2$ and nutrient transport, *Marine Chemistry*, *156*, 120–129, 2013.

Cai, W.-J., Estuarine and coastal ocean carbon paradox: $CO_2$ sinks or sites of terrestrial carbon incineration?, *Annual Review of Marine Science*, *3*, 123–145, 2011.

Cai, W.-J., M. Dai, and Y. Wang, Air-sea exchange of carbon dioxide in ocean margins: A province-based synthesis, *Geophysical Research Letters*, *33*, 2006.

Cai, W.-J., L. Chen, B. Chen, Z. Gao, S. H. Lee, J. Chen, D. Pierrot, K. Sullivan, Y. Wang, X. Hu, W.-J. Huang, Y. Zhang, S. Xu, A. Murata, J. M. Grebmeier, E. P. Jones, and H. Zhang, Decrease in the $CO_2$ uptake capacity in an ice-free arctic ocean basin, *Science*, *329*, 556–559, 2010.

Cao, L., M. Eby, A. Ridgwell, K. Caldeira, D. Archer, A. Ishida, F. Joos, K. Matsumoto, U. Mikolajewicz, A. Mouchet, J. C. Orr, G.-K. Plattner, R. Schlitzer, K. Tokos, I. Totterdell, T. Tschumi, Y. Yamanaka, and A. Yool, The role of ocean transport in the uptake of anthropogenic $CO_2$, *Biogeosciences*, *6*, 375–390, 2009.

Chapman, D. C., and R. C. Beardsley, On the origin of shelf water in the Middle Atlantic Bight, *Journal of Physical Oceanography*, *19*, 384–391, 1989.

Chavez, F. P., J. T. Pennington, R. P. Michisaki, M. Blum, G. M. Chavez, J. Friederich, B. Jones, R. Herlien, B. Kieft, B. Hobson, et al., Climate variability and change: response of a coastal ocean ecosystem, *Oceanography*, *30*, 128–145, 2017.

Chen, C.-T. A., and A. V. Borges, Reconciling opposing views on carbon cycling in the coastal ocean: Continental shelves as sinks and near-shore ecosystems as sources of atmospheric $CO_2$, *Deep Sea Research Part II: Topical Studies in Oceanography*, *56*, 578–590, 2009.

Chen, C.-T. A., T.-H. Huang, Y.-C. Chen, Y. Bai, X. He, and Y. Kang, Air sea exchanges of $CO_2$ in the world's coastal seas, *Biogeosciences*, *10*, 6509–6544, 2013.

Claret, M., E. D. Galbraith, J. B. Palter, D. Bianchi, K. Fennel, D. Gilbert, and J. P. Dunne, Rapid coastal deoxygenation due to ocean circulation shift in the northwest atlantic, *Nature climate change*, *8*, 868–872, 2018.

Conover, R. J., Comparative life histories in the genera *Calanus* and *Neocalanus* in high latitudes of the northern hemisphere, *Hydrobiologia*, *167-168*, 127–142, 1988.

Craig, S. E., H. Thomas, C. T. Jones, W. K. W. Li, B. J. W. Greenan, E. H. Shadwick, and W. J. Burt, The effect of seasonality in phytoplankton community composition on $CO_2$ uptake on the Scotian Shelf, *Journal of Marine Systems*, *147*, 52–60, 2015.

Curran, K., and K. Azetsu-Scott, Ocean acidification: State of the Scotian Shelf report, *Tech. rep.*, Fisheries and Oceans Canada, 2012.

Dee, D. P., S. Uppala, A. Simmons, P. Berrisford, P. Poli, S. Kobayashi, U. Andrae, M. Balmaseda, G. Balsamo, d. P. Bauer, et al., The era-interim reanalysis: Configuration and performance of the data assimilation system, *Quarterly Journal of the Royal Meteorological Society*, *137*, 553–597, 2011.

Deleersnijder, É., J. M. Campin, and É. J. M. Delhez, The concept of age in marine modelling I. Theory and preliminary model results, *Journal of Marine Systems*, *28*, 229–267, 2001.

Delhez, É. J. M., Transient residence and exposure times, *Ocean Science*, *2*, 1–9, 2006.

Delhez, É. J. M., and É. Deleersnijder, The boundary layer of the residence time field, *Ocean Dynamics*, *56*, 139–150, 2006.

Delhez, É. J. M., J. M. Campin, A. C. Hirst, and É. Deleersnijder, Toward a general theory of the age in ocean modelling, *Ocean Modelling*, *1*, 17–27, 1999.

Delhez, É. J. M., A. W. Heemink, and É. Deleersnijder, Residence time in a semi-enclosed domain from the solution of an adjoint problem, *Estuarine, Coastal and Shelf Science*, *61*, 691–702, 2004.

Delworth, T. L., A. Rosati, W. Anderson, A. J. Adcroft, V. Balaji, R. Benson, K. Dixon, S. M. Griffies, H.-C. Lee, R. C. Pacanowski, et al., Simulated climate and climate change in the GFDL CM2. 5 high-resolution coupled climate model, *Journal of Climate*, *25*, 2755–2781, 2012.

Dever, M., D. Hebert, B. Greenan, J. Sheng, and P. Smith, Hydrography and coastal circulation along the Halifax Line and the connections with the Gulf of St. Lawrence, *Atmosphere-Ocean*, *54*, 199–217, 2016.

Doney, S. C., The growing human footprint on coastal and open ocean biogeochemistry, *Science*, *328*, 1512–1516, 2010.

Drinkwater, K., B. Petrie, and W. Sutcliffe, Seasonal geostrophic volume transports along the Scotian Shelf, *Estuarine and Coastal Marine Science*, *9*, 17–27, 1979.

Dufour, C. O., S. M. Griffies, G. F. de Souza, I. Frenger, A. K. Morrison, J. B. Palter, J. L. Sarmiento, E. D. Galbraith, J. P. Dunne, W. G. Anderson, et al., Role of mesoscale eddies in cross-frontal transport of heat and biogeochemical tracers in the Southern Ocean, *Journal of Physical Oceanography*, *45*, 3057–3081, 2015.

Egbert, G. D., and S. Y. Erofeeva, Efficient inverse modeling of barotropic ocean tides, *Journal of Atmospheric and Oceanic Technology*.

England, M. H., The age of water and ventilation timescales in a global ocean model, *Journal of Physical Oceanography*, *25*, 2756–2777, 1995.

Environment and Climate Change Canada, Canadadian greenhouse gas measurement program, 2017, [online], Accessed at: https://www.canada.ca/en/environment-climate-change/services/climate-change/science-research-data/greenhouse-gases-aerosols-monitoring/canadian-greenhouse-gas-measurement-program.html.

Evans, W., B. Hales, P. G. Strutton, R. K. Shearman, and J. A. Barth, Failure to bloom: Intense upwelling results in negligible phytoplankton response and prolonged $CO_2$ outgassing over the oregon shelf, *Journal of Geophysical Research: Oceans*, *120*, 1446–1461, 2015.

Feely, R. A., C. L. Sabine, J. M. Hernandez-Ayon, D. Ianson, and B. Hales, Evidence for upwelling of corrosive "acidified" water onto the continental shelf, *Science*, *320*, 1490–1492, 2008.

Fennel, K., and J. Wilkin, Quantifying biological carbon export for the northwest North Atlantic continental shelves, *Geophysical Research Letters*, *36*, L18605, 2009.

Fennel, K., J. Wilkin, J. Levin, J. Moisan, J. O'Reilly, and D. Haidvogel, Nitrogen cycling in the Middle Atlantic Bight: Results from a three-dimensional model and implications for the North Atlantic nitrogen budget, *Global Biogeochemical Cycles*, *20*, 2006.

Fennel, K., J. Wilkin, M. Previdi, and R. Najjar, Denitrification effects on air-sea $CO_2$ flux in the coastal ocean: Simulations for the northwest North Atlantic, *Geophysical Research Letters*, *35*, 2008.

Fennel, K., S. Alin, L. Barbero, W. Evans, T. Bourgeois, S. Cooley, J. Dunne, R. A. Feely, J. M. Hernandez-Ayon, X. Hu, S. Lohrenz, F. Muller-Karger, R. Najjar, L. Robbins, E. Shadwick, S. Siedlecki, N. Steiner, A. Sutton, D. Turk, P. Vlahos, and Z. A. Wang, Carbon cycling in the North American coastal ocean: a synthesis, *Biogeosciences*, *16*, 1281–1304, 2019.

Fiechter, J., E. N. Curchitser, C. A. Edwards, F. Chai, N. L. Goebel, and F. P. Chavez, Air-sea $CO_2$ fluxes in the california current: Impacts of model resolution and coastal topography, *Global Biogeochemical Cycles*, *28*, 371–385, 2014.

Fine, R. A., Tracers, time scales, and the thermohaline circulation: The lower limb in the North Atlantic Ocean, *Reviews of Geophysics*, *33*, 1353–1365, 1995.

Fleminger, A., and K. Hulsemann, Geographical range and taxonomic divergence in North Atlantic *Calanus* (*C. helgolandicus*, *C. finmarchicus* and *C. glacialis*), *Marine Biology*, *40*, 233–248, 1977.

Fournier, R. O., J. Marra, R. Bohrer, and M. V. Det, Plankton dynamics and nutrient enrichment of the Scotian Shelf, *Journal of the Fisheries Board of Canada*, 1977.

Fratantoni, P. S., and R. S. Pickart, The western North Atlantic shelfbreak current system in summer, *Journal of Physical Oceanography*, *37*, 2509–2533, 2007.

Galbraith, E. D., J. P. Dunne, A. Gnanadesikan, R. D. Slater, J. L. Sarmiento, C. O. Dufour, G. F. De Souza, D. Bianchi, M. Claret, K. B. Rodgers, et al., Complex functionality with minimal computation: Promise and pitfalls of reduced-tracer ocean biogeochemistry models, *Journal of Advances in Modeling Earth Systems*, *7*, 2012–2028, 2015.

Galbraith, P., J. Chassé, P. Larouche, D. Gilbert, D. Brickman, B. Pettigrew, L. Devine, and C. Lafleur, Physical oceanographic conditions in the Gulf of St. Lawrence in 2012, *Tech. Rep. 89*, Fisheries and Oceans Canada, 2013.

Gawarkiewicz, G. G., R. E. Todd, A. J. Plueddemann, M. Andres, and J. P. Manning, Direct interaction between the Gulf Stream and the shelfbreak south of New England, *Scientific reports*, *2*, 1–6, 2012.

Geshelin, Y., J. Sheng, and R. J. Greatbatch, Monthly mean climatologies of temperature and salinity in the western North Atlantic, *Tech. rep.*, Canadian Data Report of Hydrography and Ocean Sciences, Fisheries and Oceans Canada, 1999.

Gilbert, D., B. Sundby, C. Gobeil, A. Mucci, and G.-H. Tremblay, A seventy-two-year record of diminishing deep-water oxygen in the St. Lawrence estuary: The northwest Atlantic connection, *Limnology and Oceanography*, *50*, 1654–1666, 2005.

Gilbert, D., N. N. Rabalais, R. J. Díaz, and J. Zhang, Evidence for greater oxygen decline rates in the coastal ocean than in the open ocean, *Biogeosciences*, *7*, 2283–2296, 2010.

Gruber, N., Carbon at the coastal interface, *Nature*, *517*, 148–149, 2015.

Gruber, N., D. Clement, B. R. Carter, R. A. Feely, S. Van Heuven, M. Hoppema, M. Ishii, R. M. Key, A. Kozyr, S. K. Lauvset, et al., The oceanic sink for anthropogenic $CO_2$ from 1994 to 2007, *Science*, *363*, 1193–1199, 2019.

Haidvogel, D., H. Arango, W. Budgell, B. Cornuelle, E. Curchitser, E. Di Lorenzo, K. Fennel, W. Geyer, A. Hermann, L. Lanerolle, J. Levin, J. McWilliams, A. Miller, A. Moore, T. Powell, A. Shchepetkin, C. Sherwood, R. Signell, J. Warner, and J. Wilkin, Ocean forecasting in terrain-following coordinates: Formulation and skill assessment of the Regional Ocean Modeling System, *Journal of Computational Physics*, *227*, 3595–3624, 2008.

Haine, T. W. N., and T. M. Hall, A generalized transport theory: Water-mass composition and age, *Journal of Physical Oceanography*, *32*, 1932–1946, 2002.

Haine, T. W. N., A. J. Watson, M. I. Liddicoat, and R. R. Dickson, The flow of Antarctic bottom water to the southwest Indian Ocean estimated using CFCs, *Journal of Geophysical Research*, *103653*, 637–27, 1998.

Hall, T. M., and T. W. N. Haine, On ocean transport diagnostics: The idealized age tracer and the age spectrum, *Journal of Physical Oceanography*, *32*, 1987–1991, 2002.

Hall, T. M., and R. A. Plumb, Age as a diagnostic of stratospheric transport, *Journal of Geophysical Research*, *99*, 1059–1070, 1994.

Han, G., Three-dimensional seasonal-mean circulation and hydrography on the eastern Scotian Shelf, *Journal of Geophysical Research: Oceans*, *108*, 3136, 2003.

Han, G., C. G. Hannah, J. W. Loder, and P. C. Smith, Seasonal variation of the three-dimensional mean circulation over the Scotian Shelf, *Journal of Geophysical Research*, *102*, 1011, 1997.

Hannah, C. G., J. W. Loder, and D. G. Wright, Seasonal variation of the baroclinic circulation in the Scotia-Maine region, in *Buoyancy Effects on Coastal and Estuarine Dynamics*, edited by D. G. Aubrey and C. T. Friedrichs, pp. 7–29, American Geophysical Union, 1996.

Hannah, C. G., J. A. Shore, J. W. Loder, and C. E. Naimie, Seasonal circulation on the western and central Scotian Shelf, *Journal of Physical Oceanography*, *31*, 591–615, 2001.

Hauri, C., C. Schultz, K. Hedstrom, S. Danielson, B. Irving, S. C. Doney, R. Dussin, E. N. Curchitser, D. F. Hill, and C. A. Stock, A regional hindcast model simulating ecosystem dynamics, inorganic carbon chemistry, and ocean acidification in the Gulf of Alaska, *Biogeosciences*, *17*, 3837–3857, 2020.

Hawke, D. J., Hydrology and near-surface nutrient distribution along the south otago continental shelf, new zealand, in summer and winter 1986, *New Zealand journal of marine and freshwater research*, *23*, 411–420, 1989.

Herman, A., D. Sameoto, C. Shunnian, M. Mitchell, B. Petrie, and N. Cochrane, Sources of zooplankton on the Nova Scotia shelf and their aggregations within deep-shelf basins, *Continental Shelf Research*, *11*, 211–238, 1991.

Hickey, B. M., Coastal oceanography of western North America from the tip of Baja California to Vancouver Island, in *The Global Coastal Ocean: Regional Studies and Syntheses*, vol. 11, pp. 345–393, Wiley & Sons, New York, 1998.

Ho, D. T., C. S. Law, M. J. Smith, P. Schlosser, M. Harvey, and P. Hill, Measurements of air-sea gas exchange at high wind speeds in the southern ocean: Implications for global parameterizations, *Geophysical Research Letters*, *33*, L16611, 2006.

Ho, D. T., S. Ferrón, V. C. Engel, W. T. Anderson, P. K. Swart, R. M. Price, and L. Barbero, Dissolved carbon biogeochemistry and export in mangrove-dominated rivers of the Florida Everglades, *Biogeosciences*, *14*, 2543–2559, 2017.

Hohmann, R., M. Hofer, R. Kipfer, F. Peeters, D. M. Imboden, H. Baur, and M. N. Shimaraev, Distribution of helium and tritium in Lake Baikal, *Journal of Geophysical Research: Oceans*, *103*, 12823–12838, 1998.

Holzer, M., and T. M. Hall, Transit-time and tracer-age distributions in geophysical flows, *Journal of the Atmospheric Sciences*, *57*, 3539–3558, 2000.

Holzer, M., and F. W. Primeau, The diffusive ocean conveyor, *Geophysical Research Letters*, *33*, L14618, 2006.

Jenkins, W. J., $^{3}$H and $^{3}$He in the beta triangle: Observations of gyre ventilation and oxygen utilization rates, *Journal of Physical Oceanography*, *17*, 763–783, 1987.

Jickells, T. D., Nutrient biogeochemistry of the coastal zone, *Science*, *281*, 217–21, 1998.

Karstensen, J., and M. Tomczak, Age determination of mixed water masses using CFC and oxygen data, *Journal of Geophysical Research*, *103*, 18599–18609, 1998.

Keeling, C. D., R. B. Bacastow, A. E. Bainbridge, C. A. Ekdahl Jr, P. R. Guenther, L. S. Waterman, and J. F. Chin, Atmospheric carbon dioxide variations at Mauna Loa observatory, Hawaii, *Tellus*, *28*, 538–551, 1976.

Landschützer, P., N. Gruber, D. C. Bakker, and U. Schuster, Recent variability of the global ocean carbon sink, *Global Biogeochemical Cycles*, *28*, 927–949, 2014.

Laruelle, G. G., H. H. Dürr, C. P. Slomp, and A. V. Borges, Evaluation of sinks and sources of $CO_2$ in the global coastal ocean using a spatially-explicit typology of estuaries and continental shelves, *Geophysical Research Letters*, *37*, 2010.

Laruelle, G. G., H. H. Dürr, R. Lauerwald, J. Hartmann, C. P. Slomp, N. Goossens, and P. A. Regnier, Global multi-scale segmentation of continental and coastal waters from the watersheds to the continental margins, *Hydrology and Earth System Sciences*, *17*, 2029–2051, 2013.

Laruelle, G. G., R. Lauerwald, B. Pfeil, and P. Regnier, Regionalized global budget of the $CO_2$ exchange at the air-water interface in continental shelf seas, *Global Biogeochemical Cycles*, *28*, 1199–1214, 2014.

Laruelle, G. G., R. Lauerwald, J. Rotschi, P. A. Raymond, J. Hartmann, and P. Regnier, Seasonal response of air-water $CO_2$ exchange along the land-ocean aquatic continuum of the northeast North American coast, *Biogeosciences*, *12*, 1447–1458, 2015.

Laruelle, G. G., P. Landschützer, N. Gruber, J.-L. Tison, B. Delille, and P. Regnier, Global high-resolution monthly $pCO_2$ climatology for the coastal ocean derived from neural network interpolation, *Biogeosciences*, *14*, 4545–4561, 2017.

Laurent, A., K. Fennel, W.-J. Cai, W.-J. Huang, L. Barbero, and R. Wanninkhof, Eutrophication-induced acidification of coastal waters in the northern Gulf of Mexico: Insights into origin and processes from a coupled physical-biogeochemical model, *Geophysical Research Letters*, *44*, 946–956, 2017.

Laurent, A., K. Fennel, and A. Kuhn, An observation-based evaluation and ranking of historical earth system model simulations in the northwest North Atlantic ocean, *Biogeosciences*, *18*, 1803–1822, 2021.

Lavoie, D., N. Lambert, and D. Gilbert, Projections of future trends in biogeochemical conditions in the northwest Atlantic using CMIP5 Earth System Models, *Atmosphere-Ocean*, *57*, 18–40, 2019.

Le Quéré, C., R. M. Andrew, P. Friedlingstein, S. Sitch, J. Pongratz, A. C. Manning, J. I. Korsbakken, G. P. Peters, J. G. Canadell, R. B. Jackson, et al., Global carbon budget 2017, *Earth System Science Data*, *10*, 405–448, 2018.

Lee, K., L. T. Tong, F. J. Millero, C. L. Sabine, A. G. Dickson, C. Goyet, G.-H. Park, R. Wanninkhof, R. A. Feely, and R. M. Key, Global relationships of total alkalinity with salinity and temperature in surface waters of the world's oceans, *Geophysical research letters*, *33*, 2006.

Lemay, J., H. Thomas, S. E. Craig, W. J. Burt, K. Fennel, and B. J. Greenan, Hurricane arthur and its effect on the short-term variability of $pCO_2$ on the Scotian Shelf, NW Atlantic., *Biogeosciences*, *15*, 2018.

Lewis, E., and D. Wallace, Program developed for $CO_2$ system calculations, *Tech. rep.*, Environmental System Science Data Infrastructure for a Virtual Ecosystem, 1998.

Lewis, M. K., and D. D. Sameoto, The vertical distribution of zooplankton and ichthyoplankton on the Nova Scotia shelf April 1984, *Tech. Rep. 717*, Canadian Data Report of Fisheries and Aquatic Sciences, 1988.

Liu, K., L. Atkinson, R. Quiñones, and L. Talaue-McManus, Carbon and nutrient fluxes in continental margins: A global synthesis, 2010.

Loder, J. W., G. Han, C. G. Hannah, D. A. Greenberg, and P. C. Smith, Hydrography and baroclinic circulation in the Scotian Shelf region: winter versus summer, *Canadian Journal of Fisheries and Aquatic Sciences*, *54*, 40–56, 1997.

Loder, J. W., B. Petrie, and G. Gawarkiewicz, The coastal ocean off northeastern North America: A large-scale view, in *The Sea, Volume 11: The Global Coastal Ocean - Regional Studies and Syntheses*, edited by Allan R. Robinson and Kenneth H. Brink, chap. 5, pp. 105–133, John Wiley & Sons, 1998.

Loder, J. W., C. G. Hannah, B. D. Petrie, and E. A. Gonzalez, Hydrographic and transport variability on the Halifax section, *Journal of Geophysical Research: Oceans*, *108*, 8003, 2003.

Loder, J. W., A. van der Baaren, and I. Yashayaev, Climate comparisons and change projections for the Northwest Atlantic from six CMIP5 models, *Atmosphere-Ocean*, *53*, 529–555, 2015.

Madec, G., NEMO ocean engine, *Note du Pôle de modélisation, Institut Pierre-Simon Laplace (IPSL), France*, 2008.

Mehrbach, C., C. H. Culberson, J. E. Hawley, and R. M. Pytkowicx, Measurement of the apparent dissociation constants of carbonic acid in seawater at atmospheric pressure, *Limnology and Oceanography*, *18*, 897–907, 1973.

Men, W., and G. Liu, Distribution of $^{226}$Ra and the residence time of the shelf water in the Yellow Sea and the East China Sea, *Journal of Radioanalytical and Nuclear Chemistry*, *303*, 2333–2344, 2014.

Millero, F. J., Thermodynamics of the carbon dioxide system in the oceans, *Geochimica et Cosmochimica Acta*, *59*, 661–677, 1995.

Mills, E. L., and R. O. Fournier, Fish production and the marine ecosystems of the Scotian Shelf, eastern canada, *Marine Biology*, *54*, 101–108, 1979.

Monsen, N. E., J. E. Cloern, L. V. Lucas, and S. G. Monismith, A comment on the use of flushing time, residence time, and age as transport time scales, *Limnology and Oceanography*, *47*, 1545–1553, 2002.

Mountain, D. G., The volume of shelf water in the Middle Atlantic Bight: Seasonal and interannual variability, 1977–1987, *Continental Shelf Research*, *11*, 251–267, 1991.

Mountain, D. G., Labrador slope water entering the Gulf of Maine—response to the North Atlantic Oscillation, *Continental Shelf Research*, *47*, 150–155, 2012.

Mucci, A., M. Starr, D. Gilbert, and B. Sundby, Acidification of lower St. Lawrence Estuary bottom waters, *Atmosphere-Ocean*, *49*, 206–218, 2011.

Neto, A. G., J. A. Langan, and J. B. Palter, Changes in the gulf stream preceded rapid warming of the northwest atlantic shelf, *Communications Earth & Environment*, *2*, 1–10, 2021.

Oliver, E. C., and N. J. Holbrook, Variability and long-term trends in the shelf circulation off eastern Tasmania, *Journal of Geophysical Research: Oceans*, *123*, 7366–7381, 2018.

Olsen, A., N. Lange, R. M. Key, T. Tanhua, H. C. Bittig, A. Kozyr, M. Álvarez, K. Azetsu-Scott, S. Becker, P. J. Brown, et al., An updated version of the global interior ocean biogeochemical data product, GLODAPv2. 2020, *Earth System Science Data*, *12*, 3653–3678, 2020.

Pershing, A. J., M. A. Alexander, C. M. Hernandez, L. A. Kerr, A. Le Bris, K. E. Mills, J. A. Nye, N. R. Record, H. A. Scannell, J. D. Scott, et al., Slow adaptation in the face of rapid warming leads to collapse of the Gulf of Maine cod fishery, *Science*, *350*, 809–812, 2015.

Petrie, B., B. J. Topliss, and D. G. Wright, Coastal upwelling and eddy development off Nova Scotia, *Journal of Geophysical Research: Oceans*, *92*, 12979–12991, 1987.

Previdi, M., K. Fennel, J. Wilkin, and D. Haidvogel, Interannual variability in atmospheric $CO_2$ uptake on the northeast U.S. continental shelf, *Journal of Geophysical Research*, *114*, G04003, 2009.

Rheuban, J. E., S. C. Doney, D. C. McCorkle, and R. W. Jakuba, Quantifying the effects of nutrient enrichment and freshwater mixing on coastal ocean acidification, *Journal of Geophysical Research: Oceans*, *124*, 9085–9100, 2019.

Ridgway, K., Seasonal circulation around Tasmania: an interface between eastern and western boundary dynamics, *Journal of Geophysical Research: Oceans*, *112*, 2007.

Rödenbeck, C., D. C. Bakker, N. Gruber, Y. Iida, A. R. Jacobson, S. Jones, P. Landschützer, N. Metzl, S. Nakaoka, A. Olsen, et al., Data-based estimates of the ocean carbon sink variability: first results of the Surface Ocean pCO2 Mapping intercomparison (SOCOM), *Biogeosciences*, *12*, 7251–7278, 2015.

Rogers, E. C., Modelling the movement of marine particles in discrete time and space with application to Scotian Shelf connectivity, Master's thesis, Dalhousie University, Halifax, NS, 2015.

Roobaert, A., G. G. Laruelle, P. Landschützer, N. Gruber, L. Chou, and P. Regnier, The spatiotemporal dynamics of the sources and sinks of $CO_2$ in the global coastal ocean, *Global Biogeochemical Cycles*, *33*, 1693–1714, 2019.

Ross, T., S. E. Craig, A. Comeau, R. Davis, M. Dever, and M. Beck, Blooms and subsurface phytoplankton layers on the Scotian Shelf: Insights from profiling gliders, *Journal of Marine Systems*, *172*, 118–127, 2017.

Rutherford, K., and K. Fennel, Diagnosing transit times on the northwestern North Atlantic continental shelf, *Ocean Science*, *14*, 1207–1221, 2018.

Rutherford, K., and K. Fennel, Elucidating coastal ocean carbon transport processes: A novel approach applied to the northwest north atlantic shelf, *Geophysical Research Letters*, subm.

Rutherford, K., K. Fennel, D. Atamanchuk, D. Wallace, and H. Thomas, A modeling study of temporal and spatial $pCO_2$ variability on the biologically active and temperature-dominated Scotian Shelf, *Biogeosciences Discussions*, pp. 1–25, 2021.

Saba, V. S., S. M. Griffies, W. G. Anderson, M. Winton, M. A. Alexander, T. L. Delworth, J. A. Hare, M. J. Harrison, A. Rosati, G. A. Vecchi, et al., Enhanced warming of the Northwest Atlantic Ocean under climate change, *Journal of Geophysical Research: Oceans*, *121*, 118–132, 2016.

Salisbury, J. E., and B. F. Jönsson, Rapid warming and salinity changes in the Gulf of Maine alter surface ocean carbonate parameters and hide ocean acidification, *Biogeochemistry*, *141*, 401–418, 2018.

Sameoto, D. D., and A. W. Herman, Life cycle and distribution of *Calanus finmarchicus* in deep basins on the Nova Scotia shelf and seasonal changes in *Calanus spp.*, *Marine Ecology Progress Series*, *66*, 225–237, 1990.

Sameoto, D. D., and A. W. Herman, Effect of the outflow from the Gulf of St. Lawrence on Nova Scotia shelf zooplankton, *Canadian Journal of Fisheries and Aquatic Sciences*, *49*, 857–869, 1992.

Sarmiento, J. L., G. Thiele, R. M. Key, and W. S. Moore, Oxygen and nitrate new production and remineralization in the North Atlantic subtropical gyre, *Journal of Geophysical Research*, *95*, 18303–18315, 1990.

Schlosser, P., J. Bullister, R. Fine, W. Jenkins, R. Key, J. Lupton, W. Roether, and W. Smethiejr, Transformation and age of water masses, in *Ocean Circulation and Climate*, edited by G. Siedler, J. Church, and J. Gould, chap. 5.8, pp. 431–452, Academic Press, 2001.

Seitzinger, S. P., J. A. Harrison, E. Dumont, A. H. W. Beusen, and A. F. Bouwman, Sources and delivery of carbon, nitrogen, and phosphorus to the coastal zone: An overview of global nutrient export from watersheds (news) models and their application, *Global Biogeochemical Cycles*, *19*, 2005.

Shadwick, E., and H. Thomas, Seasonal and spatial variability in the $CO_2$ system on the Scotian Shelf (Northwest Atlantic), *Marine Chemistry*, *160*, 42–55, 2014.

Shadwick, E., H. Thomas, A. Comeau, S. E. Craig, C. W. Hunt, and J. E. Salisbury, Air-sea $CO_2$ fluxes on the Scotian Shelf: Seasonal to multi-annual variability, *Biogeosciences*, *7*, 3851–3867, 2010.

Shadwick, E., H. Thomas, K. Azetsu-Scott, B. Greenan, E. Head, and E. Horne, Seasonal variability of dissolved inorganic carbon and surface water $pCO_2$ in the Scotian Shelf region of the Northwestern Atlantic, *Marine Chemistry*, *124*, 23–37, 2011.

Shan, S., J. Sheng, K. Ohashi, and M. Dever, Assessing the performance of a multi-nested ocean circulation model using satellite remote sensing and in situ observations, *Satellite Oceanography and Meteorology*, *1*, 39–59, 2016.

Sharples, J., J. J. Middelburg, K. Fennel, and T. D. Jickells, What proportion of riverine nutrients reaches the open ocean?, *Global Biogeochemical Cycles*, *31*, 39–58, 2017.

Sherwood, O. A., M. F. Lehmann, C. J. Schubert, D. B. Scott, and M. D. McCarthy, Nutrient regime shift in the western north atlantic indicated by compound-specific $\delta$15n of deep-sea gorgonian corals, *Proceedings of the National Academy of Sciences*, *108*, 1011–1015, 2011.

Signorini, S. R., A. Mannino, R. G. Najjar, M. A. Friedrichs, W. J. Cai, J. Salisbury, Z. A. Wang, H. Thomas, and E. Shadwick, Surface ocean $pCO_2$ seasonality and sea-air $CO_2$ flux estimates for the North American east coast, *Journal of Geophysical Research: Oceans*, *118*, 5439–5460, 2013.

Smith, P. C., Seasonal and interannual variability of current, temperature and salinity off southwest Nova Scotia, *Canadian Journal of Fisheries and Aquatic Sciences*, *46*, s4–s20, 1989.

Smith, P. C., R. W. Houghton, R. G. Fairbanks, and D. G. Mountain, Interannual variability of boundary fluxes and water mass properties in the Gulf of Maine and on Georges Bank: 1993–1997, *Deep Sea Research Part II: Topical Studies in Oceanography*, *48*, 37–70, 2001.

Stevens, C. L., J. M. O'Callaghan, S. M. Chiswell, and M. G. Hadfield, Physical oceanography of New Zealand/Aotearoa shelf seas–a review, *New Zealand Journal of Marine and Freshwater Research*, *55*, 6–45, 2021.

Sutcliffe, W. H., R. H. Loucks, and K. F. Drinkwater, Coastal circulation and physical oceanography of the Scotian Shelf and the Gulf of Maine, *Journal of the Fisheries Research Board of Canada*, *33*, 98–115, 1976.

Takahashi, T., S. C. Sutherland, C. Sweeney, A. Poisson, N. Metzl, B. Tilbrook, N. Bates, R. Wanninkhof, R. A. Feely, C. Sabine, J. Olafsson, and Y. Nojiri, Global sea air $CO_2$ flux based on climatological surface ocean $pCO_2$, and seasonal biological and temperature effects, *Deep Sea Research Part II: Topical Studies in Oceanography*, *49*, 1601–1622, 2002.

Takahashi, T., S. C. Sutherland, R. Wanninkhof, C. Sweeney, R. A. Feely, D. W. Chipman, B. Hales, G. Friederich, F. Chavez, C. Sabine, et al., Climatological mean and decadal change in surface ocean $pCO_2$, and net sea–air $CO_2$ flux over the global oceans, *Deep Sea Research Part II: Topical Studies in Oceanography*, *56*, 554–577, 2009.

Thiele, G., and J. L. Sarmiento, Tracer dating and ocean ventilation, *Journal of Geophysical Research*, *95*, 9377, 1990.

Tremblay, M. J., and J. C. Roff, Community gradients in the Scotian Shelf zooplankton, *Canadian Journal of Fisheries and Aquatic Sciences*, *40*, 598–611, 1983.

Trites, R. W., and A. Walton, A Canadian coastal sea - The Gulf of St. Lawrence, *Tech. rep.*, Bedford Institute of Oceanography, Darthmouth, 1975.

Tsunogai, S., S. Watanabe, and T. Sato, Is there a "continental shelf pump" for the absorption of atmospheric $CO_2$?, *Tellus*, *51B*, 701–712, 1999.

Turi, G., Z. Lachkar, and N. Gruber, Spatiotemporal variability and drivers of $pCO_2$ and air–sea $CO_2$ fluxes in the california current system: an eddy-resolving modeling study, *Biogeosciences*, *11*, 671–690, 2014.

Umlauf, L., and H. Burchard, A generic length-scale equation for geophysical turbulence models, *Journal of Marine Research*, *61*, 235–265, 2003.

Urrego-Blanco, J., and J. Sheng, Interannual variability of the circulation over the Eastern Canadian shelf, *Atmosphere-Ocean*, *50*, 277–300, 2012.

Vandemark, D., J. E. Salisbury, C. W. Hunt, S. M. Shellito, J. Irish, W. McGillis, C. Sabine, and S. Maenner, Temporal and spatial dynamics of $CO_2$ air-sea flux in the Gulf of Maine, *Journal of Geophysical Research: Oceans*, *116*, 2011.

Wang, Z., D. Brickman, and B. J. Greenan, Characteristic evolution of the Atlantic Meridional Overturning Circulation from 1990 to 2015: An eddy-resolving ocean model study, *Deep Sea Research Part I: Oceanographic Research Papers*, *149*, 103056, 2019.

Wang, Z. A., G. L. Lawson, C. H. Pilskaln, and A. E. Maas, Seasonal controls of aragonite saturation states in the g ulf of m aine, *Journal of Geophysical Research: Oceans*, *122*, 372–389, 2017.

Warner, J. C., C. R. Sherwood, H. G. Arango, and R. P. Signell, Performance of four turbulence closure models implemented using a generic length scale method, *Ocean Modelling*, *8*, 81–113, 2005.

Weiss, R. F., Carbon dioxide in water and seawater: The solubility of a non-ideal gas, *Marine Chemistry*, *2*, 203–215, 1974.

Winton, M., W. G. Anderson, T. L. Delworth, S. M. Griffies, W. J. Hurlin, and A. Rosati, Has coarse ocean resolution biased simulations of transient climate sensitivity?, *Geophysical Research Letters*, *41*, 8522–8529, 2014.

Wu, H., and J. Zhu, Advection scheme with 3rd high-order spatial interpolation at the middle temporal level and its application to saltwater intrusion in the Changjiang Estuary, *Ocean Modelling*, *33*, 33–51, 2010.

Wunsch, C., Oceanic age and transient tracers: Analytical and numerical solutions, *Journal of Geophysical Research*, *107*, 3048, 2002.

Xiu, P., F. Chai, E. N. Curchitser, and F. S. Castruccio, Future changes in coastal upwelling ecosystems with global warming: The case of the California Current System, *Scientific reports*, *8*, 2866, 2018.

Xue, L., L. Zhang, W.-J. Cai, and L.-Q. Jiang, Air–sea $CO_2$ fluxes in the southern Yellow Sea: An examination of the continental shelf pump hypothesis, *Continental Shelf Research*, *31*, 1904–1914, 2011.

Zeebe, R. E., and D. A. Wolf-Gladrow, *$CO_2$ in Seawater - Equilibrium, Kinetics, Isotopes*, 65, 2001, $1^{st}$ Ed. Amsterdam: Elsevier Science B.V.

Zhang, W. G., J. L. Wilkin, and O. M. E. Schofield, Simulation of water age and residence time in New York Bight, *Journal of Physical Oceanography*, *40*, 965–982, 2010.

Zhang, X., R. D. Hetland, M. Marta-Almeida, and S. F. DiMarco, A numerical investigation of the Mississippi and Atchafalaya freshwater transport, filling and flushing times on the Texas-Louisiana Shelf, *Journal of Geophysical Research: Oceans*, *117*, 2012.

Zisserson, B., and A. Cook, Impact of bottom water temperature change on the southernmost snow crab fishery in the Atlantic Ocean, *Fisheries Research*, *195*, 12–18, 2017.